DEVELOPMENT OF A PARAMETER-INSENSITIVE ARTIFICIAL IMMUNE SYSTEM FOR STRUCTURAL HEALTH MONITORING

by

Jiachen Zhang

A Thesis

Submitted to the Faculty

of the

WORCESTER POLYTECHNIC INSTITUTE

in partial fulfillment of the requirements for the

Degree of Master of Science

in

Mechanical Engineering

by

_____

May 2014

APPROVED:

_____

Dr. Zhikun Hou, Major Advisor

_____

Dr. Mikhail F. Dimentberg, Committee Member

_____

Dr. John R. Hall, Committee Member

_____

Dr. Stephen S. Nestinger, Graduate Committee Representative

Abstract

An innovative artificial immune system (AIS) is proposed herein for structural health monitoring (SHM) to ensure the structural integrity and functionality. While satisfactory results were obtained by previous AIS schemes, their performance is strongly structural-parameter-value (SPV) dependent and deviations of SPVs in testing from training due to modeling errors and measurement noises significantly deteriorates the AIS' performance. This thesis presents a less SPV-dependent AIS with a three-phase architecture, including damage-existence-detection, damage-location-determination, and damage-severity-estimation, using specially designed feature vectors (FVs) based on structural modal parameters. The maximum-relative-modal-parameter-change is used to detect the damage's existence and estimate its severity, and the pattern in normalized-modal-parameter-change is used to determinate the damage's location. Comparisons between the proposed FVs and their existing counterparts were conducted for 2/3/4-degree-of-freedom structures to illustrate the superior performance and less SPV-dependence of the proposed method, particularly in determining damage location. The proposed AIS was tested on a 4-degree-of-freedom model using 440 randomly generated damage conditions with a different SPV set per condition. A success rate of 95.23% in the determination of damage's existence and its location was obtained. The trained AIS for the 4-degree-of-freedom model was further evaluated by a four-story and two-bay by two-bay prototype structure used in the benchmark problem proposed by the IASC-ASCE Structural Health Monitoring Task Group. Results have shown great potentials of the proposed approach in its real-world applications.

Acknowledgments

I would like to show my deepest gratitude to my major advisor, Dr. Zhikun Hou, who has been continuously offering me insightful suggestions and guidance through the whole process of this thesis writing.

I would also like to thank Wenchang Xiao for the work she did in her MS thesis, which places a solid foundation for the discussions in this thesis. Besides, I am grateful for all the help I received from Dr. John R. Hall, Dr. Mikhail F. Dimentberg, and Dr. Stephen S. Nestinger, who serve as my thesis committee members and the graduate committee representative.

The George C. Gordon library plays an important role in the literature collecting and reviewing for this thesis. I owe my sincere thanks to this magnificent library and its enthusiastic and helpful librarians.

Additionally, I would like to express my appreciation to Dr. Erik A. Johnson in University of Southern California, for providing me with the programs of the benchmark problem, which are used to evaluate the performance of the proposed system, and Dr. Bo Chen in Michigan Technological University, for her inspiring studies in the artificial immune system's applications to the structural health monitoring tasks, which work as one of the starting point of the artificial immune system approach developed in this work.

Table of Contents

List of Figures

List of Tables

1 Introduction

This section introduces the two most important concepts in this thesis: the structural health monitoring (SHM) and the artificial immune system (AIS). Some previous studies in the AIS' application to SHM tasks are reviewed, from which the topic of this thesis is derived. Besides, the major differences between the proposed methodology and the conventional ones are also stated in this section.

1.1 Structural Health Monitoring (SHM)

From a coffee machine to the Burj Khalifa (also known as the Burj Dubai, the tallest man-made structure ($829.8\,m$) in the world (Burj Khalifa n.d.)), engineering structures work as the foundation of our modern world. People rely on these engineering structures in almost every aspect of their lives. The reliability of an engineering structure not only decides its ability to perform the designed tasks in a expected period of time, but also affects the safety of people's life and property in many occasions.

To ensure this vitally important reliability, health checks for a structure need to be performed periodically in its lifespan and also immediately after unexpected events. However, conventional approaches for the health checks rely heavily on the expertise and experience of professional workers, which makes the health check a time and money consuming process. Besides, manual health checks usually interfere with the structural functionality, which puts the structure partially or completely out of work when the check

is undergoing. In addition its high cost and associated inconvenience, the manual health check's accuracy is significantly influenced by the executor and is susceptible to all kinds of human errors.

With the aforementioned disadvantages of the conventional approach for structural health checks, the engineering area calls for the development of a technique to monitor the structural health condition in an automatic, efficient, and effective fashion. And the structural health monitoring (SHM) technique emerges at this demand.

1.1.1 Definition of SHM

Structural health monitoring (SHM) refers to the process of implementing a strategy to identify the damage and its status in engineering infrastructures. The damage here can be changes in the material and/or geometric properties, boundary conditions and system connectivity of a structure (Farrar and Worden 2007). Engineering infrastructures include, but are not limited to, beams, trusses, plates, shells and frames, bridges, offshore platforms, other large civil engineering structures, aerospace structures, and composites (Doebling, et al. 1996). The specific objectives of the SHM systems can be described as determining (i) the damage existence, (ii) the damage location, (iii) the damage type, and (iv) the damage severity (Worden, et al. 2007).

An effective SHM system is supposed to be capable of detecting the structural damage in its early stage, well before catastrophic structural failures that threaten the safety of

people's life and property. With this early knowledge about the damage, timely actions can be taken to prevent further developments of the damage, which not only exclude the possibility of structure failures, but also reduce the required expense for the structure maintenance and repair.

Besides, SHM systems can be invaluable in more dramatic scenarios, such as the structural health screening in the aftermath of earthquakes, hurricanes, explosions, and many other unexpected destructive events. The information provided by the SHM systems can be extremely helpful for the post-event damage assessments and the repair priority development.

1.1.2 Development of SHM and Its Application

Because of its benefits and potential in both the routine structure maintenance and the quick screening in emergency situations, SHM technique attracts increasing attentions from researchers, engineers, and also government officials through its development.

SHM systems aim to automatically evaluate the structural-damage-conditions based on the measurements taken actively or passively by sensors. Various methodologies have been proposed in the literature. Several classifications of the SHM techniques exist, one of which divides the methodologies into two categories: the global methods and the local methods.

The global methods are able to detect the damage that affects the overall characteristic of a structure. They can detect the damage in a wide range of locations in the structure, but are usually less competent in determining the damage type and severity. The structural modal parameters, such as the natural frequencies and the mode shapes, are usually employed as the damage-sensitive-variable in the global SHM methods. Doebling, et al. (1996) and Sohn, et al. (2004) presented excellent literature reviews on the global SHM methods.

The methods in the other category, i.e. the local methods, are only good at detecting the damage that exists in a limited area near the monitoring sensors. On the other side, the local methods exhibit preeminent performance in determining the damage type and severity, which is not the global methods' area of expertise. An example of the local method is presented by Honarvar, et al. (2013), who successfully took advantage of the ultrasonic method to detect a thinning rate as low as $10\,\mu m/year$ with an uncertainty of $\pm 1.5\,\mu m/year$ in industrial piping systems.

The SHM technique has been applied to many structures all over the world to assistant the conventional manual structural health checks. For instance, a sophisticated system named the Wind and Structural Health Monitoring System (WASHMS) was installed in the Tsing Ma, Ting Kau, and Kap Shui Mun bridges to monitor the health conditions of these bridges. Besides this, other similar systems have been deployed all across the world, including Europe (Casciati 2003), United States of America (Pines and Aktan 2002), and China (Ou and Li 2006).

1.2 Biological Immune System (BIS)

Human bodies are protected from pathogenic organisms and other invaders by our biological immune system (BIS), through a series of processes and reactions named the immune response. The immune response involves unnumbered cooperations between related cells, tissues, and organs.

Cells involved in the immune response are mainly the white blood cells, i.e. the leukocytes, which have two basic types: phagocytes and lymphocytes. Lymphocytes allow the BIS to memorize previous invaders, recognize them if they attack again in the future, and then destroy them in a much faster fashion than the speed in the first encounter. The two kinds of lymphocytes in our bodies are B-lymphocytes and T-lymphocytes, or simply B-cells and T-cells.

A foreign substance (such as a bacterium or a virus) that invades the body is called an antigen, which can be neutralized by a portion of a B-cell named an antibody. When immune cells detect new antigens, a primary-immune-response is initiated: B-cells having high affinities with this antigen undergo clone and mutation processes to generate more B-cells with similar antibodies, which are specialized proteins that can neutralize specific antigens. These antibodies react with this antigen and prevent it from harming our bodies.

After the invading antigens have been neutralized, some immune cells become memory

cells and stay in the immune system with a longer lifespan. If the same kind of antigen intrudes again, these memory cells will initiate a secondary-immune-response, which is much faster and also more efficient than the primary-immune-response, to eliminate these intruders. Details about the basic mechanisms and concepts in the BIS can be found in the reference (Lerner and Lerner 2008)**.**

1.3 Artificial Immune System (AIS)

Biological immune system (BIS) makes itself more and more efficient and effective by continuously learning from its own experiences, and keeps these "memories" in its memory-cell-set. This learning capacity has attracted attentions from a significant number of researchers, who explored the possibility of introducing this capacity into other disciplines to seek new approaches for the problems that are difficult or even impossible to solve using conventional methods.

As one of these explorations' results, artificial immune system (AIS) is an interdisciplinary area relating to immunology, computer science, and engineering (Dasgupta, Yu and Nino 2011). AIS takes advantages of the BIS' learning capacity and the computer' computational power. It advances forward with the development of modern computers, and becomes more sophisticated, powerful and affordable in recent decades. Many algorithms have been proposed in this area, such as the negative selection algorithm (Forrest, et al. 1994), the positive selection algorithm (Nguyen, Nguyen and Luong 2013), and the clonal selection algorithm (de Castro and Von Zuben 2002).

Despite its relative short history (since the mid-1980s), the AIS has been successfully applied to many areas, such as data mining (Puteh, et al. 2008), optimization (Vieira, de Lima and Jacob 2008), text processing (Albergante 2008), pattern recognition (Li, Wang and Wang 2009), anomaly detection (Gadi, Wang and do Lago 2008), and SHM (Chen and Zang 2009, 2011 and Xiao 2012). Applications of the AIS in these areas have brought new approaches and promised new possibilities to achieve their corresponding objectives. With its satisfactory performance in these aforementioned areas, the AIS has become an active research area and the related studies are undergoing all around the world.

1.4 Previous Work in Literature

This thesis focuses on the artificial immune system's (AIS') application in the structural health monitoring (SHM) area. As mentioned earlier, researchers have investigated the possibility of applying the AIS to SHM tasks, and satisfactory results have been obtained.

Chen and Zang (2009, 2011) proposed a methodology of applying the artificial-immune-pattern-recognition to the structure damage classification (different damage location and severity) task. Detailed discussions about the principles, concepts, and procedures of their method are presented in their articles. The principle-component-analysis and the multiple-regression-analysis were employed to extract the feature vectors (FVs) from the structural dynamic response in the time domain. This method's performance was evaluated for two structures: the benchmark structure proposed by the International

Association for Structural Control - American Society of Civil Engineers (IASC-ASCE) Structural Health Monitoring Task Group; and a three-story frame provided by Los Alamos National Laboratory. Their results showed that their method is suitable for the structure damage classification.

Xiao (2012) explored the feasibility of using the natural frequencies and the mode shapes as the FVs for the AIS in SHM tasks. The structural damage was detected, located, and estimated by the proposed AIS, which was trained using limited known damage conditions. Both FVs (formed by the natural frequencies or the mode shapes) occupy different positions in the feature space when representing different damage conditions. A comparison between the analytical calculation results and the numerical simulation results was provided in her thesis. Her method was tested by the simulation data and also in a real seismic scenario. Satisfactory results were acquired and analyzed in both cases.

The AIS constructed in these pioneering studies successfully introduced the advantages of the biological immune system (BIS) into the SHM area, and achieved promising results. Because the AIS derives from the BIS, many concepts and mechanisms in the AIS are directly borrowed from the BIS. A comparison is presented in Table 1-1 to clarify the differences between the definitions of some frequently used terminologies in the BIS and in the AIS for SHM tasks.

Table 1-1: Comparison between some terminologies used in the BIS and the AIS.

Terminology	Definition in BIS	Definition in the AIS for SHM
Antigen	A molecular pattern that can cause the reaction of the immune system, which is usually harmful to the human body.	A data structure that consists of some related information about a structural-damage-condition.
Antibody	A portion of a receptor molecule that can bind with a specific molecular pattern.	A data structure that consists of some related information about a structural-damage-condition. This structure is generated mathematically by the AIS.
Affinity	A measurement of the binding strength between an antigen and an antibody.	A criterion defined to scale the relationship between the FV of an antigen and the one of an antibody.
Memory Cell	An immune cell that contains information about previously invading antigens. It stays in the immune system and will initiate a secondary-immune-response if it recognizes known antigens.	A member in a database of AIS, which stores the data structures of previous invading antigens. This database is used by AIS to recognize unknown structure damage conditions.
Immune Response	The process taken by the immune system to neutralize invading antigens.	The recognition process performed by AIS to determine unknown structural damage conditions.

1.5 Thesis Contribution

As explained earlier, one attractive feature of the biological immune system (BIS) is its learning capacity, using which the BIS can continuously evolve itself to be more efficient and effective. In the artificial immune system (AIS), this learning process is named as the AIS training process. The antigens used in this AIS training process are referred to as known antigens, which means the information of the damage conditions represented by these antigens are known to the AIS. The AIS learns from these known antigens and obtain the ability to recognize unknown antigens, which means the information of the damage conditions represented by these antigens are unavailable to the AIS.

The AIS training process is a key step in the construction of an AIS. Although the aforementioned pioneering studies acquired satisfactory results, they have one common issue in the AIS training: The accuracy of the structure-parameter-values (SPVs) used in the AIS training (i.e. the training SPVs) significantly affects the overall performance of the trained AIS. In other words, the AIS needs accurate training SPVs to guarantee its satisfactory performance.

This reliance of the AIS' performance on its training SPVs' accuracy limits the AIS' applicability in the SHM area, as a result of the following reasons: If the AIS is trained using the simulated measurements, the discrepancy between the training SPVs and the SPVs of the structure under monitoring is unavoidable, because a simulation model is always a simplification and an approximation of the actual structure. Limited by the associated difficulty and cost, an accurate simulation model is usually unavailable in many real world scenarios. Because the AIS' performance depends on the accuracy of the training SPVs, this unavoidable discrepancy will deteriorate the AIS' performance, and therefore limit its applicability in the SHM area.

Alternatively, if the AIS is trained by the measurements from an interested physical structure, the difference between the SPVs of different structures will prevent this trained AIS from being applicable to other structures, due to the reliance of the AIS's performance on its training SPVs. As a result, each structure needs an uniquely trained AIS to perform SHM tasks. Also, the AIS needs re-training if the SPVs of the interested structure change, which is not uncommon for some structures (e.g. offshore oil platforms).

To tackle the problem caused by the reliance of the AIS' performance on its training SPVs and extend the AIS' applicability in the SHM area, an AIS is proposed in this these, which differentiates itself from existing methodologies by its SPV insensitive feature vectors (FVs) and a three-phase recognition process.

Results from some comparisons, a case study and a benchmark study prove that, the performance of the proposed AIS does not obviously rely on its training SPVs. Namely, the negative effect of the SPVs change on the AIS' performance is reduced to an unnoticeable level in the proposed AIS.

With this ameliorated characteristic, the proposed AIS can be applied to the physical structures if it is trained by the simulation data, or it can be applied to other similar structures if it is trained by one physical structure. The proposed AIS in this thesis is more applicable to the SHM area with this high tolerance to the discrepancy between the training SPVs and the SPVs of the structure under monitoring, compared to the AIS that was previously proposed in the literature.

2 Construction of Artificial Immune System (AIS)

In the artificial immune system (AIS) applied to structural health monitoring (SHM) tasks, one antigen or one antibody is defined to be a data structure representing one structural-damage-condition. This data structure consists of a damage flag (Is the structure damaged?), a damage-location-label (Where is the damage?), a damage-severity-label (How serious is the damage?), and a feature vector (FV) containing characteristics of this damage (Figure 2-1). Similar with the biological immune system (BIS), antigens are external invaders to the AIS, while antibodies are generated by the AIS to react with invading antigens. Namely, antigens in the AIS are generated from the dynamic responses of structures, while antibodies are mathematically calculated inside the AIS.

The proposed AIS consists of three phases, including damage-existence-detection, damage-location-determination, and damage-severity-estimation. Output of a previous phase works as the input for its next phase: Phase 2 (damage-location-determination) is performed only when Phase 1 (damage-existence-detection) suggests that there is some damage in the structure; Phase 3 (damage-severity-estimation) is executed only when Phase 2 has determined the damage's location, which will be used as the known information in Phase 3.

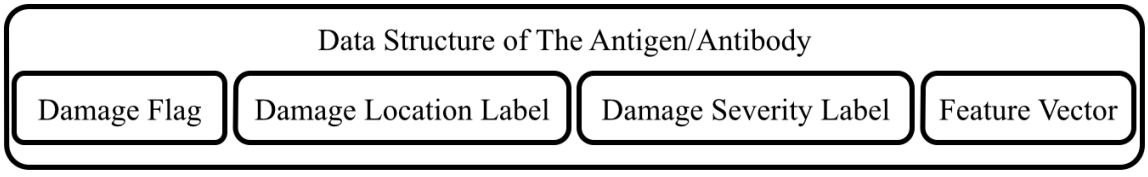

Figure 2-1: Data structure of the antigen/antibody in the AIS.

Imitating the BIS, the memory-cell-set in the AIS is the core of its learning capacity. The training process used to generate a mature memory-cell-set is described as follows: Firstly, a number of training antigens are generated from the known structural-damage-conditions. All entries of a training antigen's data structure (FV and the labels) are known to the AIS. These training antigens interact with an initial antibody set, which is randomly created by the AIS, to stimulate these antibodies' primary-immune-response. This interaction process is detailed in the following paragraphs.

For convenience, the FVs of a training antigen and an antibody are denoted by ag and ab, respectively. To quantify the intimacy between ag and ab, a variable named the affinity value is defined to be

$$\mathrm{aff}(\mathrm{ab},\mathrm{ag}) = \frac{1}{1+\mathrm{dis}(\mathrm{ab},\mathrm{ag})} \tag{3-1}$$

where $\mathrm{dis}(\mathrm{ab},\mathrm{ag})$ is the Euclidean distance between ab and ag in the feature space. With the stimulation from a training antigen, initial antibodies carry out a clone process. In the BIS, antibodies having higher affinity values with the training antigen will generate more clones in the clone process. Correspondingly in the AIS, an antibody with a higher affinity value calculated from Equation (3-1) will have more clones in this process. Thus, the clone number (CN) of an antibody under stimulation is calculated using

$$\mathrm{CN} = \mathrm{round}\left(\mathrm{CR}\cdot\mathrm{aff}(\mathrm{ab},\mathrm{ag})\right) \tag{3-2}$$

where CR is a pre-specified clone rate and $\mathrm{round}(\cdot)$ is a function that returns the integer nearest its argument.

The cloned antibodies undergo a mutation process, which is intended to increase the diversity of the antibody set and possibly generate antibodies having higher affinity values with the training antigen. To be consistent with the principles in the BIS, antibodies having higher affinity values with the training antigen experience smaller mutation extent. Therefore the mutation process is defined by

$$\mathrm{ab}_m = \mathrm{ab} + \mathrm{MR} \cdot \delta \tag{3-3}$$

where ab_m is the FV of a mutated antibody (The subscript "m" stands for the word "mutation"), δ is a standard normal random variable having the same dimensional structure with ab, and MR is the mutation rate, which is defined as

$$\mathrm{MR} = 1 - \mathrm{aff}(\mathrm{ab}, \mathrm{ag}). \tag{3-4}$$

Following the clone and mutation processes, the affinity values between all antibodies and the training antigen are calculated using Equation (3-1). Antibodies with an affinity value higher than a pre-specified candidate-selection-threshold (CST) are sifted as the candidate-memory-cells (CMCs), and their damage locations are labeled using the damage-location-label of the training antigen. Afterwards, these candidates are introduced into the existing memory-cell-set one-by-one. It is notable that the memory-cell-set is empty at the very beginning of the training process.

For one candidate-memory-cell, if there is no existing memory cell having the same location label with it, it will be injected into the memory-cell-set directly. Otherwise, if there are memory cells having the same location label with it, the affinity values between this candidate and these memory cells will be calculated (Equation (3-1)). If the

maximum of these affinity values is lower than a pre-specified candidate-injection-threshold (CIT), this candidate will be injected into the memory-cell-set. If not, this candidate will be discarded. This process repeats for every candidate. The AIS' reaction to a training antigen ends when all candidate-memory-cells have been introduced into the memory-cell-set. This process is schematically described in Figure 2-2. The AIS training process finishes when all training antigens have gone through this interaction process. At this point, the AIS' memory-cell-set is named as the mature-memory-cell-set.

The mature-memory-cell-set is used by the AIS in Phase 2 to determinate the damage's location of an unknown structural-damage-condition, in which the unknown antigen interacts with memory cells and binds with one selected-memory-cell that has the highest affinity value with it. The unknown antigen is labeled using the damage-location-label of the selected-memory-cell. Besides Phase 2, the AIS also needs Phase 1 and Phase 3 to determinate the damage's existence and severity, where the maximum-relative-modal-parameter-change (MRMPC) is used. The MRMPC's relationships with the damage's severity are built for all damage's locations. In Phase 1, the unknown condition will be labeled as "damaged" if the MRMPC is bigger than a pre-specified threshold. And in Phase 3, the damage's severity is estimated using its relationship with the MRMPC and the information of the damage's location.

After the mature-memory-cell-set and the relationships between the MRMPC and the damage's severity are obtained, this AIS is trained and ready to be applied to SHM tasks to classify new-coming unknown structural-damage-conditions.

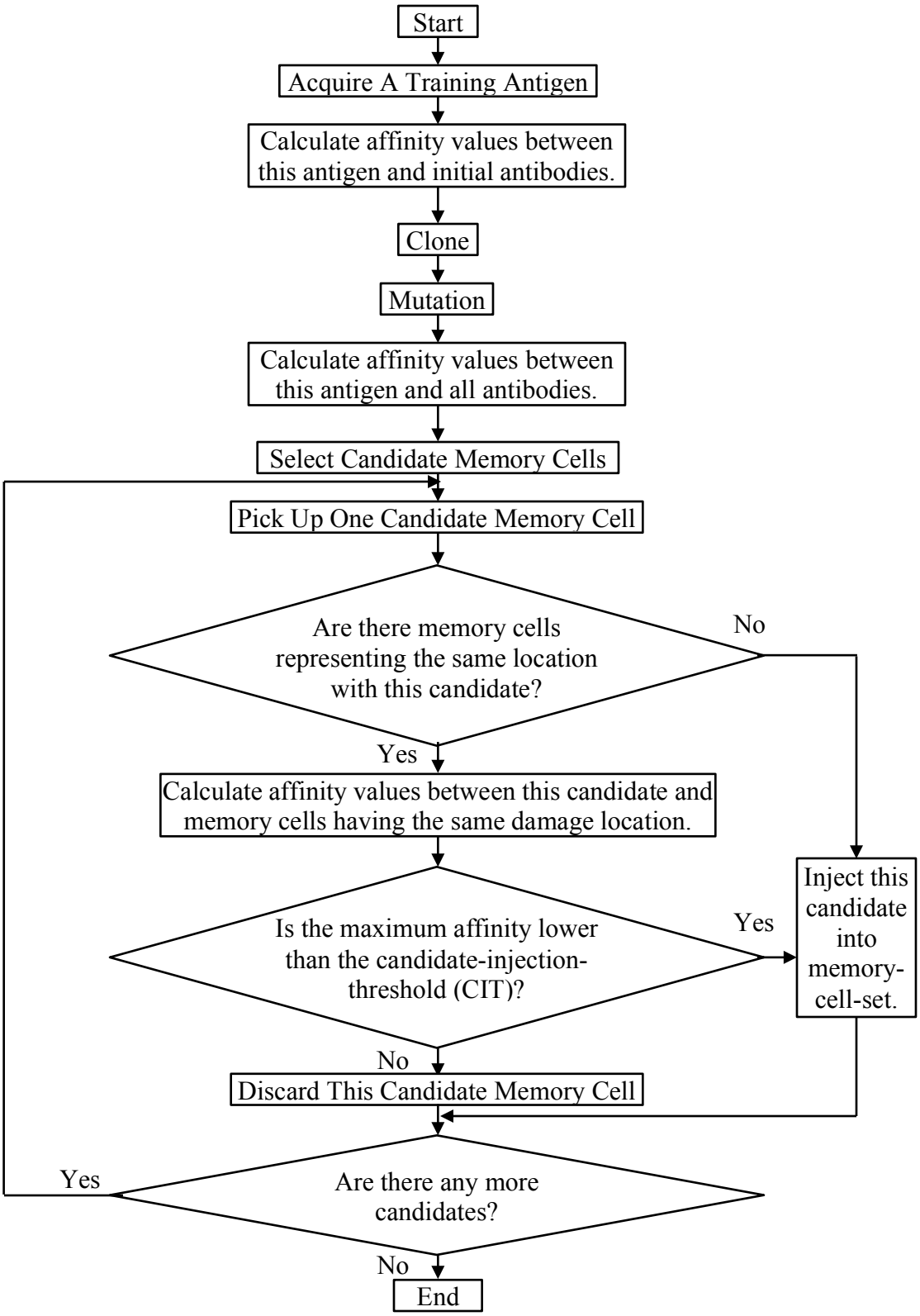

Figure 2-2: Schematic illustration of the AIS' reaction process to a training antigen.

3 Feature Vector

3.1 Introduction to Feature Vector

The feature vector (FV) in this context refers to a mathematical expression of the key characteristics of a structural-damage-condition, and therefore is an important component in the data structure of an antigen/antibody. AIS uses FVs to recognize different structural-damage-conditions. Due to its significance, the performance of the FV affects the overall performance of the AIS to a significant extent.

Following parts in this section compares the performance of the proposed FV with its conventional counterpart, both of which are based on structural modal parameters. Their performance is evaluated by the extent of the separation between FVs representing different conditions, and the concentration of FVs standing for the same condition in the feature space.

The modal parameters are functions of the physical properties (such as mass and stiffness) of the structure. Changes in the physical properties, as a result of damage, will cause changes in the modal parameters (Doebling, et al. 1996). This dependence of modal parameters on physical properties attracts many researchers to use modal parameters as the damage-sensitive-variable for SHM techniques. And many techniques have been proposed to extract modal parameters from the structural dynamic responses.

In the previous study about the AIS' application in SHM tasks, modal parameters are also employed to form FVs (Xiao 2012). However, modal parameter values heavily rely on the structural-parameter-values (SPV). As a result, the FVs formed by modal parameters are also profoundly dependent on specific SPV. The limitations and disadvantages caused by this dependence have been discussed in Section 1.5.

In this thesis, FVs for the AIS are proposed to be formed using the pattern in modal-parameter-change, instead of using the modal parameters directly (conventional approach). Comparisons are made between the proposed and the conventional approaches to construct FVs in the subsequent parts of this section. Results suggest that the FVs formed in the proposed method are less dependent on the SPV and the damage severity, while at the same time, more sensitive to the damage location, which makes them much more appropriate for the damage-location-determination in SHM tasks.

3.2 Simulation Setup

Performance of the proposed FVs and the ones is compared in three structure models, including a 2-degree-of-freedom (2-DOF), a 3-degree-of-freedom (3-DOF), and a 4-degree-of-freedom (4-DOF) structure model. These three models are simplified to the 2/3/4-DOF mass-spring-damping model, respectively. These structure models and their corresponding simplified models are illustrated in Figure 3-1 (n is the number of DOF (2, 3, or 4 in this thesis)).

The governing equation for the n-DOF mass-spring-damping model in Figure 3-1 is

$$M\ddot{X} + C\dot{X} + KX = F \tag{4-1}$$

where

$$M = \begin{bmatrix} m_1 & 0 & \cdots & 0 \\ 0 & m_2 & \cdots & 0 \\ \vdots & \vdots & \ddots & \vdots \\ 0 & 0 & \cdots & m_n \end{bmatrix}$$

and

$$K = \begin{bmatrix} k_1 + k_2 & -k_2 & 0 & \cdots & 0 & 0 \\ -k_2 & k_2 + k_3 & -k_3 & \cdots & 0 & 0 \\ 0 & -k_3 & k_3 + k_4 & \cdots & 0 & 0 \\ \vdots & \vdots & \vdots & \ddots & \vdots & \vdots \\ 0 & 0 & 0 & \cdots & k_{n-1} + k_n & -k_n \\ 0 & 0 & 0 & \cdots & -k_n & k_n \end{bmatrix}$$

are the system's mass and stiffness matrices, respectively.

$$X = \begin{bmatrix} x_1 & x_2 & \cdots & x_n \end{bmatrix}^{\mathrm{T}} \text{ and } F = \begin{bmatrix} f_1 & f_2 & \cdots & f_n \end{bmatrix}^{\mathrm{T}}$$

are the story displacement vector and the external force vector, respectively. x_i and f_i are the displacement and the external force on the i-th story, respectively.

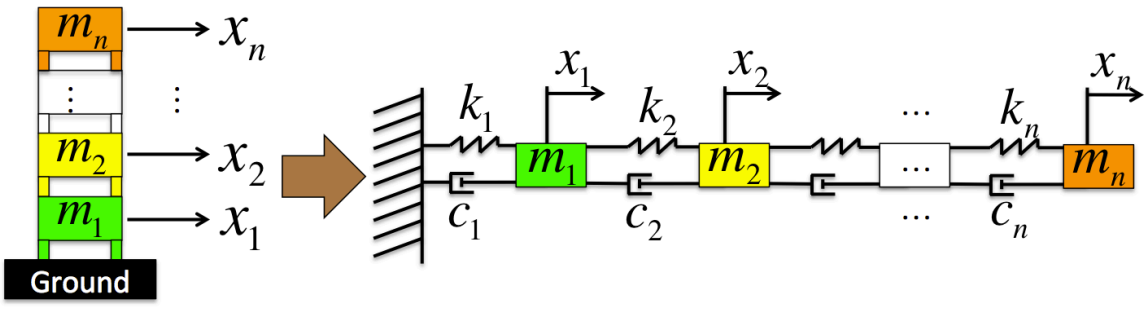

Figure 3-1: n-DOF chain structure and its mass-spring-damping model.

Rayleigh damping is assumed as

$$C = \alpha M + \beta K \tag{4-2}$$

where α and β are pre-specified parameters.

Simulations are performed using the fourth-order Runge-Kutta (RK4) algorithm with MATLAB. Non-zero initial displacement condition is used to excite the structure into free vibrations. The dynamic response of the structure (displacement and velocity of each story) is recorded up to 30s with the sampling rate of 1000Hz. Then the fast Fourier transform (FFT) is performed to transfer the first story displacement data from the time domain to the frequency domain, from where the modal parameters, including the natural frequencies and the mode shape information, are extracted.

There are two points need attention: 1) In this thesis, modal parameters are extracted from the structural dynamic response in free-vibrations. However, the forced-vibration is more frequently used in real-world scenarios. The free-vibration is used herein because the modal parameter extraction from dynamic response is easier and also more accurate in the free-vibration situation. The focus of this thesis is the development and the proof-of-concept demonstration of the proposed methodology. Issues related to the more realistic and more complicated excitation methods are out of this thesis' scope, and need to be investigated in future studies. 2) Only the displacement data of the 1st story is used to extract modal parameters for the proposed AIS. In this way, sensors on one single story (the 1st story) are sufficient for the AIS. Generally, a method with less demanding requirement has better feasibility and applicability in real-world scenarios.

To simulate different damage on a story, the stiffness value of this story is reduced to different extents. In this thesis, damage is assumed to be present on only one of the stories (single-damage-situation), which means only one stiffness value is reduced in each damage condition.

3.3 Performance Comparison of Feature Vectors

In this subsection, natural frequencies and mode shape information are employed separately as the damage-sensitive-variable to build FVs. FVs are constructed using the conventional approach and also the proposed approach. Comparisons are made between the conventional FV and the proposed one.

3.3.1 Natural Frequency and Pattern in Natural Frequency Change

In order to perform the comparison, the FVs are first formed in the conventional approach by the natural frequencies directly, according to the following formula:

$$\mathrm{FV} = \begin{bmatrix} f_1 & f_2 & \cdots & f_n \end{bmatrix}^{\mathrm{T}} \tag{4-3}$$

where f_i ($i = 1, 2, \ldots, n.n$ is the number of natural frequencies considered) is the i-th natural frequency (arranged from the lowest to the highest) acquired from the structural dynamic response.

The proposed approach to construct FVs based on changing patterns is derived in following sections, after which comparisons are carried out with the 2/3/4-DOF structure models.

3.3.1.1 2-DOF Structure Model

Simulation Parameter

In this part, the 2-DOF chain structure and its corresponding 2-DOF mass-spring-damping model are employed for simulations. The SPV sets used for this model are partially listed in Table 3-1.

The "original set" in Table 3-1 is selected based on (Ellis and Bougard 2001) and (Xiao 2012). And the "mutated set" in Table 3-1 is generated by adding random deviations, which are within the range of 15%, to the "original set". Employing mathematical expressions, the SPV values in the "mutated set" is calculated using following equations:

$$m_{i,\text{new}} = m_{i,\text{original}} + 15\% \times m_{i,\text{original}} \times \delta \tag{4-4}$$

$$k_{i,\text{new}} = k_{i,\text{original}} + 15\% \times k_{i,\text{original}} \times \delta \tag{4-5}$$

$$c_{i,\text{new}} = c_{i,\text{original}} + 15\% \times c_{i,\text{original}} \times \delta \tag{4-6}$$

where $i = 1, 2, \ldots, n$. n is the number of structural DOF. $m_{i,\text{original}}$, $k_{i,\text{original}}$, and $c_{i,\text{original}}$

Table 3-1: SPV sets used for the 2-DOF structural model (incomplete).

Name	Mass (10^5kg)		Stiffness (10^8 kg/s^2)		Damping	
	m_1	m_2	k_1	k_2	α (10^{-1}s^{-1})	β (10^{-3}s)
Original Set	2.50	2.50	3.00	2.50	2.00	1.50
Mutated Set	2.84	2.49	3.27	2.23	1.95	1.70

are the values in the "original set", and $m_{i,\text{new}}$, $k_{i,\text{new}}$, and $c_{i,\text{new}}$ are the values in a new generated SPV set (the "mutated set" in this case). δ is a uniformly distributed random number generated by MATLAB and $\delta \in (-1, 1)$.

The SPV sets for the 3-DOF and 4-DOF structural models are selected and generated in the same fashion. This process will not be explained again in their sections to avoid repetitions. Other simulation parameters such as the calculation algorithm and the measurement sampling rate have already been described in Section 3.2.

Feature Vector Performance

The natural frequencies of the 2-DOF structure are extracted from simulated dynamic responses, which is obtained with the previously described simulation parameters and the "original set" in Table 3-1.

The FVs are first constructed using natural frequencies directly (conventional approach, Equation (4-3) for $n = 2$). The feature space with these conventional FVs is plotted in Figure 3-2. In Figure 3-2, black, red, and blue colors are used to denote the FVs representing "healthy", "1st story damage", and "2nd story damage" conditions, respectively. The "healthy" condition is emphasized by a star mark in the figure. The number annotated beside a point in Figure 3-2 (b) is the damage severity of the damage condition represented by that specific point. For all other following figures in this thesis,

the implications of the colors and the numbers near points are the same as in Figure 3-2, and therefore will not be explained again unless necessary.

Figure 3-2 shows that a FV gets closer to the "healthy" point when the damage severity of the condition represented by it becomes smaller, no matter where the damage location is. The distance between FVs from different damage locations are not significant, compared to the distance between FVs from the same damage location. For example, the distance between the "10% damage on the 1st story" and the "10% damage on the 2nd

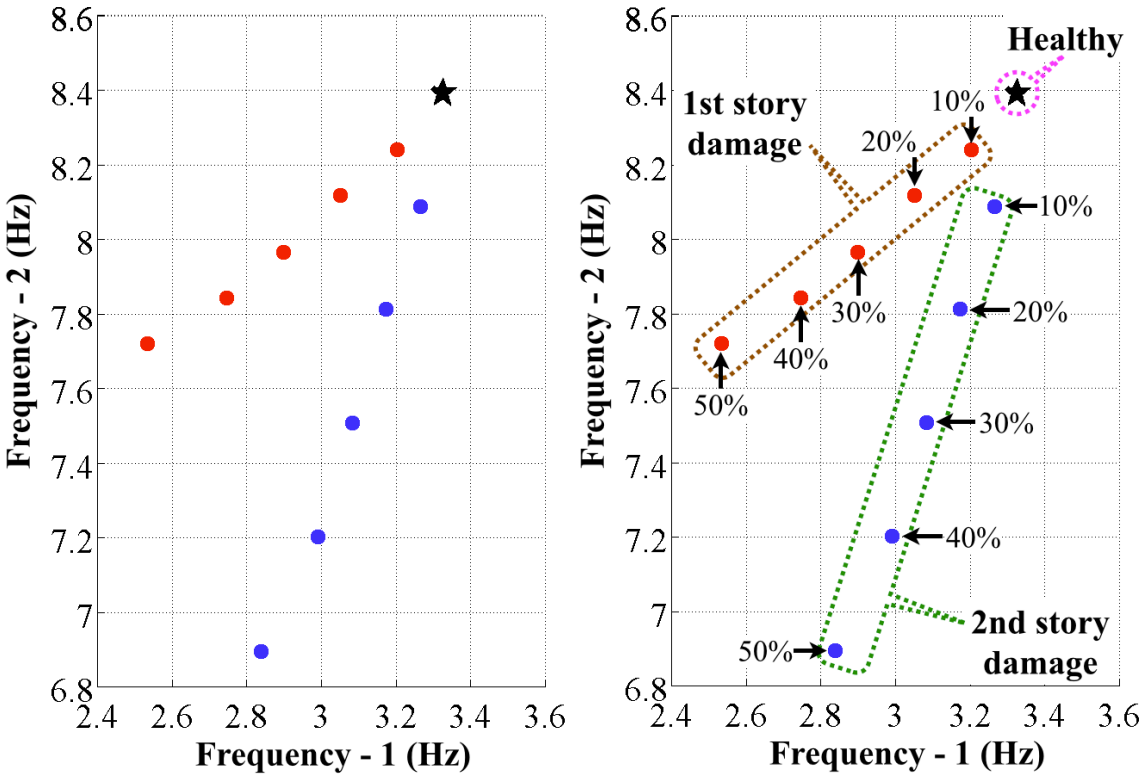

(a) (b)

Figure 3-2: Feature space of the 2-DOF model with conventional FVs in one SPV set. (a): original graph; (b): graph with annotations.

story" is smaller than the distance between the "10% damage on the 2nd story" and the "20% damage on the 2nd story". This distribution of FVs in the feature space is not desirable for AIS, because AIS discriminates different damage conditions by the distinctness of their FVs. The adjacent positions of the FVs from different damage locations increase the difficulty for AIS to distinguish one damage location from another.

In contrast to the FVs formed by natural frequencies directly, an approach of forming FVs by the pattern in natural-frequency-change is proposed as a more preferable option for the AIS in SHM tasks. To reveal this pattern, vectors are drawn from the "healthy" point to different "damaged" points in the feature space (Figure 3-3).

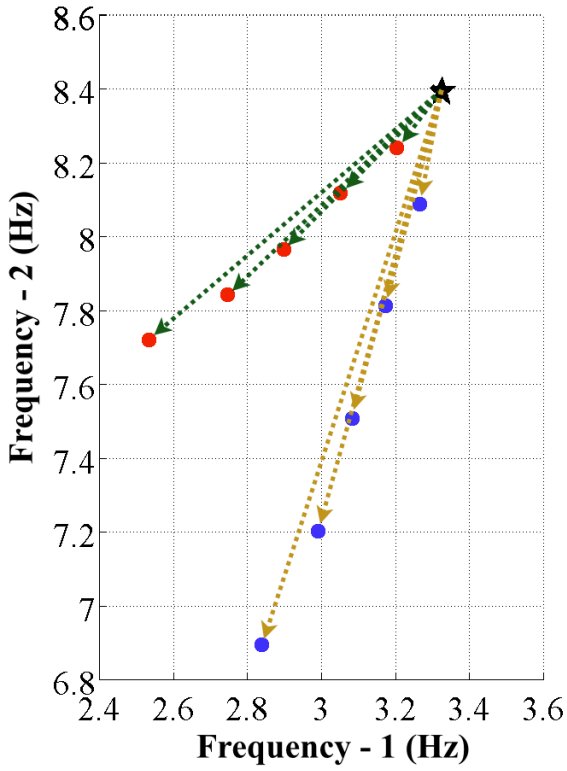

Figure 3-3: Feature space of the 2-DOF model with conventional FVs in one SPV set. Arrows are drawn from the "healthy" point to damaged points.

It is shown in Figure 3-3 that the direction and magnitude of a vector (arrow) are decided by the damage location and severity of its "ending point", respectively. In other worlds, the pattern in natural-frequency-change with different damage can be summarized as: Damage moves the FV away from the "healthy" position in the feature space. The direction of this movement is decided by the damage location. While the distance of this movement is controlled by the damage severity. Taking advantage of this pattern in natural-frequency-change, directions and magnitudes of these arrows are used for the damage-location-determination (Phase 2) and the damage-severity-estimation (Phase 3), respectively.

To extract the direction of arrows in the feature space, a variable named the normalized frequency change (NFC) is defined as follows:

$$\mathrm{NFC}_i = \frac{\Delta_i}{\sqrt{\Delta_1^2 + \Delta_2^2 \cdots + \Delta_n^2}} \tag{4-7}$$

where

$$\Delta_i = f_{\mathrm{healthy},\,i} - f_i$$

where $i = 1, 2, \ldots, n$ (n is the number of natural frequencies considered). f_i is the i-th natural frequency, and $f_{\mathrm{healthy},\,i}$ is the value of the i-th natural frequency in the healthy condition. With the NFC, the proposed FVs are constructed in the following format:

$$\mathrm{FV} = \begin{bmatrix} \mathrm{NFC}_1 & \mathrm{NFC}_2 & \cdots & \mathrm{NFC}_n \end{bmatrix}^{\mathrm{T}}. \tag{4-8}$$

According to this new definition, FVs are constructed using simulated dynamic responses of the 2-DOF structure model in different damage conditions with the "original set" in

Table 3-1. The feature space with these FVs is plotted in Figure 3-4. Compared with Figure 3-2, FVs representing the same damage location in Figure 3-4 are better clustered, and the FVs from different damage locations are better separated.

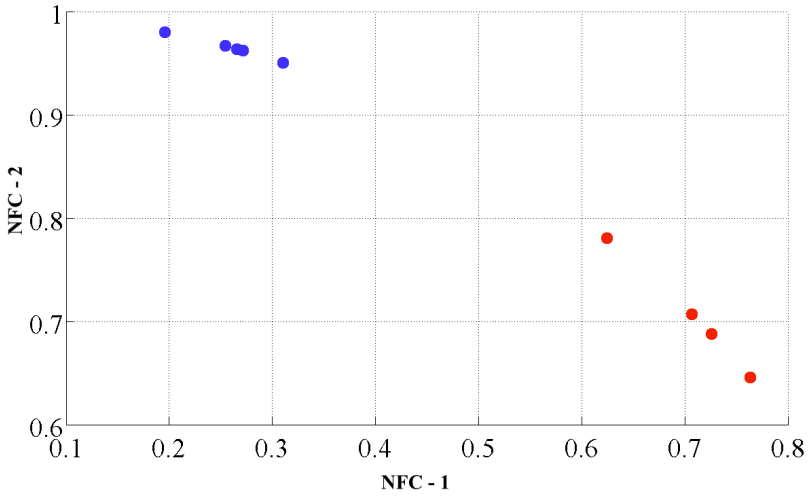

(a)

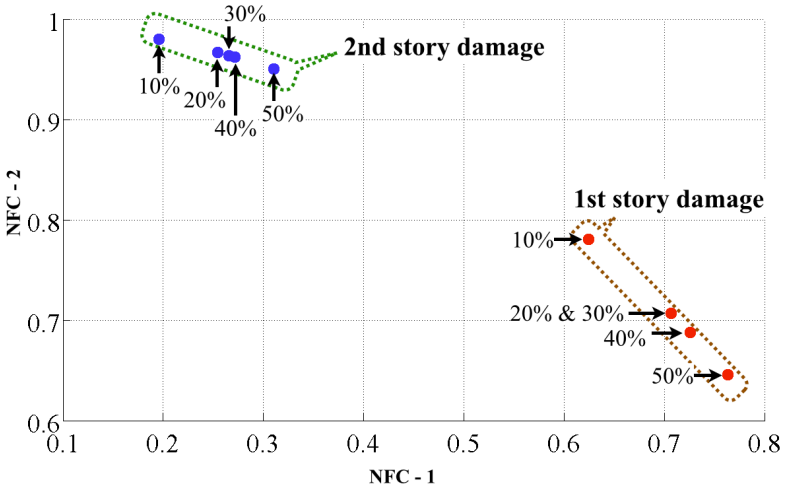

(b)

Figure 3-4: Feature space of the 2-DOF model with proposed FVs in one SPV set. (a): original graph; (b): graph with annotations.

Since AIS discriminates different damage conditions based on their characteristic FVs, it is apparently easier for AIS to correctly recognize different damage locations with this better separation between FVs from different damage locations in Figure 3-4. In brief, the characteristics of FVs in Figure 3-4 are more desirable from the perspective of AIS in SHM tasks, compared with the ones in Figure 3-2.

In addition, one point should be noted that the "healthy" point in Figure 3-2 disappears in Figure 3-4. The reason is that, the NFC is defined to be the normalized difference between frequency values in "healthy" and damaged conditions (Equation (4-7)). For the "healthy" condition itself, this difference will become zero, and therefore cannot be normalized using Equation (4-7) or plotted in Figure 3-4.

Because the NFC definition does not include the "healthy" condition, FVs formed by NFCs can only be used to instances that are known to have damage somewhere in the structure. Therefore, a damage existence detection phase is required before the damage location determination phase. Also because the NFC definition, which only considers the direction information of arrows drawn in Figure 3-3, another damage severity estimation phase employing the arrows' magnitude information is added after the damage location determination phase. These three phases of the proposed AIS will be demonstrated in later sections.

Structure-Parameter-Value Variation

As functions of the structural physical properties, structural natural frequencies change correspondingly with the SPV changes. FVs based on natural frequencies also change their positions in the feature space with the change in SPV. As explained earlier, the sensitivity of FVs to the SPV change limits the applicability of the AIS in the SHM area.

To evaluate and compare the effects of the SPV change on the conventional FVs and the proposed FVs, the dynamic responses of the 2-DOF structure model in different damage conditions were simulated using two different SPV sets (the "original set" and the "mutated set") in Table 3-1. And natural frequencies of the structure model in different damage severities with these two different SPV sets are extracted from simulation results.

Using the conventional approach, FVs are constructed using natural frequencies directly, according to Equation (4-3). The feature space with theses FVs is plotted in Figure 3-5. In Figure 3-5 and all following figures, points and circles are used to denote the FVs generated with the "original set" and the "mutated set" in Table 3-1 (or other corresponding tables), respectively.

It is shown clearly in Figure 3-5 that, the SPV change significantly affect the locations of FVs in the feature space, which are constructed from natural frequencies directly. The FVs representing "2nd story damage" ("original set") mix with the ones from "1st story damage" ("mutated set"). Due to this mixture, the challenge faced by the AIS in the

damage-location-determination task has been significantly exacerbated, which is evidently not desirable.

In contrast to the situation in Figure 3-5, FVs constructed by the changing pattern (NFC) exhibit desirable characteristics. The NFCs of the 2-DOF structure under these two SPV sets (Table 3-1) are acquired from the simulated dynamic responses using Equation (4-7), and are then employed to form FVs according to Equation (4-8). It is notable that, the proposed FVs are calculated using the healthy natural frequencies as the reference. Thus for a new SPV set, the healthy natural frequencies under this SPV set have to be known, in order to calculate the proposed FVs for damage conditions with this SPV set. The feature space with the proposed FVs is shown in Figure 3-6.

In Figure 3-6, the positions of FVs formed by the NFCs are not obviously affected by the SPV difference. More specifically, even though there are two different SPV sets in Figure 3-6, FVs representing the same damage location are still clustered together, and the ones from different damage locations are still well separated. This suggests the proposed FV is less dependent on the SPV than the conventional one. Because of this less, the trained AIS using the proposed FV will be able to maintain satisfactory performance, even when there is a discrepancy between the training SPV and the SPV of the structure under monitoring. Therefore, the proposed FVs are desirable and superior for the AIS in SHM tasks, compared to FVs formed in conventional approaches.

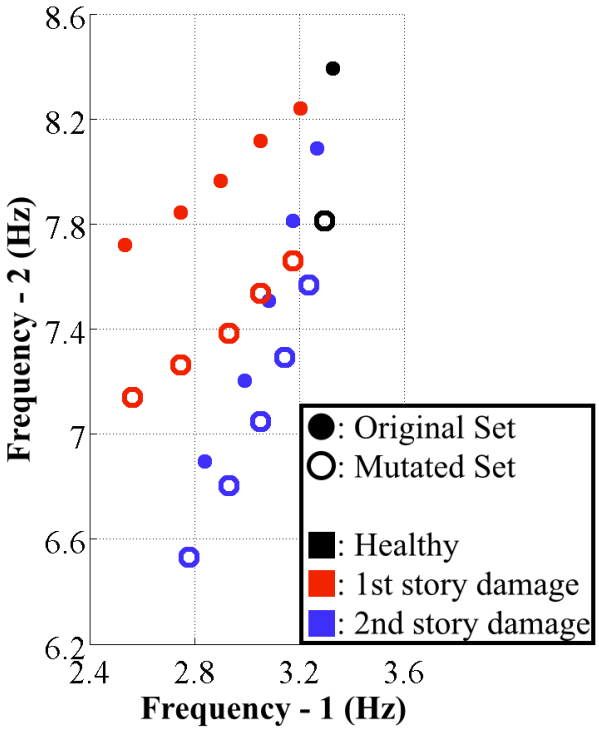

Figure 3-5: Feature space of the 2-DOF model with conventional FVs in two SPV sets.

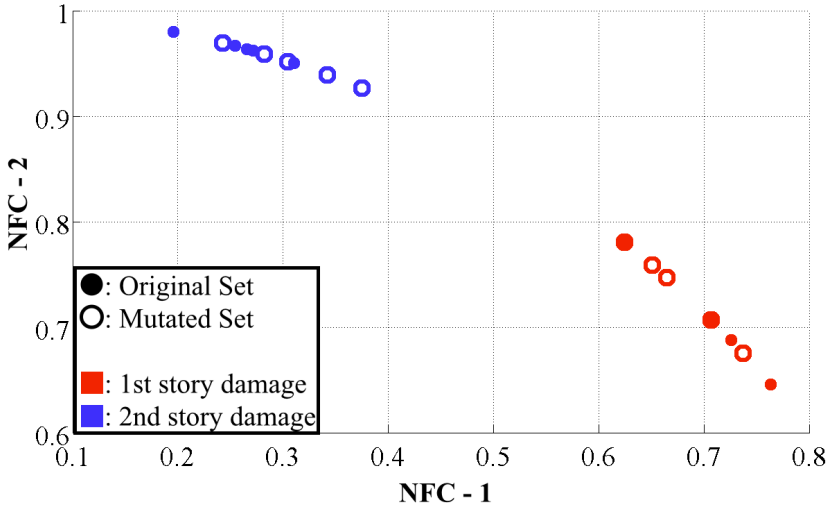

Figure 3-6: Feature space of the 2-DOF model with proposed FVs in two SPV sets.

Structure-Parameter-Value Uncertainty

Previous comparisons suggest that, the proposed FVs, which are formed by changing patterns, are more suitable for the AIS in SHM tasks than the conventional FVs, which are formed by natural frequencies directly. However, the previous comparisons are based on two specific SPV sets: the "original set" and the "mutated set" in Table 3-1. A study with more SPV sets is needed to testify that the superiority of the proposed FVs is not an exception caused by specific SPVs. Therefore, the "original set" in Table 3-1 is used as the nominal SPV set. 300 more SPV sets are generated by this nominal set with a 15% uncertainty for each value in this set (Equation (4-4) through Equation (4-6)).

With these 300 SPV sets and 11 damage conditions per SPV set (5 for each damage location and one for the "healthy"), there are 3300 new structural-damage-conditions here. Dynamic responses of the 2-DOF structure with these 3300 new conditions are simulated using the aforementioned simulation setup. Natural frequencies of the 2-DOF structure in each condition are extracted from these simulation results.

With the obtained natural frequency values, FVs are first formed by the conventional approach based on natural frequencies directly (Equation (4-3) for $n = 2$). The feature space with points representing these 3311 FVs is plotted in Figure 3-7, including the 11 ones from the nominal SPV set (the "original set" in Table 3-1).

Figure 3-7 shows that, with significant SPV difference, FVs representing "healthy" condition are overwhelmed by the ones standing for "damaged" conditions. And within the "damaged" conditions, FVs representing "1st story damage" and the ones standing for "2nd story damage" are mixed with each other. In brief, FVs from different damage conditions are not clearly recognizable, and they mix with each other when the SPV set changes.

To complete the comparison, FVs are reformed by the proposed approach based on the pattern in natural-frequency-change. The NFCs of the 2-DOF structure model under the 301 SPV sets are acquired using Equation (4-7) and FVs are constructed using Equation

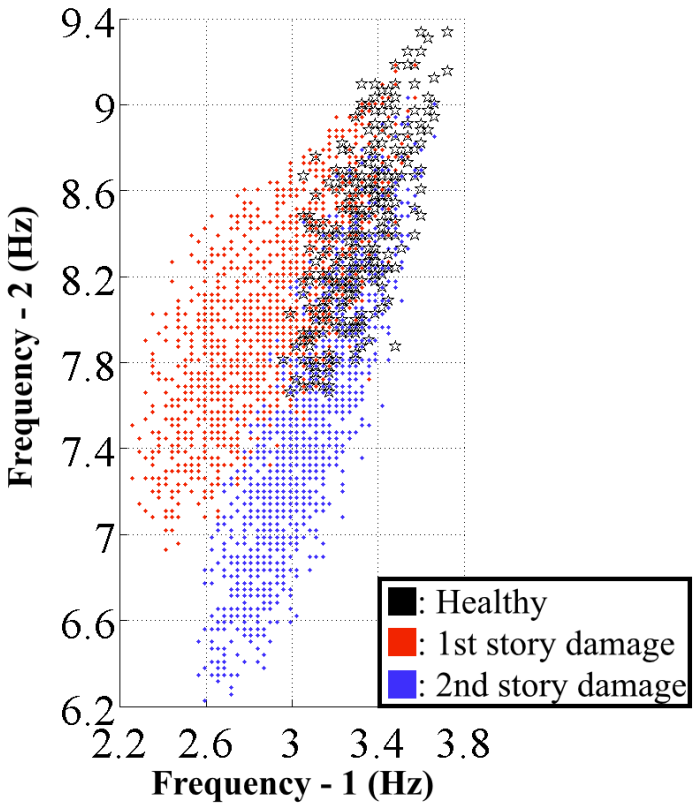

Figure 3-7: Feature space of the 2-DOF model with conventional FVs in 301 SPV sets.

(4-8). The feature space with points representing these FVs is plotted in Figure 3-8.

Figure 3-8 shows that the FVs with damage on the 1st story and the ones with damage on the 2nd story are still well separated, despite the significant difference existing in the 301 SPV sets. This good separation results in the high tolerance of AIS to the discrepancy between the training SPV and the SPV of the structure under monitoring.

The trained AIS may be employed to assess a newly-occurred unknown strucdtural-damage-condition by comparing its FV with the known memory cells obtained after training. Because of the poor separation exhibited in Figure 3-7, the AIS trained by one SPV set will not be reasonably accurate if being applied to a structure with another SPV set. In other words, the performance of a trained AIS will be deteriorated by an unacceptable extent, if there exists a significant discrepancy between the training SPVs and the SPVs of the structure in monitoring, which is unavoidable in many occasions.

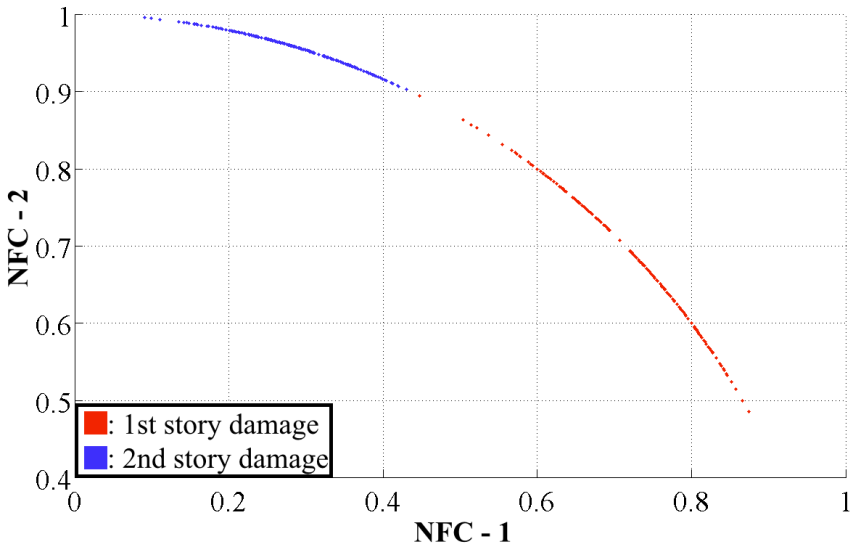

Figure 3-8: Feature space of the 2-DOF model with proposed FVs in 301 SPV sets.

Thus, the dependence of the AIS' performance on specific SPV set significantly limits its application in practical SHM tasks.

In contrast, the proposed FVs formed by the changing pattern are sensitive to the damage location but insensitive to the SPV changes, as compared to the conventional FVs formed by natural frequencies directly. This characteristic makes the proposed FVs more suitable for the damage-location-determination in SHM tasks. With FVs formed by the pattern in natural-frequency-change, the discrepancy between the training SPV and the SPV of the structure in monitoring will not significantly degrade the AIS' performance. Therefore, the proposed FVs are more applicable to the SHM tasks with practical limitations.

3.3.1.2 3-DOF Structure Model

Simulation Parameter

In this section, a more complicated structure model with more DOFs is employed: a 3-DOF structure model and its corresponding 3-DOF mass-spring-damping model. The SPV sets for this 3-DOF model are listed in Table 3-2, excluding the 300 SPV sets employed in the statistic study section.

Table 3-2: SPV sets used for the 3-DOF structural model (incomplete).

Set Name	Mass (10^5kg)			Stiffness (10^8 kg/s^2)			Damping	
	m_1	m_2	m_3	k_1	k_2	k_3	α (10^{-1}s^{-1})	β (10^{-3}s)
Original Set	2.50	2.50	1.50	3.00	2.50	2.00	2.00	1.50
Mutated Set	2.44	2.81	1.63	3.41	2.62	1.72	2.21	1.70

The values listed in Table 3-2 are selected ("original set") or calculated ("mutated set") using the same method that previously worked for the 2-DOF model and has been explained in Section 3.3.1.1. Other simulation parameters such as the calculation algorithm and the measurement sampling rate are the same with those described in Section 3.2.

Feature Vector Performance

The characteristics of the two kinds of FVs are presented and compared in this section, one of which is constructed by natural frequencies directly (conventional approach) and the other one is formed by pattern in natural-frequency-change.

In order to generate these two kinds of FVs, dynamic responses of the 3-DOF model under different conditions with the "original set" (Table 3-2) are simulated. And natural frequencies of the 3-DOF model in each damage condition are extracted from these simulated dynamic responses.

Firstly, FVs are constructed in the conventional fashion using Equation (4-3) ($n = 3$). It is worthy of attention that, the feature space involved here is a 3-dimensional (3-D) Cartesian coordinate system, because there are three natural frequencies in the 3-DOF model. The 3-D feature space with these conventional FVs is shown in Figure 3-9.

Similar with the situation in the 2-DOF model, Figure 3-9 shows that a FV moves closer to the "healthy" point when its damage severity get smaller, regardless of its damage location. This causes poor separations between FVs representing different damage locations in the adjacent area of the "healthy" point.

Besides, the separations between FVs with same damage location but different damage severities are equally obvious, if not more so, with the separations between the "healthy" point and "damaged" points. For example, the separation between the FVs of "10% damage in 3rd story" and "20% damage in 3rd story" is approximately the same distinct

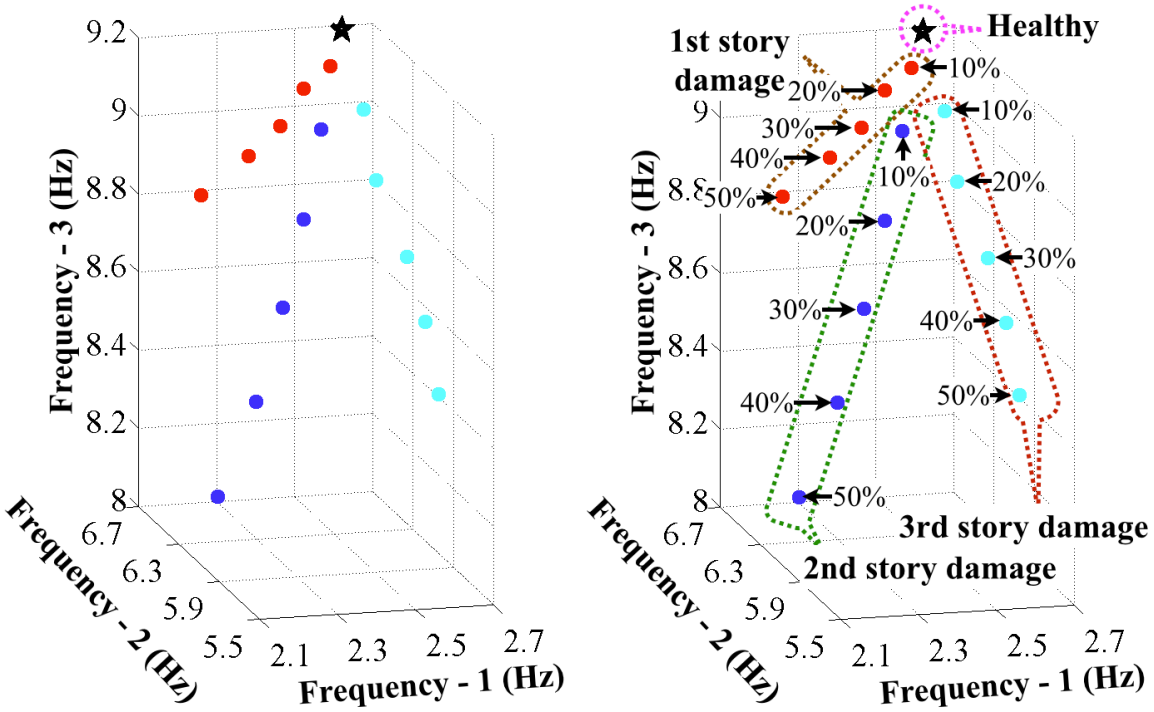

(a) (b)

Figure 3-9: Feature space of the 3-DOF model with conventional FVs in one SPV set. (a): original graph; (b): graph with annotations.

with the separation between the "healthy" point and the FV of "10% damage in 3rd story". In brief, FVs constructed from natural frequencies directly (conventional approach) exhibit poor performance in the feature space: FVs representing same damage location are not well clustered, while the separation between FVs from different damage locations are not significant.

In the other approach, NFCs are calculated using Equation (4-7) ($n = 3$), and are used to form FVs according to Equation (4-8) ($n = 3$). Because NFC stands for the normalized frequency change, which means the square sum of all entries of NFC equals one, a conversion from the 3-D Cartesian coordinate to the spherical coordinate is performed to reduce one unnecessary dimensionality. This conversion is performed using

$$\begin{cases} \theta = \tan^{-1} \dfrac{\mathrm{NFC}_2}{\mathrm{NFC}_1} \\ \varphi = \cos^{-1} \mathrm{NFC}_3 \end{cases} . \tag{4-9}$$

After this conversion, FVs are constructed in the form of

$$\mathrm{FV} = \begin{bmatrix} \theta & \varphi \end{bmatrix}^{\mathrm{T}} . \tag{4-10}$$

With Equation (4-9) and Equation (4-10), FVs of the 3-DOF model in different damage conditions with the "original set" (Table 3-2) are obtained fro simulated dynamic responses. The 2-D feature space based on the two spherical coordinates is plotted in Figure 3-10, together with FVs formed in the proposed approach.

It is evident from the comparison between Figure 3-9 and Figure 3-10 that, the proposed FVs representing different damage locations are better separated in the feature space, and the ones standing for the same damage location are better clustered. As explained earlier, this characteristic of the proposed FVs is beneficial to the AIS in the damage-location-determination of SHM tasks.

Structure-Parameter-Value Variation

As explained earlier, SPV changes cause the changes in the natural frequencies, which further results in the changes in the FVs. The FVs constructed in the conventional approach are especially susceptible to the SPV changes, and therefore have limited

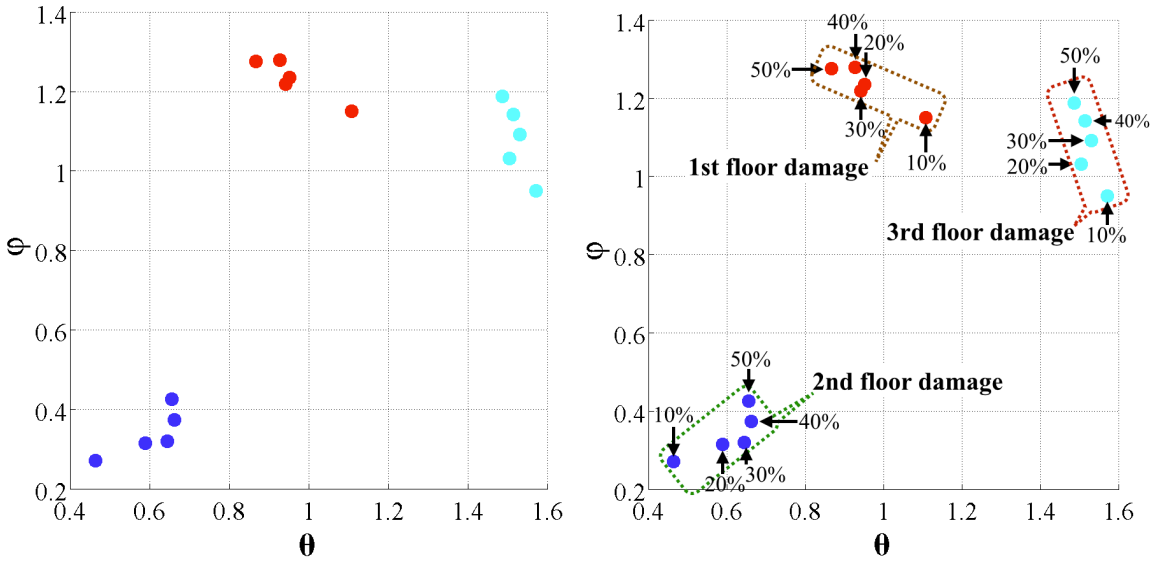

(a) (b)

Figure 3-10: Feature space of the 3-DOF model with proposed FVs in one SPV set. (a): original graph; (b): graph with annotations.

applications in real world SHM scenarios.

To compare the effects of the SPV change on the conventional FVs and the proposed FVs, two SPV sets ("original set" and "mutated set" in Table 3-2) are employed. Natural frequencies of the 3-DOF structure models under these two SPV sets are acquired from simulated dynamic responses.

The conventional FVs are formed according to Equation (4-3). The feature space with points representing these FVs is plotted in Figure 3-11, where lines are drawn between points representing the same damage location in order to make the architecture clearer. Similar with the situation in the 2-DOF structure model, FVs representing different damage locations from different SPV sets mix with each other in Figure 3-11.

On the other hand, the proposed FVs are formed by the NFCs using Equation (4-7), Equation (4-9), and Equation (4-10). The two SPV sets ("original set" and "mutated set" in Table 3-2) are considered. The feature space with FVs from these two SPV sets is plotted in Figure 3-12.

It can be seen in Figure 3-12 that, Regardless of the significant difference existing between the two SPV sets, the FVs representing different damage locations are still well separated, while at the same time the FVs from the same damage location still tend to occupy the same area in the feature space.

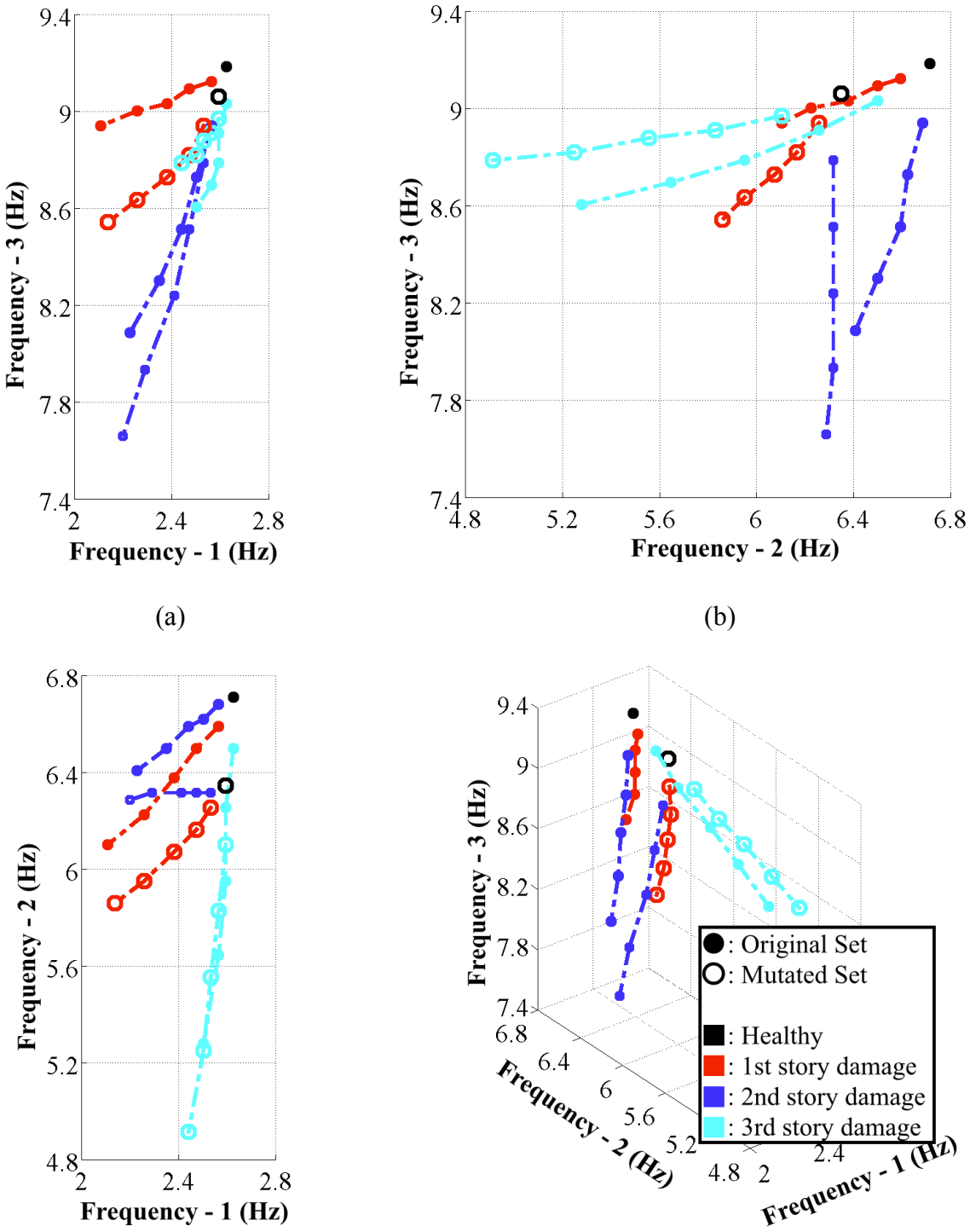

Figure 3-11: Feature space of the 3-DOF model with conventional FVs in two SPV sets. (a), (b) and (c) are three orthographic views of the graph in (d).

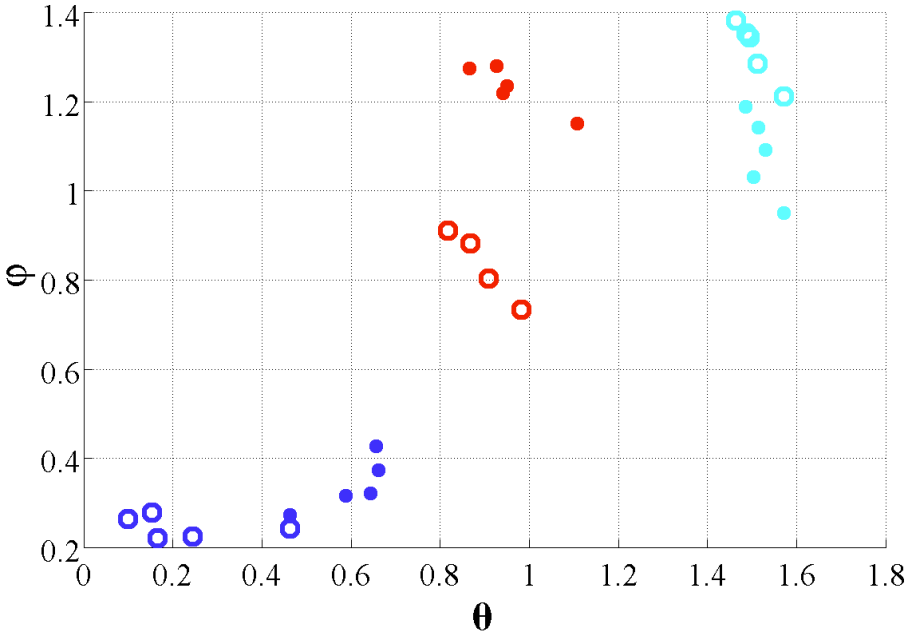

(a)

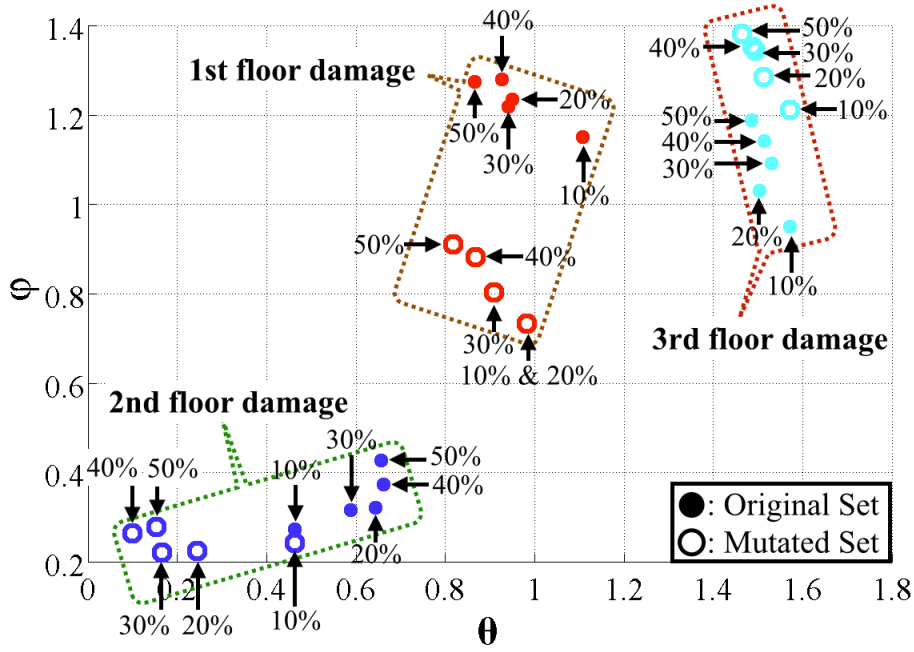

(b)

Figure 3-12: Feature space of the 3-DOF model with proposed FVs in two SPV sets. (a): original graph; (b): graph with annotations.

Structure-Parameter-Value Uncertainty

Previous comparisons suggest that, the proposed FVs (formed by changing patterns) are more suitable for the AIS in SHM tasks than the conventional FVs (formed by natural frequencies directly). However, the previous comparisons are based on two specific SPV sets: the "original set" and the "mutated set" in Table 3-2. A study with more SPV sets is needed to testify that the superiority of the proposed FVs is not an exception caused by specific SPVs. Thus, the "original set" in Table 3-2 is used as the nominal SPV set. 300 more SPV sets are calculated by this nominal set with a 15% uncertainty for each value in this set (Equation (4-4) through Equation (4-6)).

With these 300 SPV sets and 16 damage conditions per SPV set, 4800 new structural-damage-conditions are simulated here, with the previously described simulation setup. Natural frequencies of the 3-DOF structure in each condition are extracted from these simulation results.

The conventional FVs with these 301 SPV sets (including the nominal set) are formed using Equation (4-3) ($n = 3$). The feature space with points representing these 4816 FVs is plotted in Figure 3-13, where lines are drawn between points from the same damage location to make the architecture clearer.

Figure 3-13 clearly shows that, FVs representing the "healthy" conditions are overwhelmed by other FVs, and FVs representing different damage locations mix with each other, when multiple different (but similar) SPV sets are considered.

If the proposed approach is employed to construct FVs, the NFCs of the 3-DOF structure model in different damage conditions with these 301 SPV sets are acquired using Equation (4-7), and used to form FVs according to Equation (4-9) and Equation (4-10). The feature space with points representing these FVs is plotted in Figure 3-14.

The difference between Figure 3-13 and Figure 3-14 is apparent: In Figure 3-14, FVs representing different damage locations are better separated, while FVs representing the same damage location are better clustered. In other words, the performance of the proposed FVs (Figure 3-14) is more suitable for the AIS in SHM tasks, comparing with the conventional FVs (Figure 3-13).

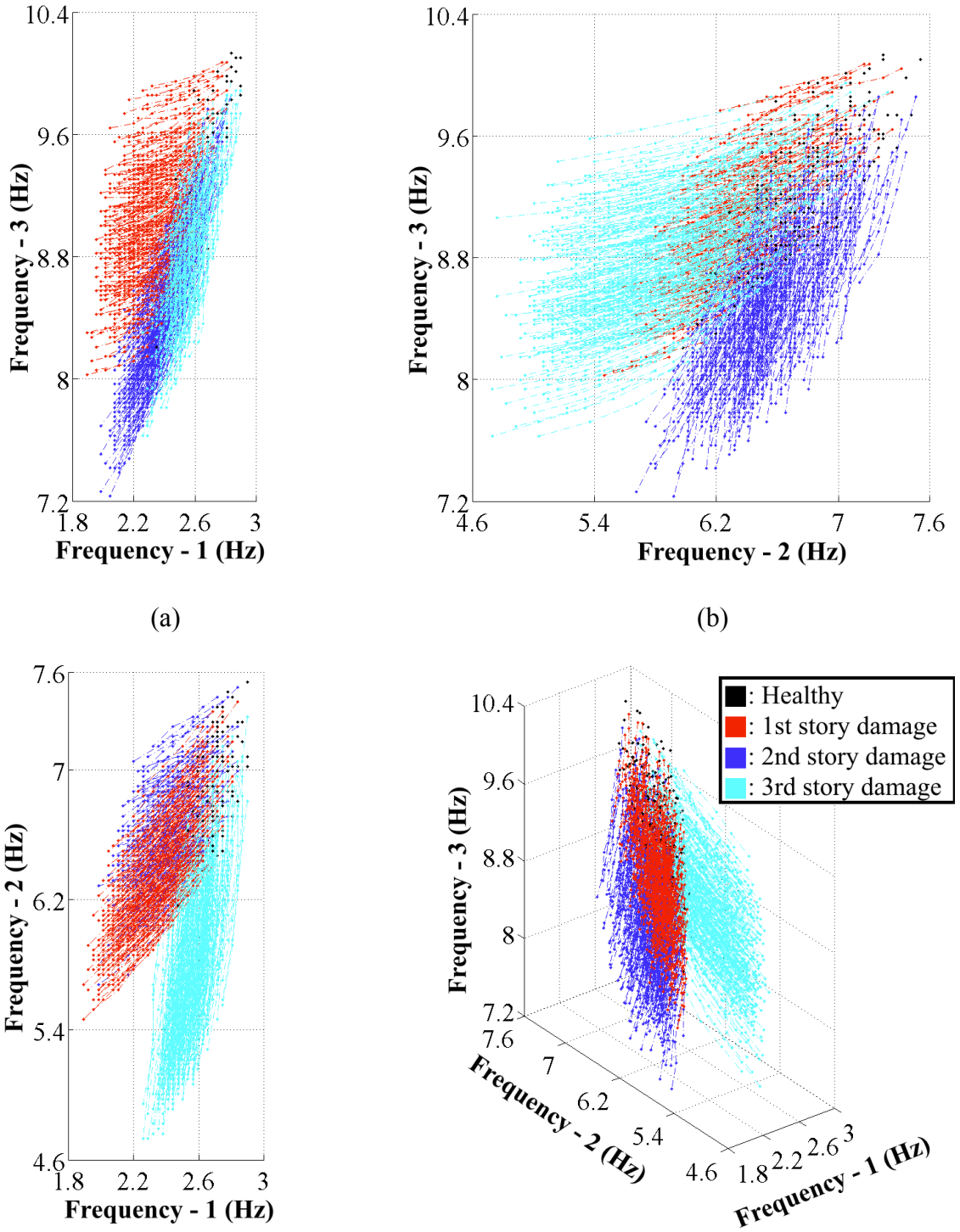

Figure 3-13: Feature space of the 3-DOF model with conventional FVs in 301 SPV sets. (a), (b) and (c) are three orthographic views of the graph in (d).

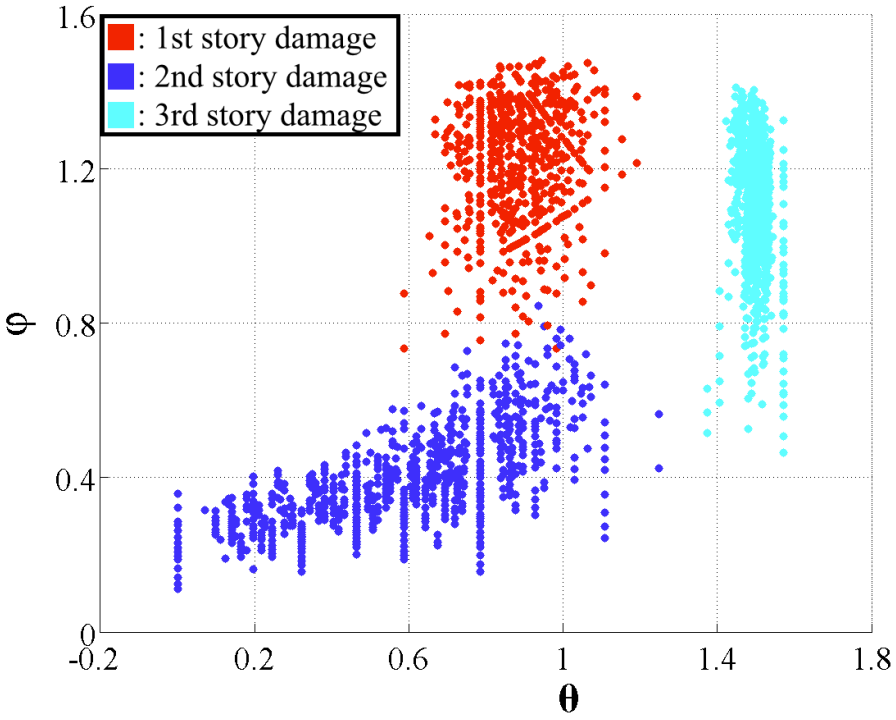

Figure 3-14: Feature space of the 3-DOF model with proposed FVs in 301 SPV sets.

3.3.1.3 4-DOF Structure Model

Simulation Parameter

In this part, the 4-DOF structure model and its corresponding 4-DOF mass-spring-damping model are employed for simulations. The SPV sets used for this model are partially listed in Table 3-3.

Table 3-3: SPV sets used for the 4-DOF structural model (incomplete).

Set Name	Mass (10^5kg)				Stiffness (10^8 kg/s^2)				Damping	
	m_1	m_2	m_3	m_4	k_1	k_2	k_3	k_4	α (10^{-1}s^{-1})	β (10^{-3}s)
Original Set	2.50	2.50	2.50	1.50	3.00	2.50	2.50	2.00	2.00	1.50
Mutated Set	2.74	2.80	2.22	1.69	3.12	2.20	2.33	2.03	2.28	1.71

The values listed in Table 3-3 is selected or calculated in the same way with the SPV for the 2-DOF structure model, which has been explained in Section 3.3.1.1. Other simulation parameters such as the calculation algorithm and the measurement sampling rate have already been described in Section 3.2.

The 4-DOF mass-spring-damping model has four distinct natural frequencies. In many real-world problems, the structural response is dominated by its low-frequency contents. Thus, the higher the natural frequency is, the more difficult or expensive it is to be measured accurately. As a result practical or cost issues, the full frequency spectrum of a structure with multiple (four or more) natural frequencies is often unavailable.

In order to improve the applicability of the proposed method, and also to guarantee the realistic significance of the discussion, the incomplete frequency spectrum is simulated by only considering the three lower frequencies of the 4-DOF structure. The 4^{th} natural frequency (also the highest frequency), is assumed to be unable to measure. Therefore it should be noted that, the discussion here is based on incomplete natural frequency information, which is different with the discussions in previous sections.

Feature Vector Performance

Natural frequencies are extracted from simulated dynamic responses of the 4-DOF structure model in different structural-damage-conditions with the "original set" in Table

3-3. The first three natural frequencies are kept and used to build FVs, while the last (also the highest) natural frequency is discarded in further discussions.

First, FVs are formed in the conventional approach using natural frequencies directly. Only the three lower natural frequencies are used to form FVs according to Equation (4-3) ($n = 3$). The feature space with points representing these FVs is plotted in Figure 3-15.

In Figure 3-15 (b), the damage severities of FVs are not annotated due to the space limitation. For FVs standing for the same damage location (points with the same color),

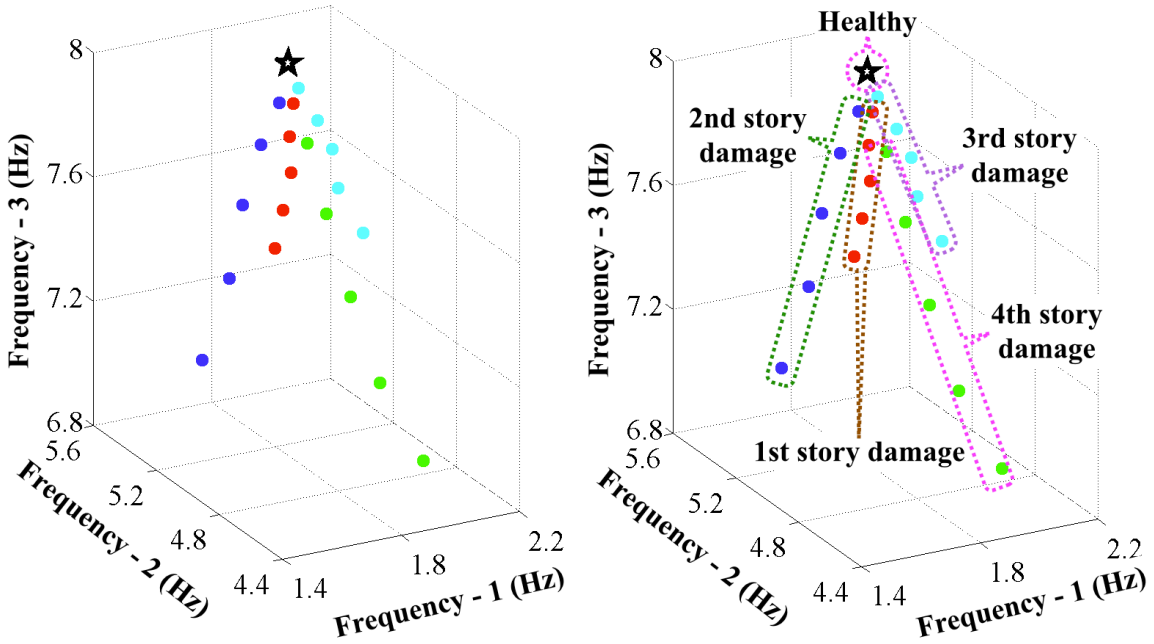

(a) (b)

Figure 3-15: Feature space of the 4-DOF model with conventional FVs in one SPV set. (a): original graph; (b): graph with annotations.

their damage severities change from 10% to 50% at an interval of 10%, with the increase in their distances to the "healthy" point in the feature space.

The situation in Figure 3-15 is similar with the situations in the 2-DOF and 3-DOF structure models: FVs representing different damage locations are not well separated, while FVs from the same damage location are not well clustered.

In the proposed approach, the NFCs of the three lower natural frequencies are calculated using Equation (4-7). FVs are formed using these calculated NFCs according to Equation (4-9) and Equation (4-10). Because only three natural frequencies are considered, the conversion from the Cartesian coordinate to the spherical coordinate is still performed to reduce unnecessary dimensionality. The feature space with points representing these FVs is plotted in Figure 3-16.

Figure 3-16 show similar situations with FVs in the 2-DOF and 3-DOF structure models, even though the frequency spectrum is incomplete (only the three lower natural frequencies are considered) in this case. The FVs formed by the changing pattern exhibit superior characteristics in the feature space: FVs from different damage locations are better separated, and FVs from the same damage location are better clustered, comparing with the FVs constructed by natural frequencies directly.

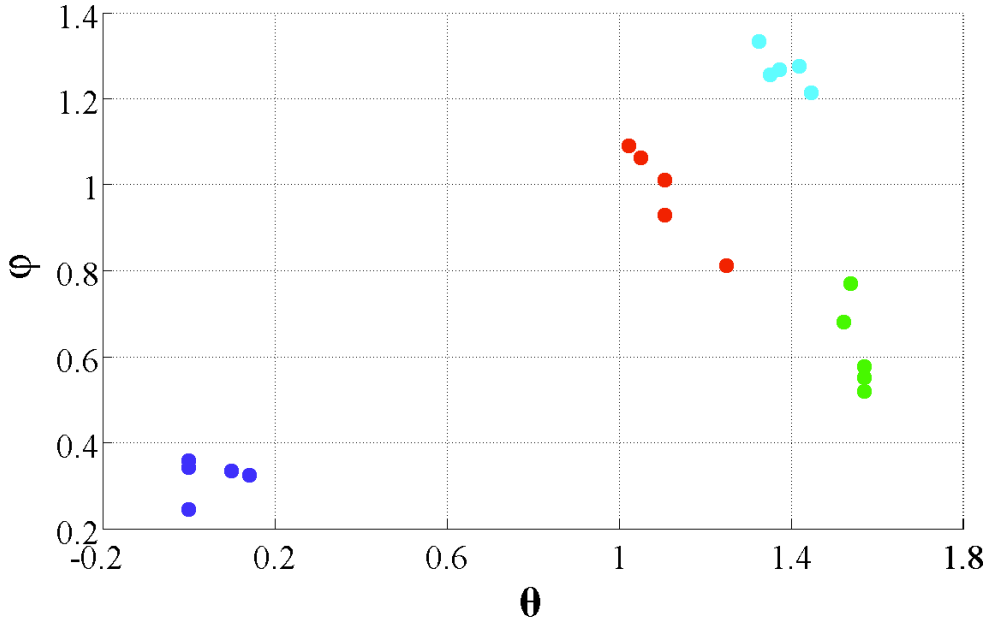

(a)

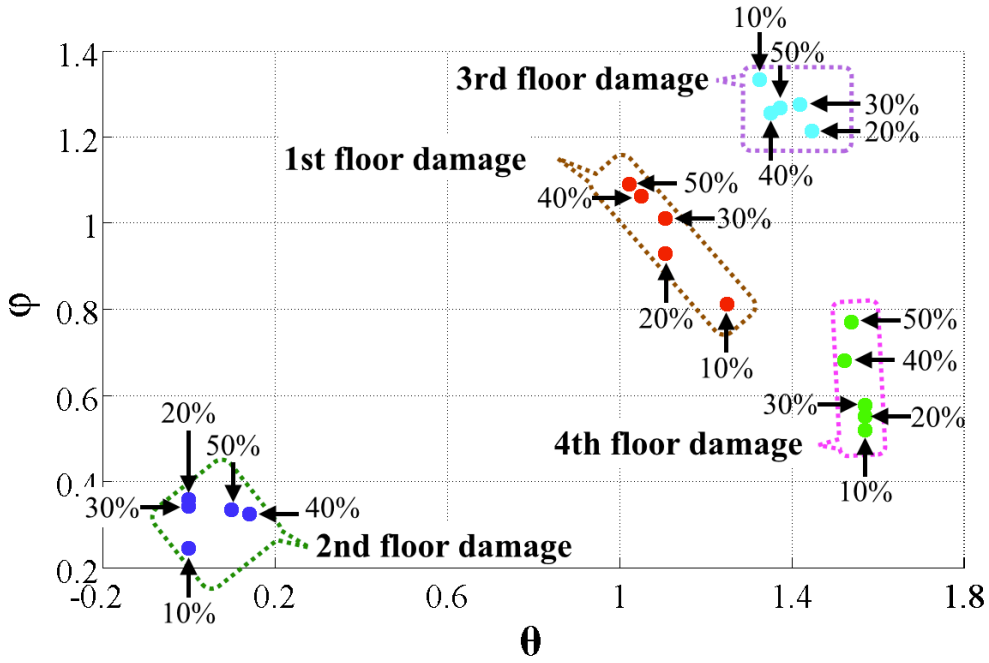

(b)

Figure 3-16: Feature space of the 4-DOF model with proposed feature in one SPV set. (a): original graph; (b): graph with annotations.

Structure-Parameter-Value Variation

As explained earlier, natural frequencies of a structure change correspondingly with its SPV. To compare the effects of SPV change on the two kinds of FVs, the natural frequencies of the 4-DOF structure model under two SPV sets ("original set" and "mutated set" in Table 3-3) are acquired.

The conventional FVs are formed according to Equation (4-3). The feature space with points representing these FVs is plotted in Figure 3-17. In Figure 3-17, lines are drawn between points representing the same damage location in order to make the architecture clearer.

Alternatively, the NFCs of the 4-DOF structure models under two SPV sets ("original set" and "mutated set" in Table 3-3) are acquired and used to form FVs according to Equation (4-7), Equation (4-9), and Equation (4-10). The feature space with points representing these FVs is plotted in Figure 3-18.

Figure 3-17 and Figure 3-18 clearly show that, the proposed FVs have better performance compared with the ones formed by natural frequencies: They are better separated when the damage locations are different, and are better clustered when the damage locations are the same. Besides, FVs representing the same damage locations with different SPV sets still occupy adjacent positions in the feature space (Figure 3-18), which indicates that the FVs formed by changing patterns are less sensitive to the SPV difference.

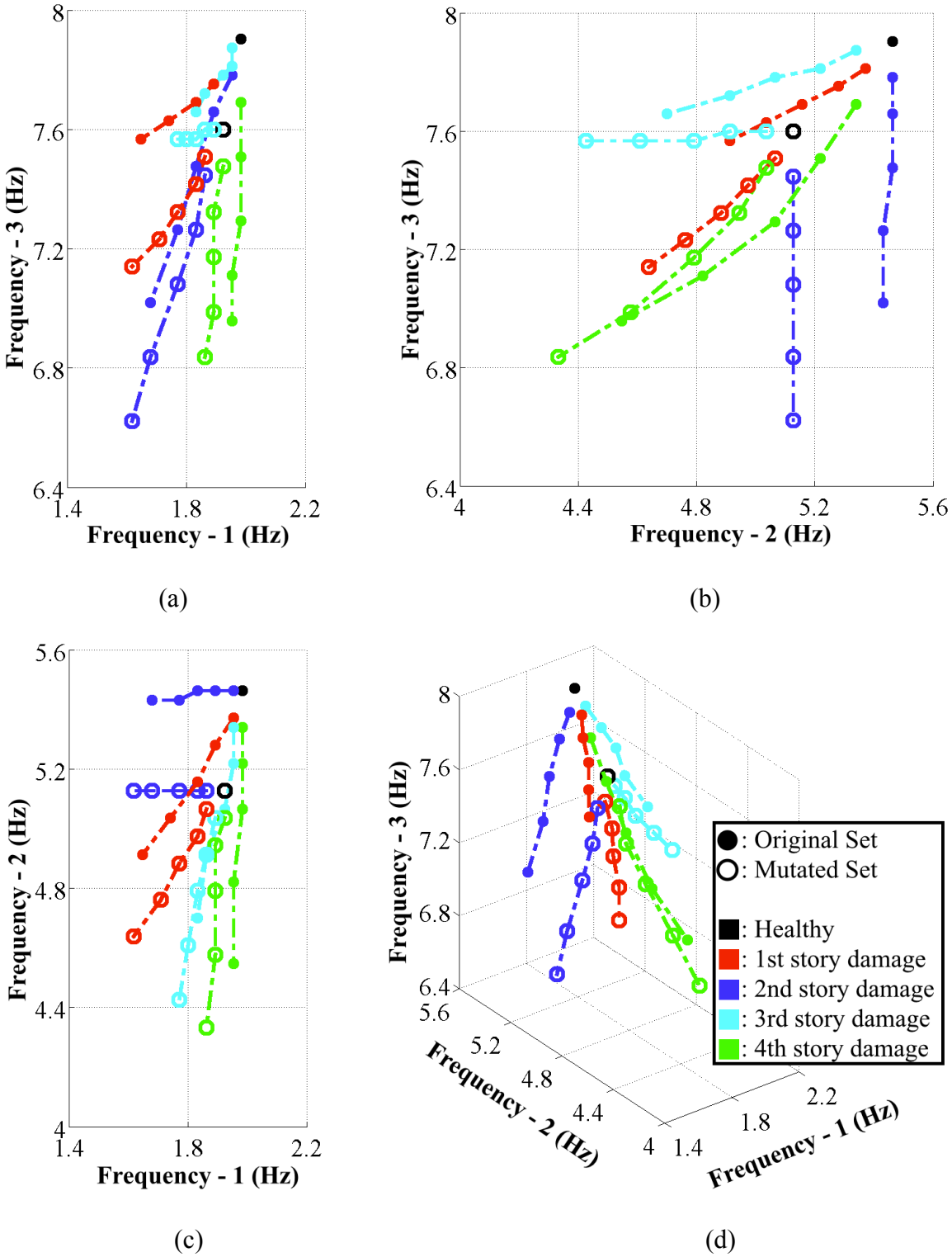

Figure 3-17: Feature space of the 4-DOF model with proposed FVs in two SPV sets. (a), (b) and (c) are three orthographic views of the graph in (d).

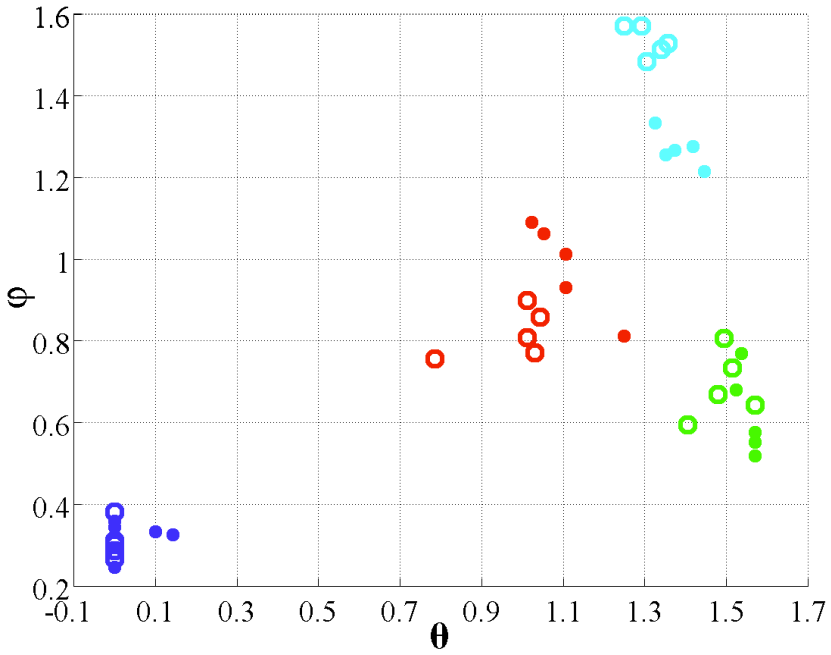

(a)

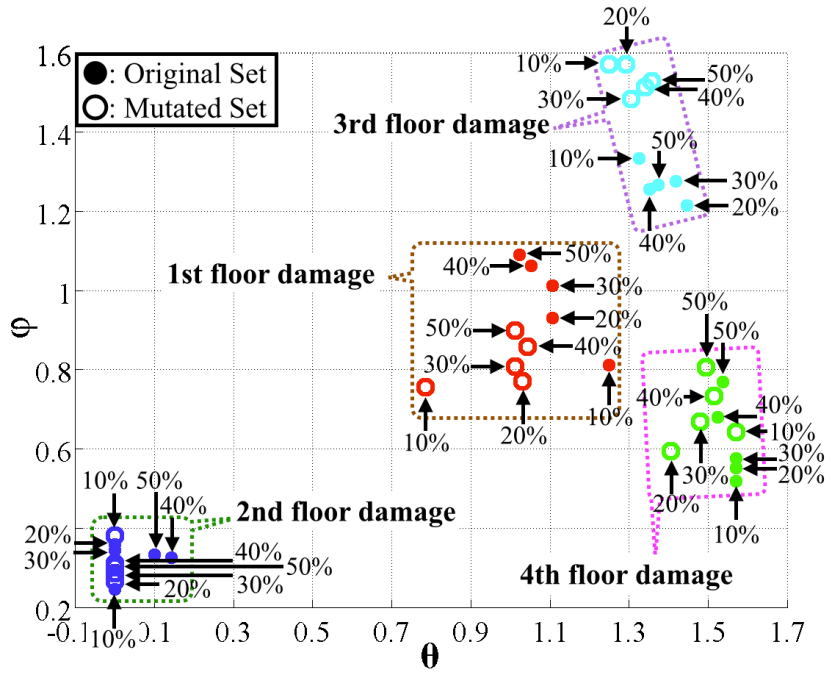

(b)

Figure 3-18: Feature space of the 4-DOF model with proposed FVs in two SPV sets. (a): original graph; (b): graph with annotations.

Structure-Parameter-Value Uncertainty

Previous comparisons suggest that, the proposed FVs (formed by changing patterns) are more suitable for the AIS in SHM tasks than the conventional FVs (formed by natural frequencies directly). Nevertheless, the previous comparisons are based on two specific SPV sets: the "original set" and the "mutated set" in Table 3-3. A study with more SPV sets is needed to testify that the advantage of the proposed FVs is not an exception caused by specific SPVs. Thus, the "original set" in Table 3-3 is considered to be the nominal SPV set. 300 more SPV sets are generated by this nominal set with a 15% uncertainty for each value in this set (Equation (4-4) through Equation (4-6)).

With these 300 SPV sets and 21 damage conditions per SPV set, there are 6300 new structural-damage-conditions here. Dynamic responses of the 4-DOF structure with these 6300 new conditions are simulated using aforementioned simulation setup. The three lower natural frequencies of the 4-DOF structure in each condition are extracted from these simulations. The conventional FVs are formed using Equation (4-3) ($n = 3$). The feature space with points representing these 6321 FVs is plotted in Figure 3-19, including the 21 ones from the nominal SPV set (the "original set" in Table 3-3).

On the other hand, the NFCs of the 4-DOF structure model under all 301 SPV sets, including the "original set", are acquired and used to form FVs in the proposed approach (Equation (4-7), Equation (4-9), and Equation (4-10)). Points representing these FVs are plotted in the feature space and shown in Figure 3-20.

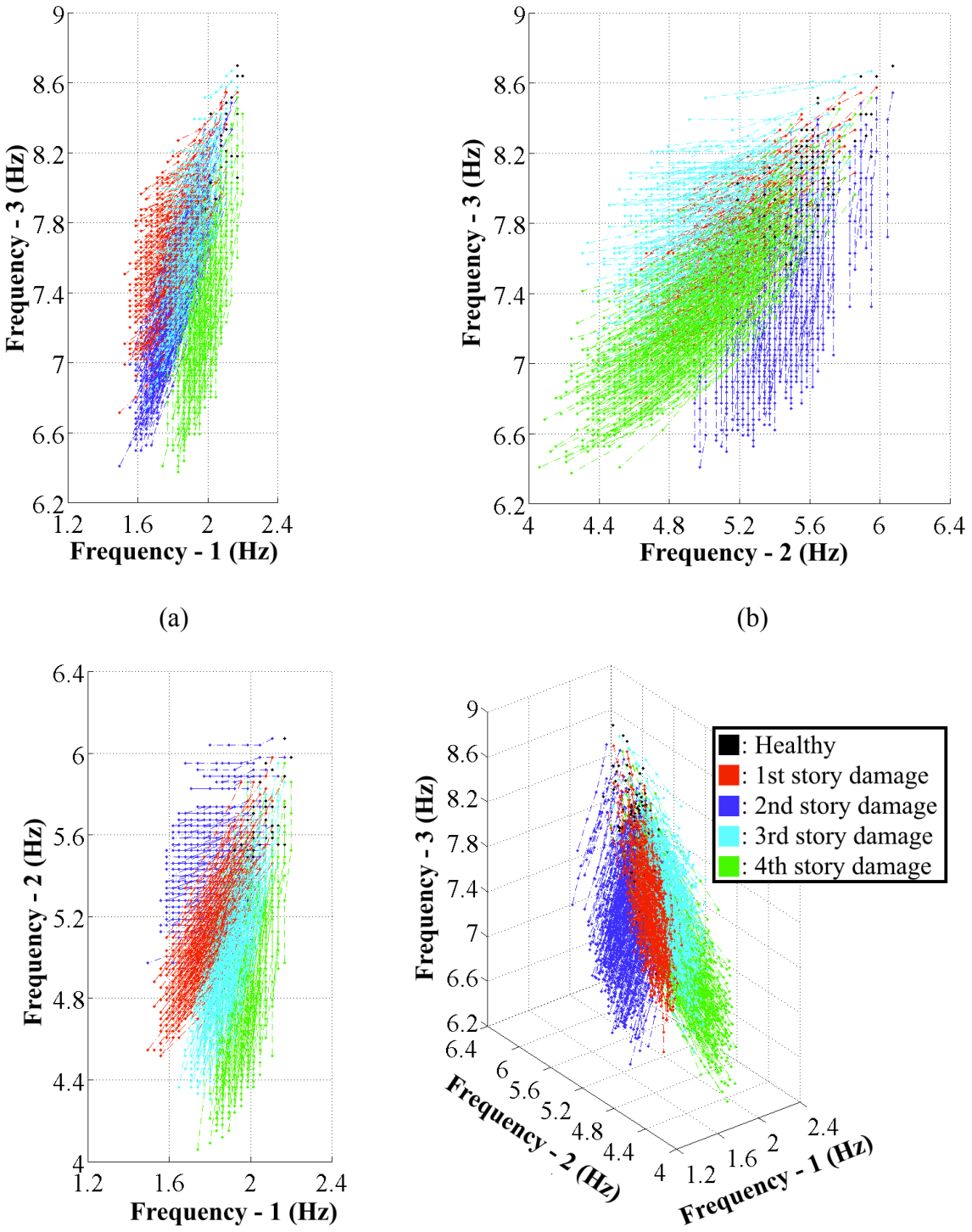

Figure 3-19: Feature space of the 4-DOF model with conventional FVs in 301 SPV sets. (a), (b) and (c) are three orthographic views of the graph in (d).

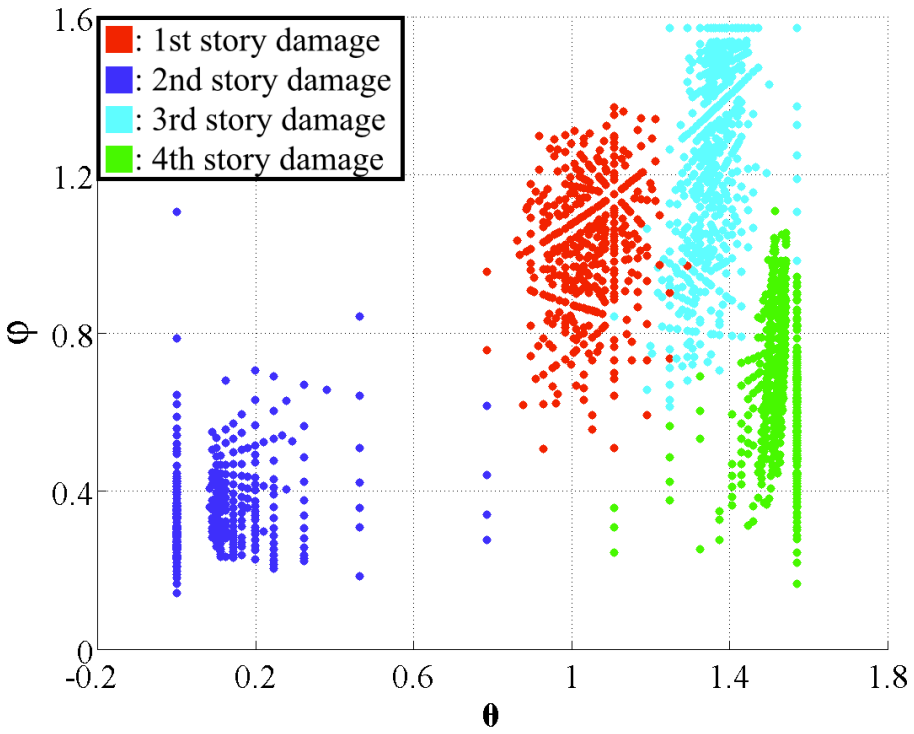

Figure 3-20: Feature space of the 4-DOF model with proposed FVs in 301 SPV sets.

Figure 3-19 and Figure 3-20 clearly show that the FVs formed by changing patterns are better clustered when damage locations are the same, and better separated when damage locations are different, even though only the lower three frequencies are considered.

Results in this section conform that the proposed approach of building FVs is more suitable for the AIS in SHM tasks compared with the conventional one, because the FVs based on changing patterns are less dependent on SPV and more sensitive to damage location.

3.3.1.4 Review

In this part, natural frequencies are used as the damage-sensitive-variable, based on which the feature vectors (FVs) are constructed. Comparisons are presented between the FVs formed by natural frequencies directly and the FVs built by changing patterns. Three different structure models with 2-, 3- and 4-DOF are employed in simulations, together with their corresponding 2-, 3- and 4-DOF mass-spring-damping mathematic models.

The proposed FVs, which are formed by the changing pattern, exhibits more desirable characteristics than the conventional FVs: They are better clustered in the feature space when representing the same damage location, and are better separated when standing for different damage locations.

The effect of SPV changes on the two kinds of FVs are also investigated and compared, using two SPV sets (the "original set" and the "mutated set" in corresponding tables). Results suggest that the proposed FVs are less dependent on SPV and more tolerant to SPV changes. This characteristic is suitable for the AIS in SHM tasks, because the discrepancy between the training SPV and the SPV of the structure under monitoring always exists in practical SHM scenarios.

To further support the conclusions acquired and eliminate the effect of specific SPV on these conclusions, 300 different SPV sets are generated by the "original" set with random

deviations, which are within a 15% range around the corresponding values in the "original set".

Results from the 2-, 3- and 4-DOF structure models and the 301 SPV sets are consistent: The proposed FVs (formed by the changing pattern) have superior performance compared with the conventional FVs (formed by natural frequencies directly). This better performance is reflected in two aspects: First, the proposed FVs are better clustered in the feature space when representing the same damage location, and are better separated when standing for different damage locations. Second, the proposed FVs are less dependent on SPV. In other words, they still occupy similar positions in the feature space even with different SPV sets.

On the other hand, FVs formed by natural frequencies exhibit less satisfactory performance. They mix with each other in the feature space regardless of different damage locations, when the damage severity is small. And their positions in the feature space are highly dependent on the SPV sets they are in. FVs representing different damage locations interfere with each other when they are in different SPV sets.

AIS recognizes unknown antigens based on the characteristics of their FVs. Therefore, the FVs formed by the changing patterns are more suitable for the AIS in the damage location determination of SHM tasks.

3.3.2 Mode Shape Information and Pattern in Mode Shape Change

As another modal parameter besides the natural frequency, the mode shape changes correspondingly with the variation in structural properties. Similar with the natural frequency, the mode shape has also been employed as the damage-sensitive-variable in many vibration-based SHM methodologies (Doebling, et al. 1996). Some researches have suggested that the mode shape is as sensitive, if not more, as the natural frequency to the damage in structures (Srinivasan and Kot 1992).

The mode shape information can be expressed in a matrix as follows

$$\begin{bmatrix} a_{11} & a_{12} & \cdots & a_{1m} \\ a_{21} & a_{22} & \cdots & a_{2m} \\ \vdots & \vdots & \ddots & \vdots \\ a_{n1} & a_{n2} & \cdots & a_{nm} \end{bmatrix}$$

where a_{ij} stands for the amplitude of the j-th natural frequency on the i-th story. m is the number of modes considered and n is the number of structural stories. The conventional definition of the mode shape refers to column vector of this matrix, as indicated by

$$\begin{bmatrix} \boxed{a_{11}} & \boxed{a_{12}} & \cdots & a_{1m} \\ \boxed{a_{21}} & \boxed{a_{22}} & \cdots & a_{2m} \\ \boxed{\vdots} & \boxed{\vdots} & \ddots & \vdots \\ \boxed{a_{n1}} & \boxed{a_{n2}} & \cdots & a_{nm} \end{bmatrix}.$$

One column vector contains the amplitudes of one natural frequency on every structural story. This definition requires the sensors to be mounted on every structural story in order to measure the mode shape information. In order to relax this demanding system

requirement, another approach is employed in this thesis to extract the mode shape information. The row vectors of the mode matrix are taken as illustrated by

$$\begin{bmatrix} \boxed{a_{11} \quad a_{12} \quad \cdots \quad a_{1m}} \\ \boxed{a_{21} \quad a_{22} \quad \cdots \quad a_{2m}} \\ \vdots \quad \vdots \quad \ddots \quad \vdots \\ \boxed{a_{n1} \quad a_{n2} \quad \cdots \quad a_{nm}} \end{bmatrix}.$$

Using this approach, the data required are the amplitudes of different natural frequencies on the same structural story. Namely, the measurement data from the sensors on one single structural story is enough to build the row vector.

The values in the mode matrix are affected by the initial condition and the external excitation. But after an appropriate normalization, both the column vector and the row vector are uniquely decided by the structural properties, and are theoretically irrelevant to the initial condition or the external excitation. Therefore, these two kinds of vectors are both suitable to work as the damage-sensitive-variable. With an attempt to minimize the requirement of the proposed methodology, the row vector is used in this thesis as the representation of the mode shape information. Therefore it is noteworthy that, the mode shape information here has a different meaning with its conventional definition. Also, considering the convenience in practical SHM systems, data of the 1st story displacement is employed to extract this mode shape information.

Same as in the previous parts, two kinds of FVs are presented here: The conventional FVs are formed using the mode shape information directly, while the proposed FVs are derived from the pattern in the mode-shape-change.

To begin with, the conventional FVs are constructed from the mode shape information directly. The normalization process is performed by dividing every entry in the row vector with the first entry. After the normalization, the format of FVs becomes

$$\mathrm{FV} = \left[\begin{array}{ccccc} 1 & \frac{a_{12}}{a_{11}} & \frac{a_{13}}{a_{11}} & \cdots & \frac{a_{1m}}{a_{11}} \end{array} \right]^{\mathrm{T}} \tag{4-11}$$

where a_{1i} is the amplitude of the i-th natural frequency (arranged from the lowest to the highest) on the 1st story, and m is the number of mode shapes considered.

3.3.2.1 2-DOF Structure Model

Simulation Parameter

The 2-DOF structure model, the SPV sets, and all the simulation parameters used in this part is the same as those in Section 3.3.1.1. The difference between this part and Section 3.3.1.1 is that, the values extracted from the simulated dynamic responses here are the y-coordinates (amplitude values) of the peaks in the frequency spectrum, while in Section 3.3.1.1 the x-coordinates (frequency values) of the peaks are considered.

Feature Vector Performance

Dynamic responses of the 2-DOF structure model in different damage conditions with the "original set" of in Table 3-1 are obtained through simulations, from which the mode shape information for each damage condition is extracted.

For the conventional FVs, Equation (4-11) ($m = 2$) is applied to generate the FV for each damage condition based on the mode shape information directly. The feature space with these 11 FVs is shown in Figure 3-21, 5 of which are for each damage location and another one for the "healthy" condition. In the figure, x stands for the first entry of the FV vector and y means the second entry (Equation (4-11)).

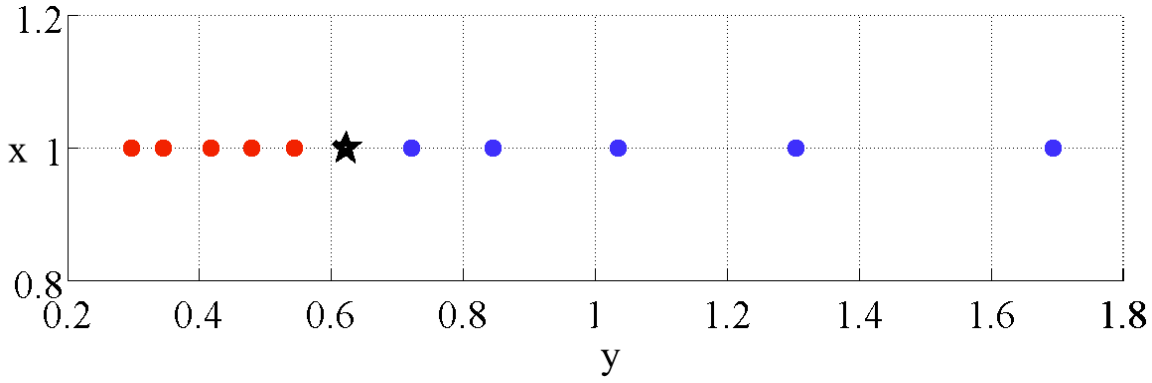

(a)

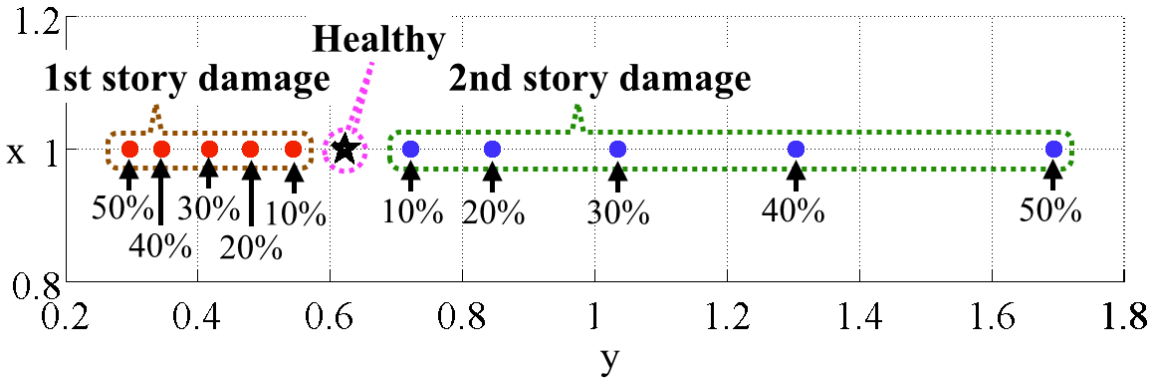

(b)

Figure 3-21: Feature space of the 2-DOF model with conventional FVs in one SPV set. The positions of x and y axes are exchanged. (a): Original graph; (b): Graph with annotations.

As suggested by Figure 3-21, points from different damage locations are distributed on different sides of the "healthy" point. But the points representing the same damage location are not well clustered in the feature space. For instance, there exists an obvious distance between the point of "40% damage on the 2nd story" and the point of "50% damage on the 2nd story". Besides, the points corresponding to small damage severities are much closer to the "healthy" point than the points representing bigger severities.

In other words, the FVs representing the same damage location are not well clustered. And the FVs representing different damage locations are not well separated. This poses significant challenge for the AIS to determine the correct damage location of an unknown condition based on the position of its FV in the feature space.

The positive information revealed by Figure 3-21 is that, the points representing different damage locations are on the different sides of the "healthy" point: The points corresponding to the "1st story damage" lie on the left side, while the points from the "2nd story damage" are on the right side.

The shape formed by FVs in Figure 3-21 has similar characteristic with the shape in Figure 3-2: If a vector is drawn from the "healthy" point to a "damaged" point, its direction and magnitude are decided by the damage severity and location of the damage condition represented by this "damaged" point, respectively.

The vectors drawn from the "healthy" point to "damaged" points are named as the modal-shape-change (MSC) in this thesis and their coordinates in the feature space are

$$\mathrm{MSC} = \left[\begin{array}{ccccc} 0 & \dfrac{a_{12,\,\mathrm{damage}}}{a_{11,\,\mathrm{damage}}} - \dfrac{a_{12,\,\mathrm{healthy}}}{a_{11,\,\mathrm{healthy}}} & \cdots & \dfrac{a_{1\mathrm{m},\,\mathrm{damage}}}{a_{11,\,\mathrm{damage}}} - \dfrac{a_{1\mathrm{m},\,\mathrm{healthy}}}{a_{11,\,\mathrm{healthy}}} \end{array} \right]^{\mathrm{T}} \tag{4-12}$$

where m is the number of mode shapes considered.

In order to make the FV representing the same damage location better clustered, the MSCs are normalized to make the square sum of all the entries of a vector equals to one. The vector after this normalization is referred to as the normalized-modal-shape-change (NMSC) in following parts and is defined as

$$\mathrm{NMSC} = \left[\begin{array}{ccccc} \dfrac{\mathrm{msc}_1}{S} & \dfrac{\mathrm{msc}_2}{S} & \cdots & \dfrac{\mathrm{msc}_m}{S} \end{array} \right]^{\mathrm{T}} \tag{4-13}$$

where

$$S = \sqrt{\mathrm{msc}_1^2 + \mathrm{msc}_2^2 + \cdots + \mathrm{msc}_m^2}$$

where msc_i is the i-th entry of the MSC vector (Equation (4-12)).

Values of the NMSCs are a proper representation of pattern in mode-shape-change. Therefore, they are proposed to be used as FVs for the AIS in SHM tasks. With Equation (4-12) and Equation (4-13), FVs of the 2-DOF structure model in all damage conditions with the "original set" in in Table 3-1 are calculated. The feature space with these FVs is plotted in Figure 3-22.

Figure 3-22 shows an impressive result: All the five FVs representing the same damage location cluster at the same position in the feature space, which results from the normalization process described by Equation (4-13). This distinct difference between FVs from different damage locations makes it easier for the AIS to determine the correct damage location of an unknown damage condition, based on the position of its FV in the feature space.

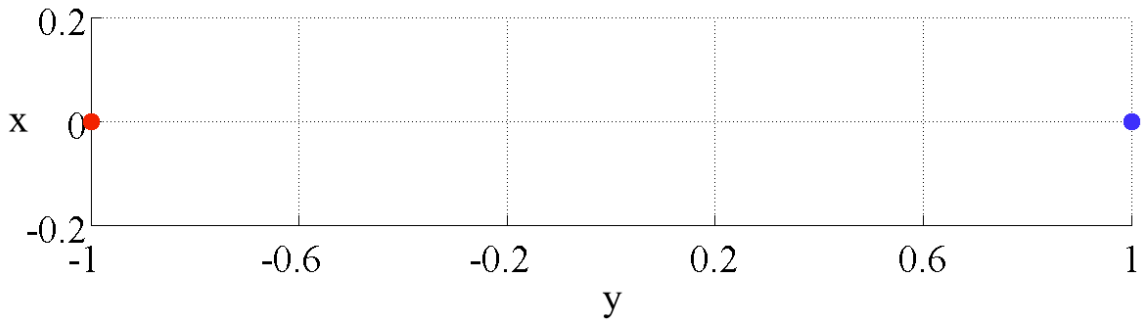

(a)

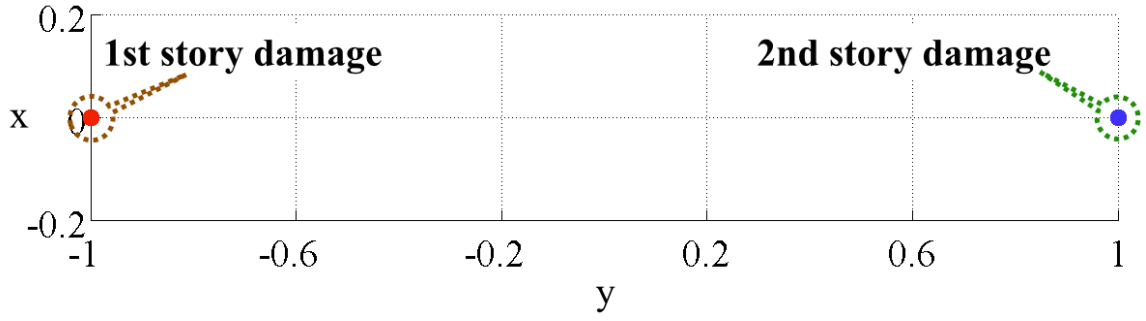

(b)

Figure 3-22: Feature space of the 2-DOF model with proposed FVs in one SPV set. The positions of x and y axes are exchanged. (a): Original graph; (b): Graph with annotations.

Structure-Parameter-Value Variation

Similar with natural frequencies, mode shapes are also dependent on the SPVs. FVs formed by the mode shape information change correspondingly when the SPV changes, which results in the AIS' low tolerance to the discrepancy between the training SPV and the SPV of the structure under monitoring. The proposed FV is less susceptible to the effect of the SPV change, and is therefore better suited for the AIS in SHM tasks. To explore the effect of the SPV change on the two kinds of FVs, the "original set" and "mutated set" in in Table 3-1 are employed for simulations.

FVs are first constructed using the conventional approach with Equation (4-11). The feature space with these FVs is plotted in Figure 3-23. It is clearly shown in Figure 3-23 that, FVs representing different damage locations mix with each other due to the SPV variation. This mixture deprives the FVs of their functionality of being used to determine damage locations of unknown conditions.

For the proposed approach to construct FVs, the NMSCs of the 2-DOF structure with the "original set" and the "mutated set" (Table 3-1) are acquired using Equation (4-12) and Equation (4-13). They are used to formed FVs, which are plotted in the feature space (Figure 3-24).

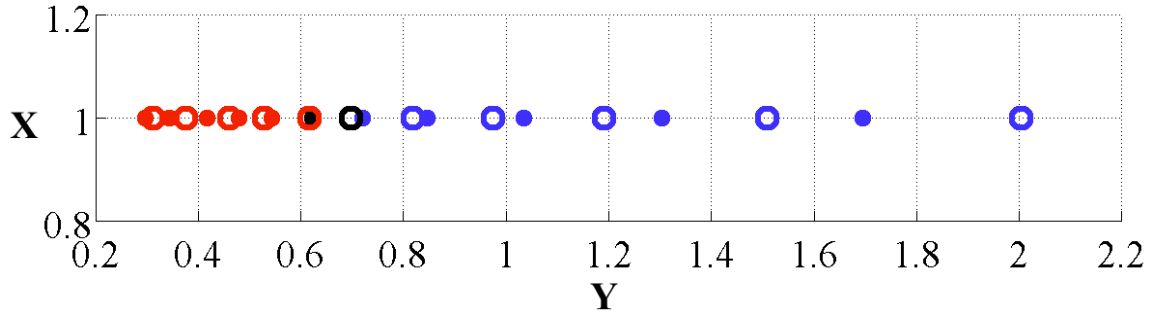

(a)

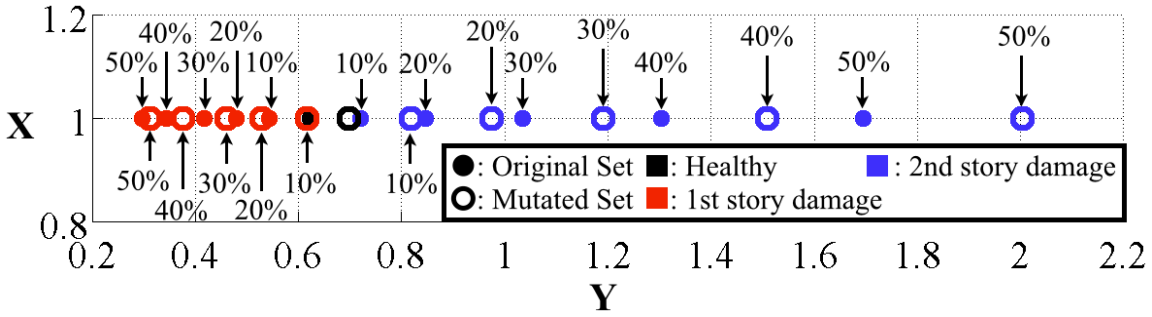

(b)

Figure 3-23: Feature space of the 2-DOF model with conventional FVs in two SPV sets. The positions of x and y axes are exchanged. (a): Original graph; (b): Graph with annotations.

Compare with FVs in Figure 3-23, positions of the FVs in Figure 3-24 are not negatively affected by the SPV change. FVs from the same damage location still occupy the same location in the feature space, despite the SPV variance. The characteristic of the proposed FVs exhibited in Figure 3-24 makes them much more appropriate for the damage-location-determination tasks than the conventional FVs.

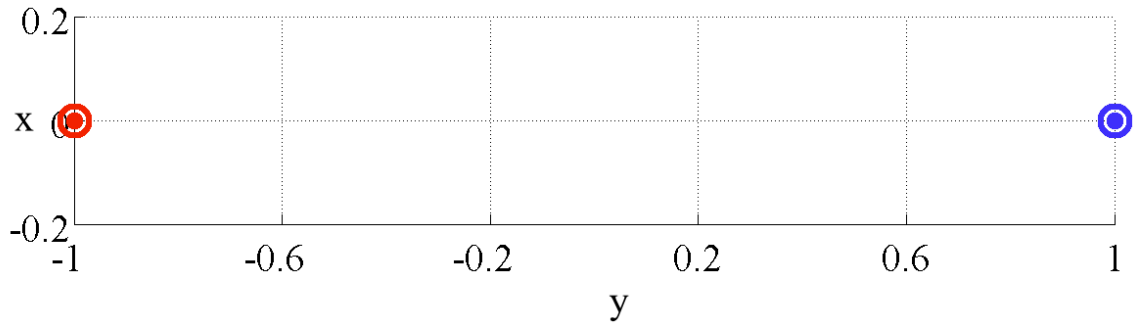

(a)

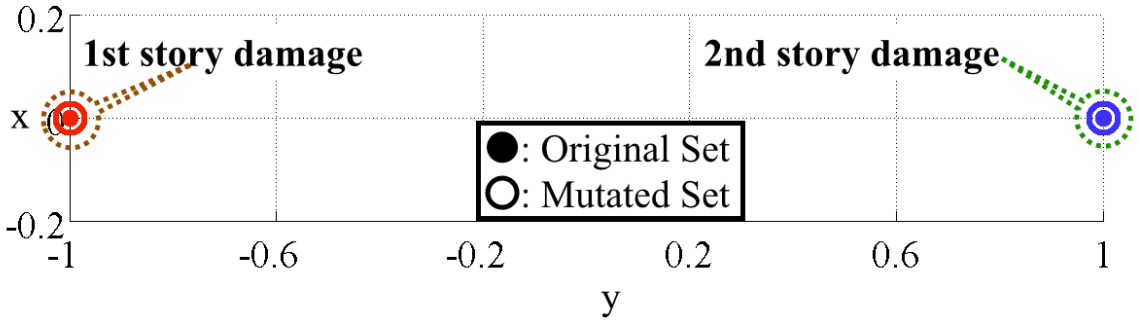

(b)

Figure 3-24: Feature space of the 2-DOF model with proposed FVs in two SPV sets. The positions of x and y axes are exchanged. (a): Original graph; (b): Graph with annotations.

Structure-Parameter-Value Uncertainty

Due to the same reason in the corresponding part of Section 3.3.1.1, a study with more SPV sets is needed to support the superiority of the proposed FVs, which is constructed by the pattern in the mode-shape-change. The "original set" in Table 3-1 is again used as the nominal SPV set. 300 more SPV sets are generated by this nominal set with a 15% uncertainty for each value in this set (Equation (4-4) through Equation (4-6)).

With these 300 SPV sets and 11 damage conditions per SPV set, there are 3300 new structural-damage-conditions here. Dynamic responses of the 2-DOF structure with these 3300 new conditions are simulated using the aforementioned setup. The mode shape information of the 2-DOF structure in each condition are extracted from these simulation results.

With this obtained mode shape information, FVs are first formed by the conventional approach (Equation (4-11) for $n = 2$). The feature space with points representing these 3311 FVs is plotted in Figure 3-25, including the 11 ones from the nominal SPV set (the "original set" in Table 3-1). Figure 3-25 shows that the FVs representing different damage locations in different SPV sets mix with each other, which is unacceptable from the AIS perspective.

Using the proposed approach, FVs are constructed using the NMSCs from the 301 SPV sets, according to Equation (4-12) and Equation (4-13). The feature space with these FVs is plotted in Figure 3-26.

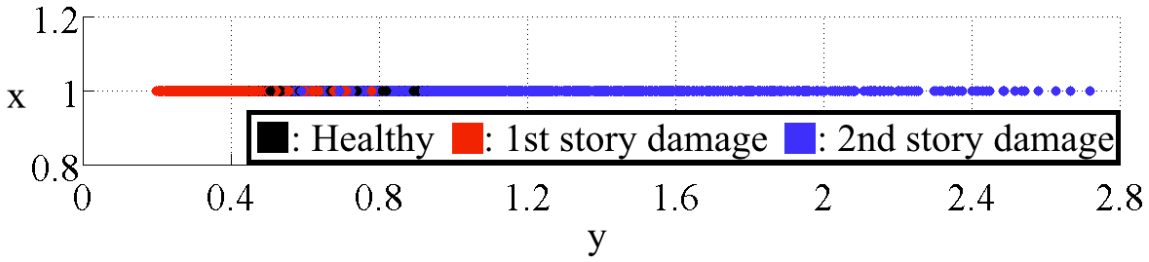

Figure 3-25: Feature space of the 2-DOF model with conventional FVs in 301 SPV sets. The positions of x and y axes are exchanged.

Figure 3-26 shows that FVs representing the same damage location still occupy the same position in the feature space, despite the significant difference existing between these 301 SPV sets. The reason behind this can be explained as: No matter what the SPVs are, for one specific SPV set, the FVs representing the "1st story damage" are always on the left side of the "healthy" point, and the FVs standing for the "2nd story damage" are always on the right side in Figure 3-25. The relative position between the FVs with the same SPV set is consistent with all the 301 SPV sets. Equation (4-12) and Equation (4-13) extract this relative position information and use it to form the new FVs, which are shown in Figure 3-26.

The characteristic of the FVs in Figure 3-26 makes the proposed FV more suitable for the damage-location-determination task than its conventional counterpart. And this superiority generally exists in different SPV sets.

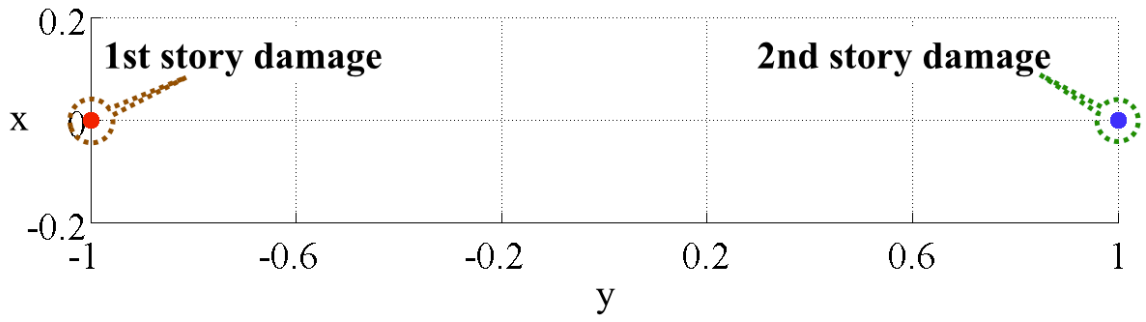

Figure 3-26: Feature space of the 2-DOF model with proposed FVs in 301 SPV sets. The positions of x and y axes are exchanged.

3.3.2.2 3-DOF Structure Model

Simulation Parameter

The 3-DOF structure model employed here is the same one that is in Section 3.3.1.2. Part of the SPV sets involved in this section is also listed in Table 3-2. All the simulation parameters are the same with Section 3.3.1.2, except that the interested value here is the y-coordinates (amplitudes) of peaks in the frequency domain, while previously it is the x-coordinates (frequencies).

Feature Vector Performance

The mode shape information is extracted from simulated dynamic responses of the 3-DOF structure model in different damage conditions with the "original set" of Table 3-2. Equation (4-11) is employed to construct the conventional FVs, which are plotted in the feature space (Figure 3-27). In Figure 3-27, x, y and z stand for the first, the second and the third entry of the FV vector (Equation (4-11)), respectively. The x-axis is hidden because the x-coordinate of every point is always 1 based on the definition.

On the other hand, the proposed FVs are constructed by the NMSCs of the 3-DOF structure model with the "original set" SPV set in Table 3-2, according to Equation (4-12) and Equation (4-13). The feature space with these FVs is plotted in Figure 3-28. In Figure 3-28, the x-axis is not shown because the x-coordinate of every point is always 0,

as a result of Equation (4-12). In addition, points in Figure 3-28 lie on a circle due to the normalization process (Equation (4-13)).

Comparing with the ones in Figure 3-27, FVs in Figure 3-28 exhibit better characteristic:

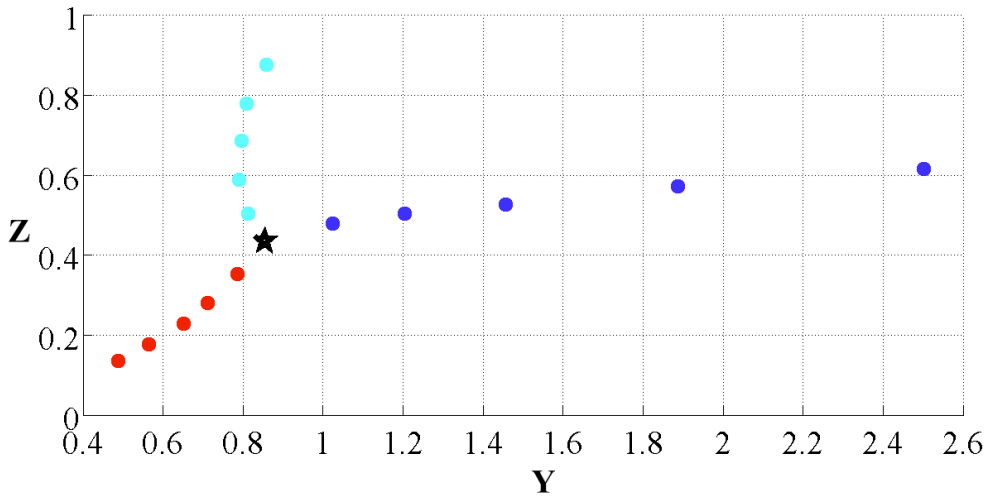

(a)

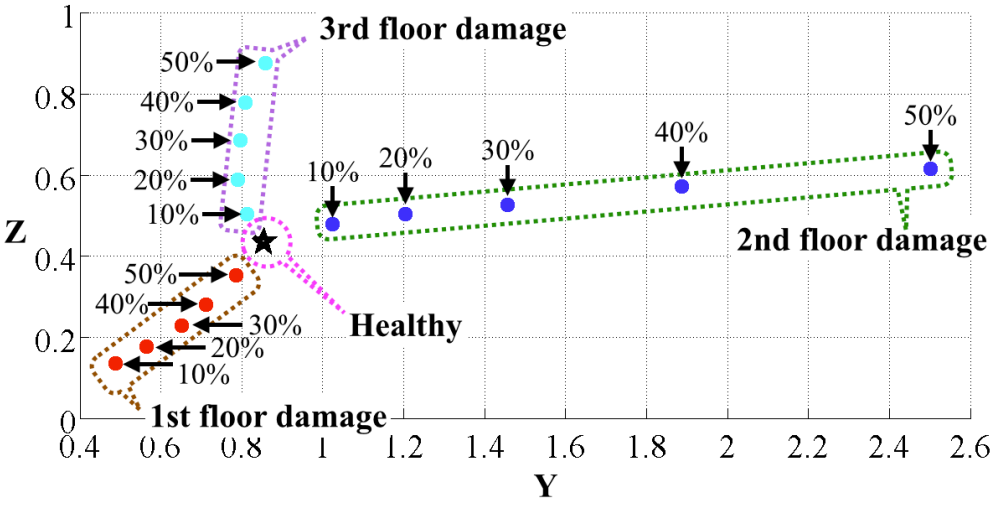

(b)

Figure 3-27: Feature space of the 3-DOF model with conventional FVs in one SPV set. (a): Original graph; (b): Graph with annotations.

FVs from the same damage location are better clustered, while the ones representing different damage locations are better separated.

Structure-Parameter-Value Variation

To explore the effect of SPV change on the two kinds of FVs, the "original set" and the "mutated set" in Table 3-2 are employed. The mode shape information is extracted from the 3-DOF structure model in different damage conditions with these two different SPV sets.

The conventional FVs are constructed by the mode shape information with Equation

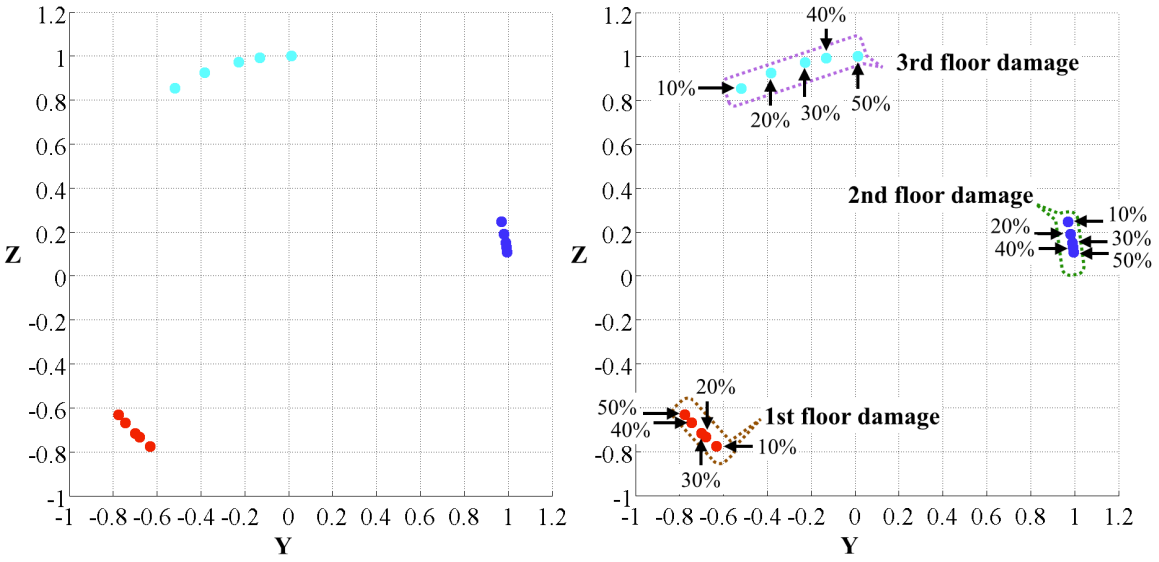

(a) (b)

Figure 3-28: Feature space of the 3-DOF model with proposed FVs. (a): Original graph; (b): Graph with annotations.

(4-11) and are plotted in the feature space (Figure 3-29). In Figure 3-29, the x-axis is not shown because the x-coordinate of every point is always 1. Figure 3-29 clearly show that the difference between the two SPV sets significantly changed the FV positions in the feature space, which is undesirable.

Alternatively, the proposed FVs are constructed using the NMSCs according to Equation (4-12) and Equation (4-13). These FVs are plotted in the feature space (Figure 3-30). In Figure 3-30, the x-axis is not shown because the x-coordinate of every point is always 0.

Compared with the ones in Figure 3-29, FVs in Figure 3-30 exhibit more desirable characteristics: FVs from the same damage location are better clustered, and the ones representing different damage locations are better separated. The proposed FV are less affected by the SPV change, and tend to occupy similar positions in the feature space with different SPV sets.

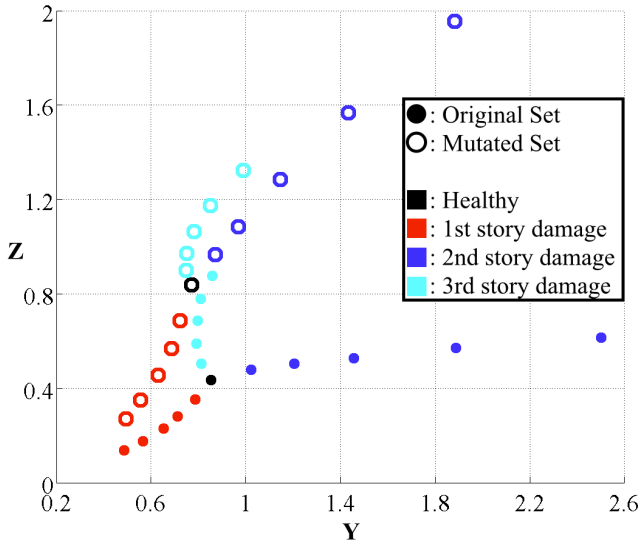

Figure 3-29: Feature space of the 3-DOF model with conventional FVs in two SPV sets.

Structure-Parameter-Value Uncertainty

Due to the same reason in the corresponding part of Section 3.3.1.2, a study with more SPV sets is needed to support the advantage of proposed FVs. The "original set" (Table 3-2) is used as the nominal SPV set. 300 more SPV sets are calculated by this nominal set with a 15% uncertainty for each value in this set (Equation (4-4) through Equation (4-6)).

With 300 SPV sets and 16 damage conditions per SPV set, there are 4800 new structural-damage-conditions here. Dynamic responses of the 3-DOF structure with these 4800 new conditions are simulated using the aforementioned setup. The mode shape information of the 3-DOF structure in each condition are extracted from these simulation results.

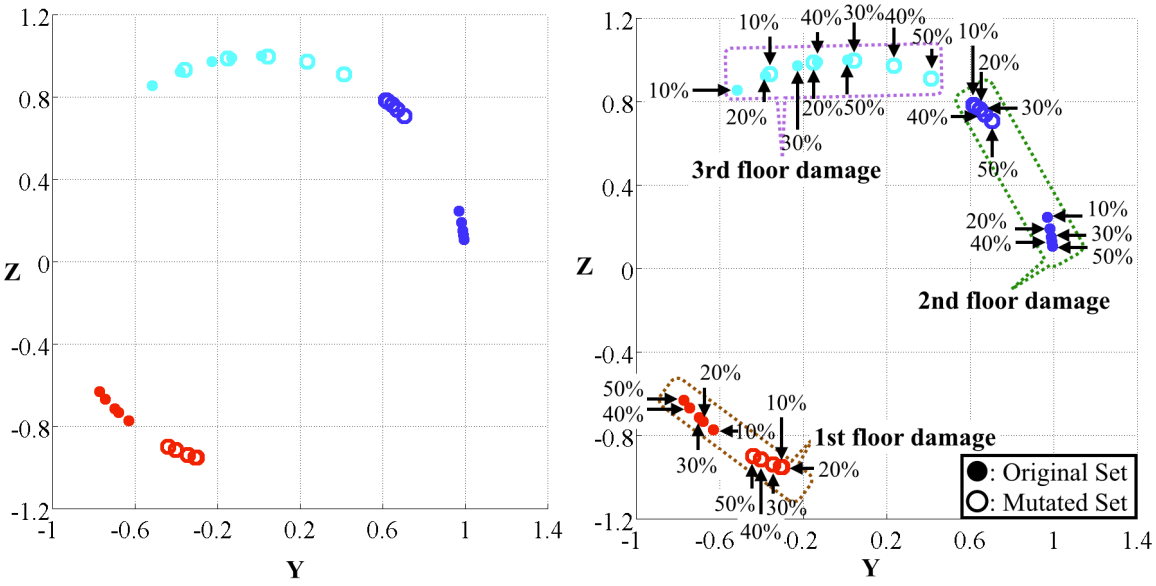

(a) (b)

Figure 3-30: Feature space of the 3-DOF model with proposed FVs in two SPV sets. (a): Original graph; (b): Graph with annotations.

With this mode shape information, FVs are first formed by the conventional approach (Equation (4-11) for $n = 3$). The feature space with points representing these 4816 FVs is plotted in Figure 3-31, including the 16 ones from the nominal SPV set. In Figure 3-31, the x-axis is not shown because the x-coordinate of every point is always 1. It is clearly shown in Figure 3-31 that, FVs representing different damage locations mix with each other, due to the difference existing between these 301 SPV sets.

To complete the comparison, the proposed FVs are formed using Equation (4-12) and Equation (4-13) and are plotted in the feature space (Figure 3-32), where the x-axis is not shown because the x-coordinate of every point is always 0 based on its definition.

Figure 3-32 shows that, even though the FVs representing the "2nd story damage" mix with the ones representing the "3rd story damage" at one side, the FVs standing for different damage locations are still clearly separated in the feature space and easy for the

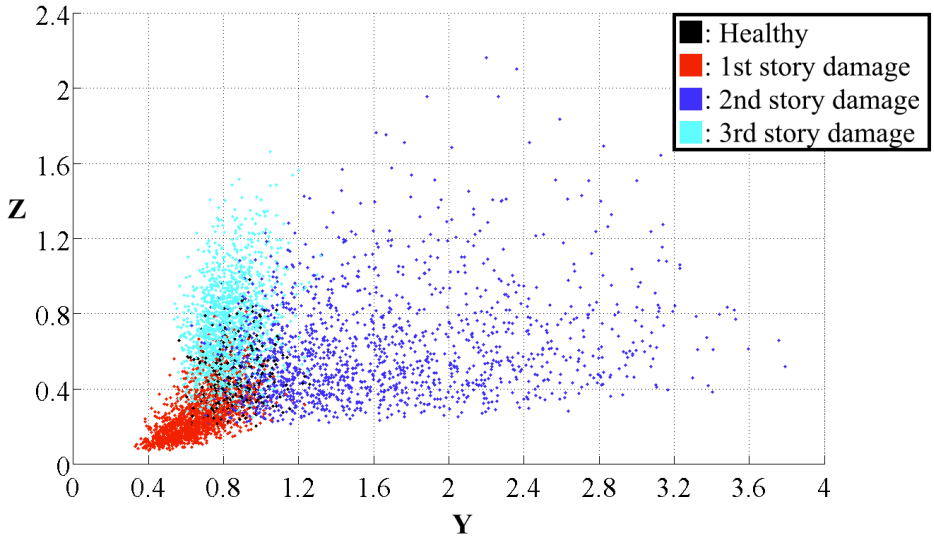

Figure 3-31: Feature space of the 3-DOF model with conventional FVs in 301 SPV sets.

AIS to recognize. The position of a FV in Figure 3-32 is decided by the vector direction from the "healthy" point to its corresponding point in Figure 3-31. Due to the significant difference existing between these 301 SPV sets, it is possible that the vectors, which are from the "healthy" points to damaged points representing different damage locations in different SPV sets, have similar directions. This may explain the mixture in Figure 3-32.

Even though mixture happens between the FVs representing the "2nd story damage" and the "3rd story damage". The performance of the proposed FV still affirms that it is more suitable for the AIS in the damage-location-determination, compared with the FVs formed in the conventional approach.

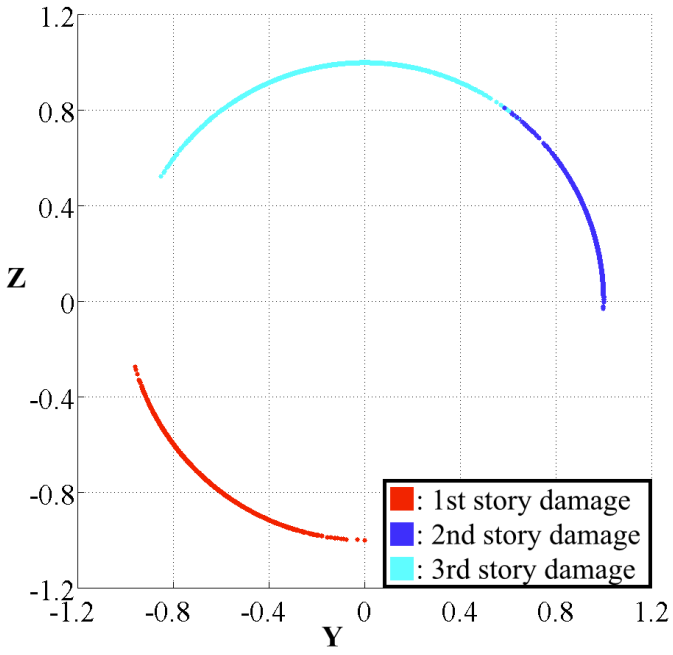

Figure 3-32: Feature space of the 3-DOF model with proposed FVs in 301 SPV sets.

3.3.2.3 4-DOF Structure Model

Simulation Parameter

The 4-DOF structure model employed here is the same one appeared in Section 3.3.1.3. Part of the SPV sets involved in this part is also listed in Table 3-3. All the simulation parameters are the same with Section 3.3.1.3, except that the information extracted here is the y-coordinates (amplitudes) of peaks in the frequency domain, while previously it is the x-coordinates (frequencies).

As mentioned earlier in Section 3.3.1.3, only the three lower natural frequencies are considered to be available in this 4-DOF structure model, in an attempt to imitate the incomplete frequency spectrum difficulty commonly present in practical SHM scenarios. Therefore, only the mode shape information corresponding to the three lower natural frequencies are employed to build FVs in this section.

Feature Vector Performance

To begin with, the mode shape information of the 4-DOF structure model is extracted from simulated dynamic responses of the structure model in different structural-damage-conditions with the "original set" in Table 3-3. This mode shape information is used to form the conventional FVs according to Equation (4-11). Constructed FVs are plotted in the feature space (Figure 3-33), where the x-axis is not shown because the x-coordinate of every point is always 1.

The five points in the same color represent the five different damage severities in the same damage location. From the point nearest the "healthy" point to the point farthest the "healthy" point, they represent 10%, 20%, 30%, 40%, and 50% stiffness loss on that specific story alone. When the damage severity is relatively small, the corresponding point becomes very close with the "healthy" point and points representing other damage locations.

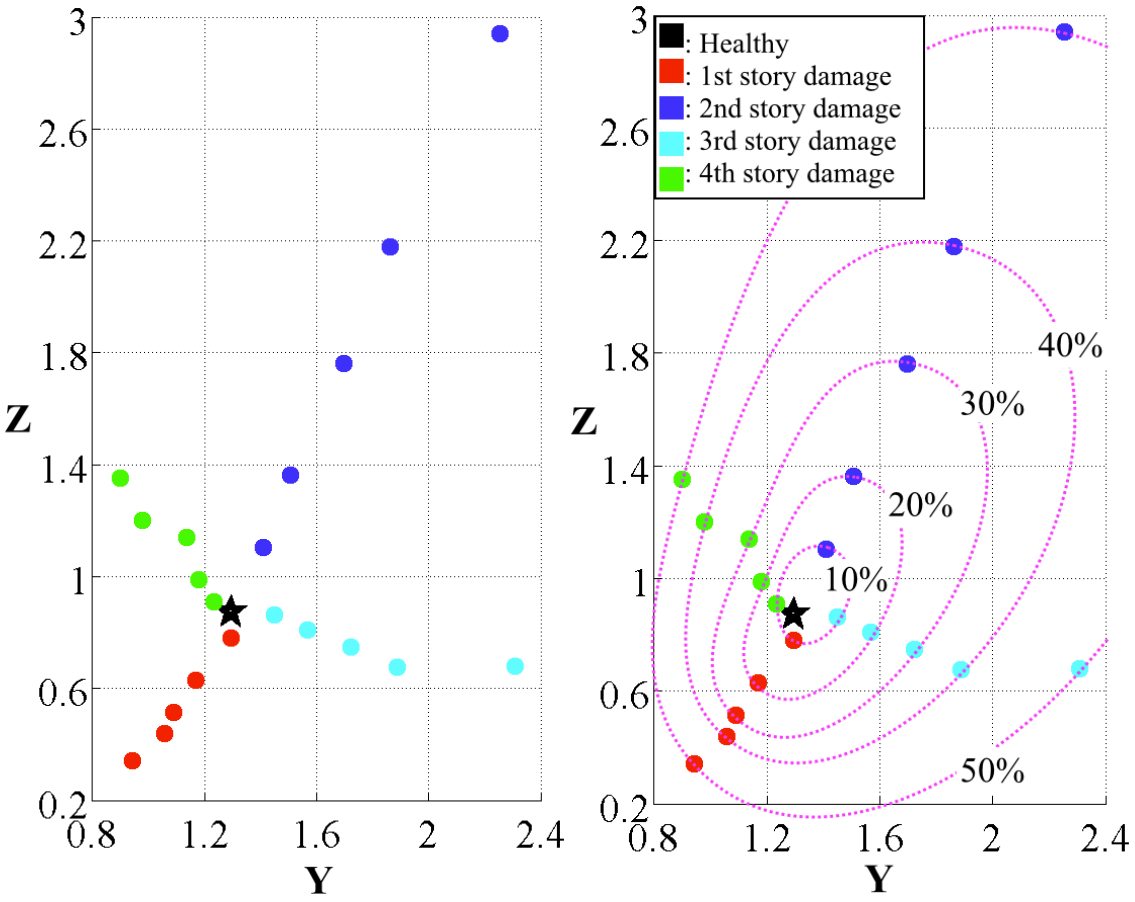

(a) (b)

Figure 3-33: Feature space of the 4-DOF model with conventional FVs in one SPV set. (a): Original graph; (b): Graph with annotations.

With the mode shape information of the 4-DOF structure model in different damage conditions with the "original set" in Table 3-3, the NMSCs are calculated using Equation (4-12) and Equation (4-13). These NMSCs are used as the proposed FVs and are plotted in the feature space (Figure 3-34), where the x-axis is not shown because the x-coordinate of every point is always 0. FVs in Figure 3-34 lie on a circle because of the normalization process (Equation (4-13)).

In Figure 3-34, FVs with the same damage location are better clustered and the ones with different damage locations are better separated, compared with FVs in Figure 3-33. Using the FV performance criteria defined earlier, FVs In Figure 3-34 possess better performance than the ones in Figure 3-33.

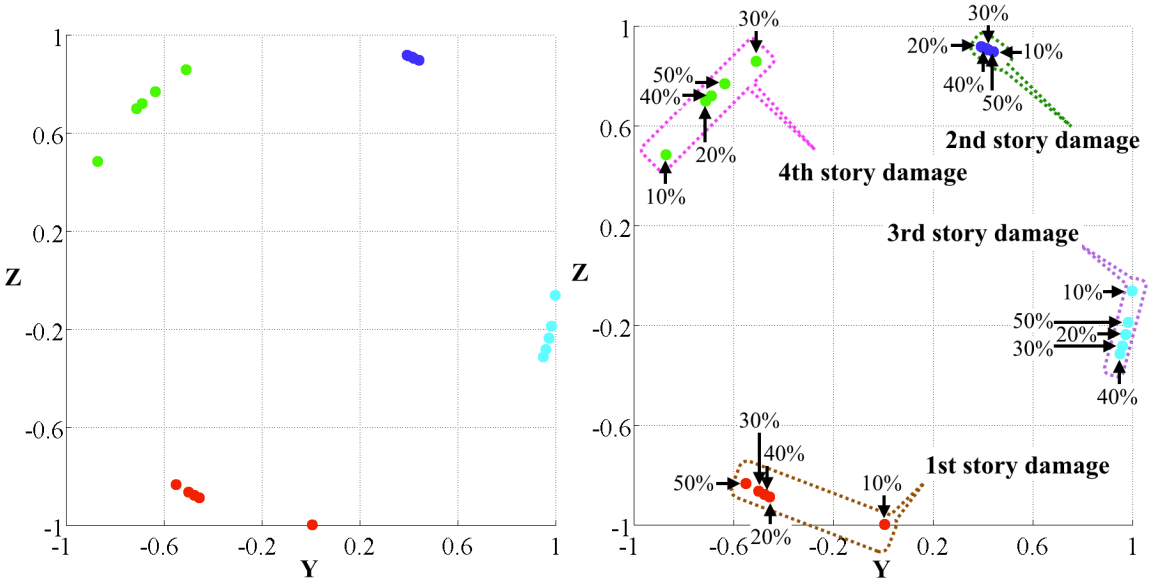

(a) (b)

Figure 3-34: Feature space of the 4-DOF model with proposed FVs in one SPV set. (a): Original graph; (b): Graph with annotations.

Structure-Parameter-Value Variation

To investigate the effect of SPV change on the positions of FVs in the feature space, the "original set" and "mutated set" in Table 3-3 are employed. The mode shape information is extracted from the simulated dynamic response of the 4-DOF structure model in different damage conditions with these two SPV sets.

This information is used to form the conventional FVs according to Equation (4-11). Constructed FVs are plotted in the feature space (Figure 3-35). In Figure 3-35, the x-axis is not shown because the x-coordinate of every point is always 1.

To use the pattern in mode-shape-change, Equation (4-12) and Equation (4-13) are

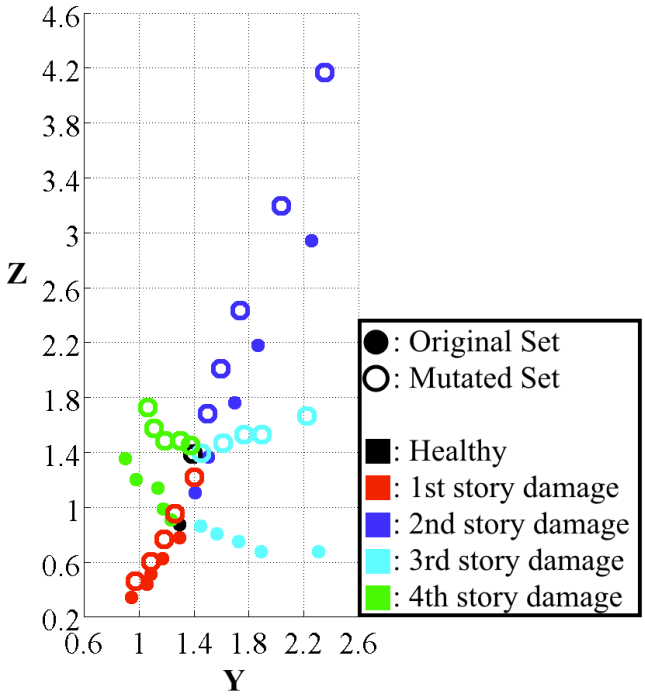

Figure 3-35: Feature space of the 4-DOF model with conventional FVs in two SPV sets.

employed to calculate the NMSCs, which are used as the FVs and are plotted in the feature space (Figure 3-36). In Figure 3-36, the x-axis is not shown because the x-coordinate of every point is always 0.

Compare Figure 3-36 with Figure 3-35, it is clear that FVs in Figure 3-36 exhibit more desirable characteristics: The FVs from the same damage location are better clustered, while the ones from different damage locations are separated more distinctly. The proposed FVs are less affected by the SPV change, and still tend to occupy similar positions in the feature space despite the difference existing between the two SPV sets.

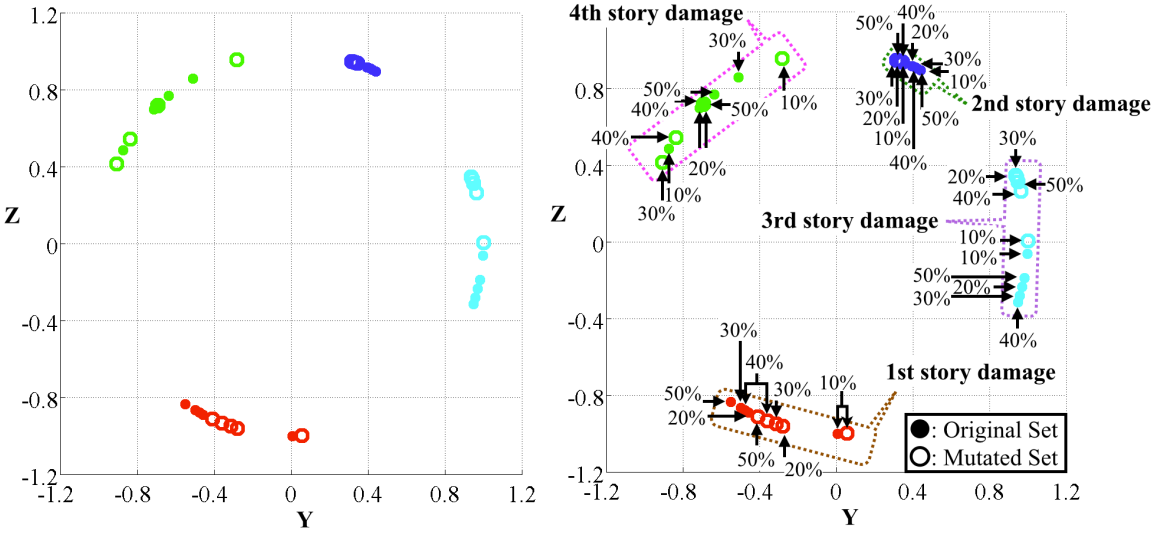

(a) (b)

Figure 3-36: Feature space of the 4-DOF model with proposed FVs in two SPV sets. (a): Original graph; (b): Graph with annotations.

Structure-Parameter-Value Uncertainty

Due to the same reason in the corresponding part of Section 3.3.1.3, a study with more SPV sets is needed to support the superiority of the proposed FVs. The "original set" in Table 3-3 is again used as the nominal SPV set. 300 more SPV sets are generated by this nominal set with a 15% uncertainty for each value in this set (Equation (4-4) through Equation (4-6)).

With these 300 SPV sets and 21 damage conditions per SPV set, there are 6300 new structural-damage-conditions here. Dynamic responses of the 4-DOF structure with these 6300 new conditions are simulated using the aforementioned setup. The mode shape information of the 4-DOF structure in each condition are extracted from these simulation results.

The 301 sets of conventional FVs are constructed from the mode shape information according to Equation (4-11) ($n = 3$) and are plotted in the feature space (Figure 3-37), where the x-axis is not shown because the x-coordinate of every point is always 1.

Alternatively, the proposed FVs are formed using the pattern in mode-shape-change according to Equation (4-12) and (4-13). These FVs are plotted in the feature space (Figure 3-38), where the x-axis is not shown because the x-coordinate of every point is always 0.

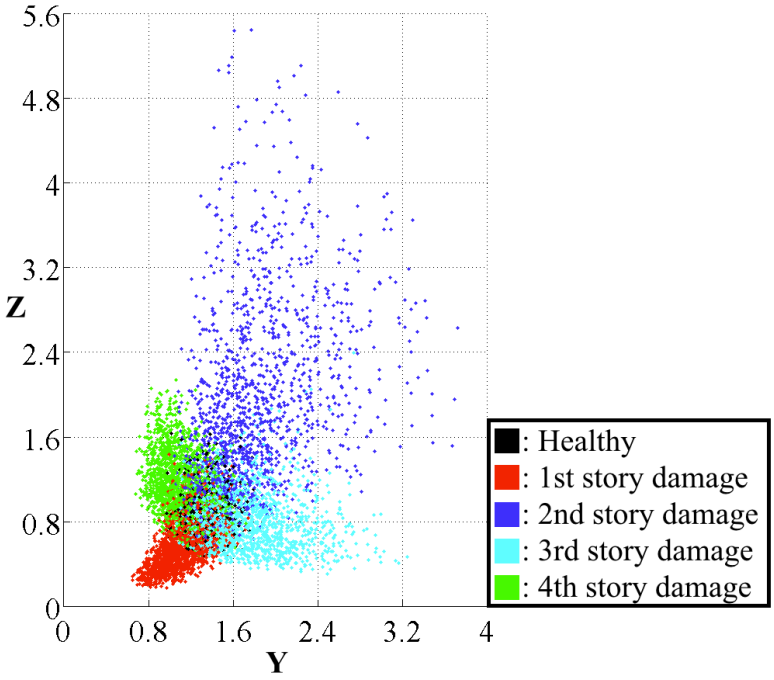

Figure 3-37: Feature space of the 4-DOF model with conventional FVs in 301 SPV sets.

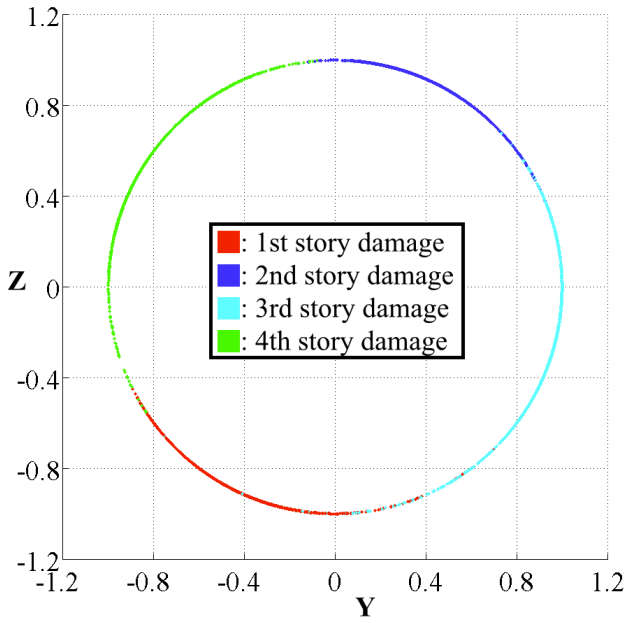

Figure 3-38: Feature space of the 4-DOF model with proposed FVs in 301 SPV sets.

The mixture between FVs representing different damage locations happens in both Figure 3-37 and Figure 3-38. However, it is obvious that the FVs in Figure 3-38 are better separated when the damage locations are different, compared with the FVs in Figure 3-37.

3.3.2.4 Review

Comparisons in this part conclude the same result with Section 3.3.1: The proposed FV, which is formed by the pattern in mode-shape-change, exhibits more desirable characteristics than the conventional FV that is constructed by the mode shape information directly. FVs based on the pattern in mode-shape-change are more sensitive to the damage location, less sensitive to the damage severity or the SPV difference. Therefore, FVs formed by the changing pattern are more suitable for the AIS in the damage location determination of SHM tasks.

3.4 Section Summary

Comparisons are made in previous sections, which are between two kinds of FVs for the AIS in SHM tasks: The conventional kind is constructed from the modal parameter directly. And the proposed one is formed by the pattern in model-parameter-change.

Three linear structure models (2/3/4-DOF) are considered. And results of comparisons are consistent in all three structure models. The proposed FVs formed by the changing

pattern exhibit better characteristics: FVs from the same damage location occupy adjacent positions, while FVs representing different damage locations are distinctly separated in the feature space.

The AIS' capacity of recognizing unknown antigens relies on the interactions between FVs of the unknown antigens and its memory cells. If the FVs representing different damage conditions mix with each other in the feature space, the AIS will become unable to distinguish one condition from another.

Based on the comparison results presented and analyzed previously, the proposed approach of constructing FVs using the pattern in modal-parameter-change is superior. FVs formed using this approach are insensitive to the SPV change and the damage severities, while they are much more sensitive to the damage location. This characteristic makes them more suitable for the damage location determination in SHM tasks.

4 Artificial Immune System (AIS) Performance

Based on the comparisons between the proposed FV and the conventional one in preceding sections, the AIS constructed in the proposed method is expected to be applicable to the SHM task, where a discrepancy exists between the training SPV and the SPV of the structure in monitoring.

In this section, the AIS formed in the proposed method is applied to recognize unknown structure-damage-conditions in two SHM scenarios and its performance is evaluated. One of the two scenarios is a 4-DOF structural model with different SPV set for each damage condition, while the other scenario is a benchmark structure with different structure models and SPV sets.

4.1 4-DOF Structure Model Test

4.1.1 Artificial Immune System (AIS) Construction

The proposed AIS is trained using simulated dynamic responses of a 4-DOF structure model with the "original set" in Table 3-3. Some known structural-damage-conditions are simulated and used as the training antigens. Damage severities of these training antigens range from 10% to 50% stiffness loss at an interval of 10%. The single-damage-situation is assumes, which means that only one story in the structure is damaged in each structural-damage-condition.

In order to make this test more realistic, only the lower three natural frequencies are used as known and the fourth one is considered to be unable to measure. Similar with the 4-DOF case in Section 3.3.1.3, the normalized-frequency-changes (NFCs) of these training damage conditions are calculated according to Equation (4-7), and an conversion is made from the Cartesian coordinates to spherical coordinates (Equation (4-9)), which are then used to build FVs with Equation (4-10). These FVs have been previously shown in Figure 3-16.

These FVs, together with the information about their corresponding damage locations and damage severities, form the training antigens for the AIS. These training antigens are employed to train the AIS using the process described in Figure 2-2.

For the AIS training process, the following parameters are specified: the clone rate (CR) is set to be 10, the candidate-selection-threshold (CST) is set to be 0.9, and the candidate-injection-threshold (CIT) is set to be 0.98. After the training process, the FVs of the mature memory-cell-set are plotted in the feature space (Figure 4-1).

As explained earlier, FVs formed by the NFCs are suitable for the damage location determination task, but not for the damage existence detection and the damage severity estimation tasks. Two phases are added before and after the damage location determination phase, respectively.

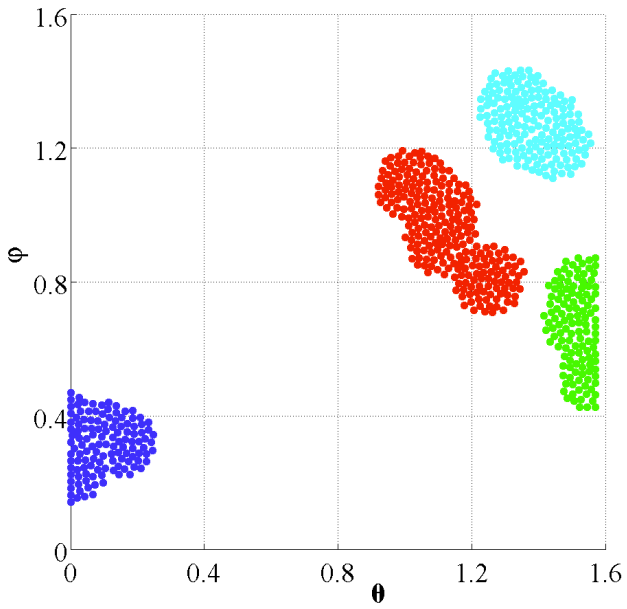

Figure 4-1: Feature space of the 4-DOF structure model with FVs of the mature memory-cell-set.

For Phase 1, AIS detects the damage existence according to the maximum-relative-frequency-change (MRFC), which is defined to be:

$$\text{MRFC} = \max\left(\frac{\Delta_1}{f_{\text{healthy},1}}, \frac{\Delta_2}{f_{\text{healthy},2}}, \cdots, \frac{\Delta_n}{f_{\text{healthy,n}}}\right) \tag{5-1}$$

where max () is a function that returns its maximum argument. And

$$\Delta_i = f_{\text{healthy},i} - f_i$$

where $i = 1, 2, \ldots, n$ (n is the number of natural frequencies considered). f_i is the i-th natural frequency, and $f_{\text{healthy},i}$ is the i-th frequency value in the healthy condition.

If the maximum-relative-frequency-change (MRFC) of an unknown condition is higher than a pre-specified threshold, named the damage-existence-threshold (DET), AIS will

consider this condition as “damaged” and passes it to Phase 2, which determines the damage location of the damage in this condition. In this section, the damage-existence-threshold is set to be 1%.

The maximum-relative-frequency-change (MRFC) is also used in Phase 3 to estimate the damage severity. Relationships between the damage severity and the maximum-relative-frequency-change (MRFC) are plotted in Figure 4-2.

The straight lines in Figure 4-2 are the least square best-fit lines of the data points. Equations of these best-fit lines and their corresponding coefficients of determination are also shown in the figure. It is clearly shown in Figure 4-2 that the relationship between the maximum-relative-frequency-change (MRFC) and the damage severity is approximately linear ($R^2 > 0.97$).

The relationships between the damage severity and the maximum-relative-frequency-change (MRFC) for each story shown in Figure 4-2 are recorded in the AIS, and are used for the damage-severity-estimation task. After the AIS has determined the damage location of one unknown structural-damage-condition, the maximum-relative-frequency-change (MRFC) of this condition is calculated and is used to calculate the damage severity with the coefficients corresponding to its damage location. The calculation formula is

$$\mathrm{DS} = \frac{1}{a}\left(\mathrm{MRFC} - b\right) \tag{5-2}$$

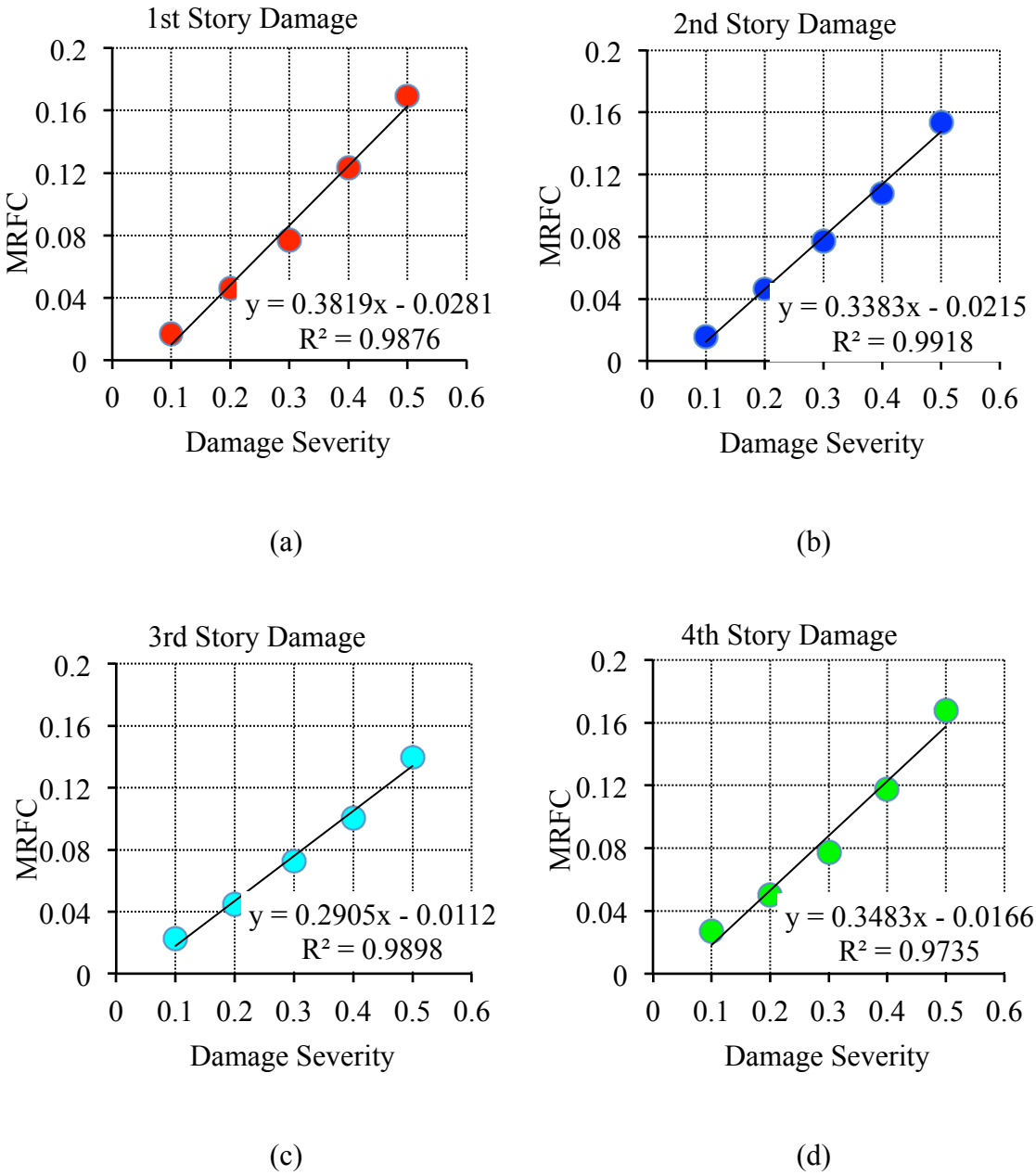

Figure 4-2: Relationships between the damage severity and the MRFC for each structural story. (a), (b), (c) and (d) are for the 1st story, the 2nd story, the 3rd story, and the 4th story, respectively.

Table 4-1: Coefficients used for the damage-severity-estimation in the SHM task.

Coefficient	1st story damage	2nd story damage	3rd story damage	4th story damage
a	0.3819	0.3383	0.2905	0.3483
b	-0.0281	-0.0215	-0.0112	-0.0166

where DS represents the damage severity, and a and b are coefficients, which are different for each damage location. After the training, the coefficients (a and b) are listed in Table 4-1, which are also shown in the equations in Figure 4-2.

4.1.2 Testing Damage Conditions

To test the performance of the proposed AIS after training, 440 different structural-damage-conditions are generated (110 conditions for each structural story) using the same 4-DOF structural model. Damage severities of these 440 conditions are randomly selected within the range from 10% to 50%, and the single-damage-situation is assumed. The SPV set of the 4-DOF structural model is different for each damage condition, and is generated in the same way with the ones used for the statistic study (Section 3.3.1.3).

FVs of these 440 unknown conditions are constructed, and are used to build unknown antigens. The FVs of these 440 unknown antigens are plotted in the feature space (Figure 4-3).

The significance of this AIS performance test is that, the AIS is trained using only 20 structural-damage-conditions with one SPV set (the "original set" in Table 3-3), while

there are 440 unknown structural-damage-conditions from 440 different SPV sets, which can be as different as 15% with the corresponding values in the SPV set used for training.

4.1.3 Testing Procedures

For each unknown structural-damage-condition, Phase 1 of the AIS recognition process is the damage-existence-detection. The MRFC of the unknown structural-damage-condition is calculated using Equation (5-1). As explained earlier, the natural frequencies of a structure change correspondingly with its healthy situation. Therefore, the MRFC can be used as an effective indicator of the damage existence: If MRFC $>$ DET, the AIS labels the damage flag of this unknown condition as "damaged" and pass its information to Phase 2 (damage-location-determination). Otherwise, if MRFC $\leq$ DET, the damage flag of this unknown antigen is set to be "healthy" and the AIS recognition process ends here.

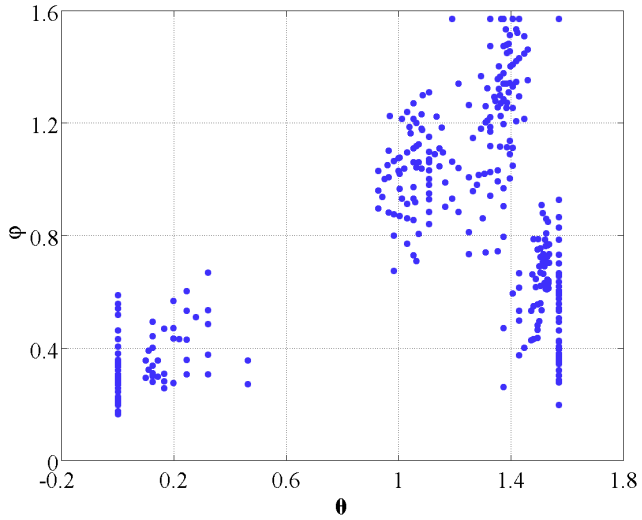

Figure 4-3: Feature space with FVs of the 440 unknown antigens used to test the performance of the trained AIS.

For the unknown conditions labeled as “damaged”, the NFCs of the structure in these conditions are calculated using Equation (4-7) and FVs of these unknown damage conditions are constructed using Equation (4-9) and Equation (4-10). With their FVs, these unknown damage conditions are packaged as unknown antigens (Figure 2-1) and introduced into the AIS’ mature memory-cell-set to stimulate a secondary-immune-response.

In this phase, the affinity values between the FV of an unknown antigen and the ones of the memory cells are calculated using Equation (3-1). Then this unknown antigen interacts with the memory cell having the highest affinity value with it, which is named the selected memory cell. The damage location represented by this selected memory cell is read out by the AIS and used to label the unknown antigen. In other word, the unknown antigen is determined to be representing a damage condition, whose damage location is the same with the selected memory cell.

After the damage location has been determined, the damage severity of the unknown antigen is estimated using Equation (5-2) and coefficients in Table 4-1 corresponding to its damage location. At the end of this process, the damage flag, the damage location, and the damage severity of the unknown antigen have been determined by the AIS.

4.1.4 Testing Results

Among the 440 unknown damage conditions, the trained AIS succeeded in detecting the damage existence and correctly pointing out the damage location in 419 cases, which results in a success rate of 95.23%.

To quantify the performance of the AIS in the damage severity estimation task, a variable named the severity deviation (SD) is defined as the difference between the estimated and the real damage severities:

$$\mathrm{SD} = \mathrm{DS}_{\mathrm{estimated}} - \mathrm{DS}_{\mathrm{real}} \tag{5-3}$$

where $\mathrm{DS}_{\mathrm{estimated}}$ and $\mathrm{DS}_{\mathrm{real}}$ are the estimated and real damage severities, respectively.

The distribution of the SD of the cases, which are correctly recognized by AIS in the damage existence detection and the damage location determination, is shown in Figure 4-4.

In Figure 4-4, the blue bars represent the distribution in a range of 0.01, and the red curve represents the "best-fit" Gauss curve generated by the curve fitting toolbox of MATLAB. The equation of this "best-fit" Gauss curve is

$$P = 13.79e^{-\left(\frac{\mathrm{SD}+0.005643}{0.04011}\right)^2} \tag{5-4}$$

where P is the percentage.

Figure 4-4 shows that the major portion of the SDs is within the $\pm 5\%$ range, which suggests a relative accurate damage severity estimation result. In order to investigate the relationship between the percentage and the SD in another perspective, the data shown in Figure 4-4 is reorganized and shown in Figure 4-5 again.

The x-axis of Figure 4-5 is the absolute value of the SD. The blue points in Figure 4-5 represent the accumulated percentage. It can be seen from Figure 4-5 that, in nearly 90% cases, the SD result of the AIS is within a range of $\pm 5\%$.

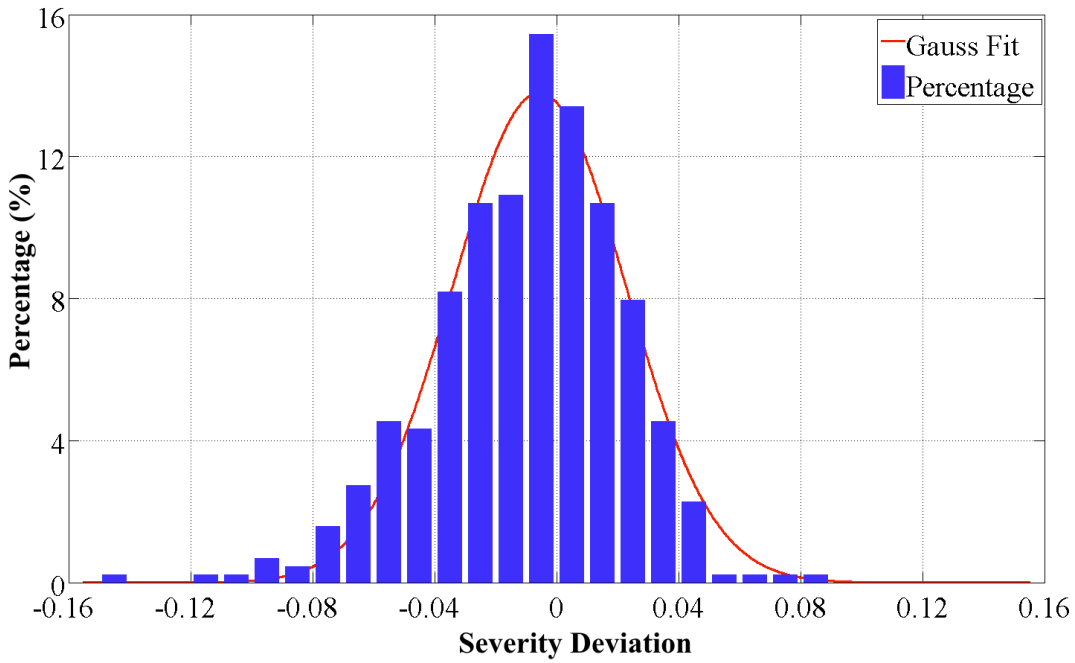

Figure 4-4: The distribution of the SDs of the damage-severity-estimation and its best-fit Gauss curve.

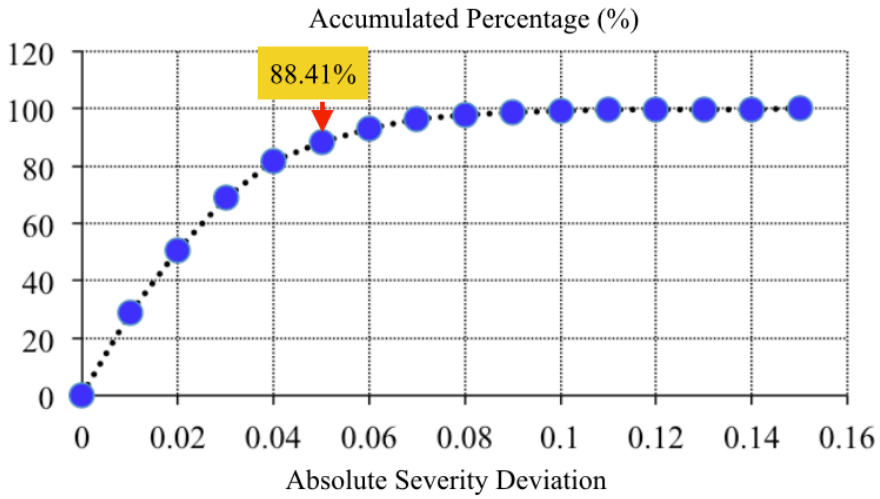

Figure 4-5: The accumulated percentage of the absolute severity deviation.

4.1.5 4-DOF Structural Model Test Summary

The proposed AIS is evaluated in a 4-DOF structure test. 21 known damage conditions (5 for each story and 1 for the "healthy" condition) with the "original set" (Table 3-3) are used to train the AIS. The trained AIS is then applied to 440 unknown damage conditions, each of which has a different SPV set.

The significance of this test is that, the AIS is trained using very limited known instances (21 cases). And unknown damage conditions are from different SPV sets, which can be as different as 15% with the SPV used for the training. This test simulates the practical challenges faced by the AIS when it is applied to similar but not identical structures after training, i.e. the discrepancy between the training SPV and the SPV of unknown conditions.

With an overall success rate of 95.23% in the damage-existence-detection and damage-location-determination, and nearly 90% of the damage-severity-estimations having a SD value less than 5%, the proposed AIS' performance is proved to be satisfactory in this 4-DOF structural test.

4.2 Benchmark Problem Test

The proposed AIS has been evaluated using the 4-DOF structure model in the preceding part, in which it exhibits satisfactory performance. Nevertheless, the previous evaluation only explores the situation when there exists a discrepancy between the training SPV and the SPV of the structure in monitoring. It remains unclear what the AIS' performance is when the structure model in monitoring is different with the structure model for training.

Even though the proposed AIS is only expected to deal with the problem when the SPV sets are different, it will still be interesting and also meaningful to evaluate the AIS in the situation where the structure model in monitoring is different with the one for training. To investigate this, a benchmark problem is employed, which is proposed by the International Association for Structural Control-American Society of Civil Engineers (IASC-ASCE) Structural Health Monitoring Task Group (Johnson, et al. 2004).

4.2.1 Introduction to Benchmark Problem

The structure in this benchmark problem is a four-story, two-bay by two-bay, steel-frame, quarter-scale model structure in the Earthquake Engineering Research Laboratory at the University of British Columbia (UBC). It has a $2.5\,m \times 2.5\,m$ plan and is $3.6\,m$ tall (Johnson, et al. 2004). An analytical diagram of the structure model with strong and weak directions annotated is shown in Figure 4-6.

There exist two analytical structure models in this benchmark problem: one is a 12-DOF shear-building model, and the other one is a 120-DOF model. Both models are finite-element-method based and their MATLAB codes are available on the website (NEEShub

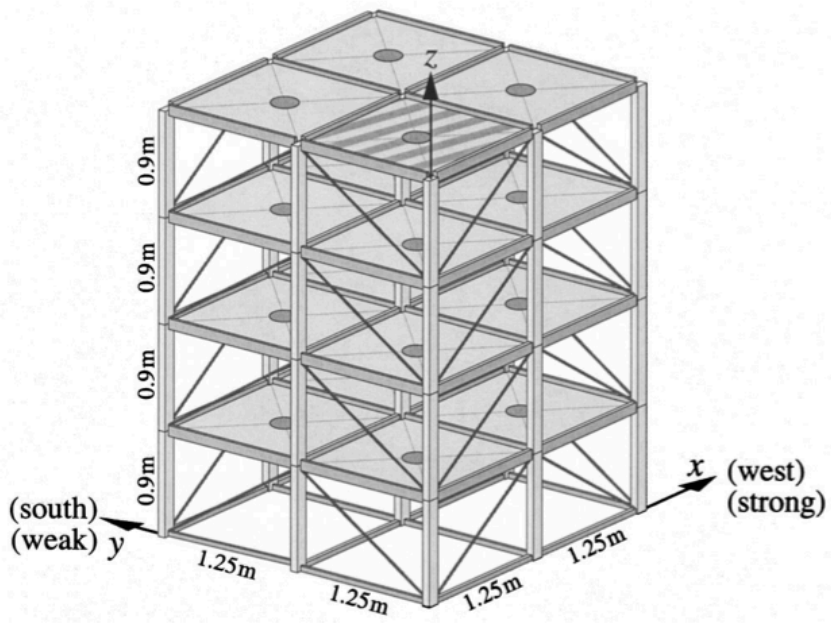

Figure 4-6: An analytical diagram of the structure model used in the benchmark problem with strong and weak directions annotated (Johnson, et al. 2004).

n.d.) for academic use. Coupled with other factors, the two analytical models result in five different model cases, which are listed in Table 4-2.

Eight damage patterns are defined for each model case. They are listed in Table 4-3, and are graphically illustrated in Figure 4-7 except for Pattern 0 (Undamaged) and Pattern 7 (User defined).

The performance of the AIS are investigated in all 5 model cases of the benchmark problem. As mentioned earlier, the single-damage-situation is assumed in the AIS. However, damage exists on two different stories in Pattern 2, 4, and 5 (Table 4-3), which violate the single-damage-situation assumption. Despite this, all the 7 damage patterns, excluding Pattern 7 (User define), are included in the investigation for each model case.

The fact that damage happens on more than one story significantly increases the difficulty in recognizing unknown structural-damage-conditions. Because the single-damage-situation is taken as a known condition by the AIS, the AIS will only point out one damage location, even though damage may also exist on another story.

Table 4-2: Configurations of the model cases in the benchmark problem.

Case Index	Number of DOF	Symmetric	Load Position
1	12	Yes	At all stories
2	120	Yes	At all stories
3	12	Yes	At roof
4	12	No	At roof
5	120	No	At roof

Table 4-3: Damage patterns in the benchmark problem.

Damage Pattern Index	Damage Location (Story)				Detailed Damage Information
	1	2	3	4	
0					Undamaged.
1	■				All braces of the 1st story are broken.
2	■		■		All braces of the 1st and the 3rd stories are broken.
3	■				One brace on one side of the 1st story is broken.
4	■		■		One brace on one side of the 1st and the 3rd stories are broken
5	■		■		Pattern 4 plus unscrew the left end of one element of the 1st story.
6	■				Area of one brace on one side of the 1st story is reduced to 2/3.
7	◥	◥	◥	◥	User defined damage conditions.

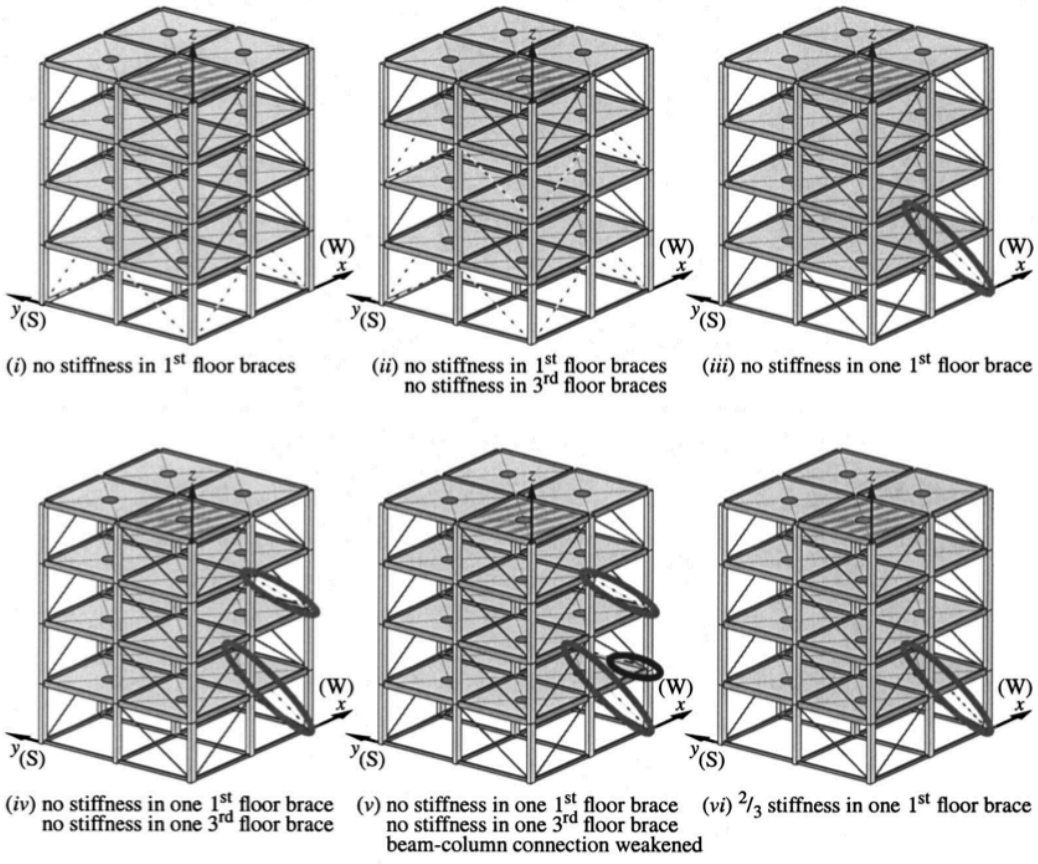

Figure 4-7: Graphical illustrations of Pattern 1 to 6 (Johnson, et al. 2004).

4.2.2 Unknown Structural-Damage-Conditions for Test

Sixteen accelerometers, two in the x and two in the y directions per story, are mounted on the outer surface of the benchmark structure. MATLAB codes of the benchmark problem provide the measured acceleration data from all sixteen accelerometers.

In real world scenarios, the measurement data from sensors are usually limited and incomplete. In order to simulate this practical limitation and therefore make this investigation more practical, only the first two of the sixteen accelerometers are used. These two sensors are mounted along the x and y directions on the 1st story, respectively. Data from them are used to extract modal parameters of the structure needed by the AIS.

To further limit the available information in an attempt to make this test more realistic, only the lower three natural frequencies in either direction are considered, which responses to the practical situation that the complete frequency spectrum is usually inconvenient or expensive to obtain.

For each model case, dynamic responses of the benchmark structure with seven different damage patterns are obtained from the provided MATLAB codes. The data associated with Pattern 0 (Undamaged) is considered to be a known condition, and is used as the reference for further calculations. Normalized-frequency-changes (NFCs) are calculated according to Equation (4-7), and are then converted to spherical coordinates using Equation (4-9). Finally, FVs are constructed based on Equation (4-10).

With these FVs, the six damage patterns generate six unknown antigens. These unknown antigens are introduced into the AIS, which is trained using the 4-DOF structure model with the "original set" in Table 3-3.

The trained AIS determine the health conditions of these unknown antigens through the three phases described earlier. Results are presented and analyzed in the ensuing part.

4.2.3 Benchmark Problem Results

4.2.3.1 Model Case 1

As indicated in Table 4-2, the excitation method in Model Case 1 is the "ambient" excitation along the y-direction at all stories. Because there is no external excitation applied along the x-direction, the data from the 1st accelerometer (x-direction at the 1st story) is discarded, and only the data from the 2nd accelerometer (y-direction at the 1st story) is used.

Antigens formed by the six damage patterns in previously described approach are introduced into the trained AIS as unknown antigens. The trained AIS recognizes these unknown antigens through the three-phase procedure, which has also been described in previous parts.

Results from the AIS about these six damage patterns are listed in Table 4-4, which shows that, the trained AIS correctly points out the damage location for the damage

Table 4-4: Results from the AIS about the damage patterns in Model Case 1.

Damage Pattern Index	Real Damage Condition						AIS Result	
	Location (Story)				Severity (Stiffness Loss)		Location (Story)	Severity (%)
	1	2	3	4	x (%)	y (%)		
1	■				45.24	71.03	1	93.78
2	■				45.24	71.03	3	146.72
			■		45.24	71.03		
3	■				0	17.76	1	21.39
4	■				0	17.76	1	21.39
			■		11.31	0		
5	■				0	17.76	1	21.39
			■		11.31	0		
6	■				0	5.92	1	11.60

patterns with the single-damage-situation (Pattern 1, 3, and 6). For the other three damage patterns (Pattern 2, 4, and 5), which have two damaged stories, the trained AIS only successfully points out one of the damaged stories.

Even though the trained AIS fails in pointing out both the damaged stories in the damage patterns with two damage locations, this mistake is understandable because the single-damage-situation is imbedded in the AIS as a known condition.

As for the damage-severity-estimation, the trained AIS overestimated the severity in every damage pattern. It is noteworthy that the estimated severity is compared with the severity along the y-direction, because the accelerometer in use is mounted along the y-direction.

For Pattern 3, 4, 5 and 6, the trained AIS generates relatively accurate damage-severity-estimation results, whose severity deviations are within 10%. The estimations made by the AIS about Pattern 1 and 2 are much bigger than the actual damage severity. Nevertheless, if the fact that the AIS is trained using a 4-DOF structure model, while Model Case 1 of the benchmark problem has 12 DOF and different SPV sets is taken into account, the overall performance of the proposed AIS in Model Case 1 is still remarkable.

4.2.3.2 Model Case 2

Model Case 2 is similar with Model Case 1, except that it has a 120-DOF model while the one in Model Case 1 is 12-DOF. The excitation method in Model Case 2 is also the "ambient" excitation along the y-direction at all stories.

Because the external excitation is only applied along the y-direction, thus the measurement data from the 2nd accelerometer (y-direction at the 1st story) is used. Results from the AIS about the six damage patterns in Mode Case 2 are listed in Table 4-5.

As suggested in Table 4-5, the AIS correctly pointed out the damage location (or one of the damage locations) in five damage patterns (Pattern 1, 2, 3, 4, and 5). Because the 2nd accelerometer (y-direction at the 1st story) is used, the damage severity estimation results from the AIS are compared with the actual severity along the y-direction. For Pattern 3, 4, and 5, the AIS' estimations are relatively accurate (severity deviations are within 5%).

For Pattern 1 and 2, the estimations from the AIS are much higher than the actual severities.

The inaccuracy of the damage-severity-estimation in Pattern 1 and 2 can be possibility attributed to the fact that, the structure is severely damaged in these two patterns: The 1st story in Pattern 1 is heavily damaged (stiffness loss 74.99 along the y-direction), and the AIS overestimated about 30% stiffness loss. In Pattern 2, the stiffness loss is 74.78% on the 1st story and 76.00% on the 3rd story along the y-direction. The AIS only detected the damage on the 3rd story and the estimated damage severity is 167.76%, which is roughly the sum of the two damage severities of the 1st and the 3rd stories. In brief, the AIS is more accurate in damage-severity-estimation when the damage is relatively small.

Even though the structural in Modal Case 2 is much different with the 4-DOF structure used for training, the AIS still exhibits acceptable performance in unknown structural-damage-condition recognitions.

Table 4-5: Results from the AIS about the damage patterns in Model Case 2.

Damage Pattern Index	Real Damage Condition						AIS Result	
	Location (Story)				Severity (Stiffness Loss)		Location (Story)	Severity (%)
	1	2	3	4	x (%)	y (%)		
1	■				54.50	74.99	1	102.07
2	■				54.14	74.78	3	167.76
			■		59.60	76.00		
3	■				0	19.15	1	23.61
4	■				0	19.15	1	23.61
			■		15.20	0		
5	■				0	20.37	1	24.06
			■		15.20	0		
6	■				0	6.30	3	12.51

4.2.3.3 Model Case 3

This model case is the same with Model Case 1 except that, the excitation method in this model case is an external force applied at the roof along the direction of $\pm(\vec{\imath} - \vec{\jmath})$. With this excitation method, the data from the 1st (x-direction at the 1st story) and the 2nd (y-direction at the 1st story) accelerometers is used. Results from the AIS about the six damage patterns are listed in Table 4-6.

As suggested by Table 4-6, the AIS successfully pointed out the damage locations in Pattern 1, 3, 4, 5, and 6, some of which (Pattern 4 and 5) have two damaged stories. And for Pattern 2, the AIS only detected the damage on the 3rd story, while ignored the damage on the 1st story.

The success of the AIS in Pattern 4 and 5 can be attributed to the fact that, the most

Table 4-6: Results from the AIS about the damage patterns in Model Case 3.

Damage Pattern Index	Real Damage Condition						AIS Result			
	Location (Story)				Severity (Stiffness Loss)		X-Direction Sensor		Y-Direction Sensor	
	1	2	3	4	x (%)	y (%)	Location	Severity	Location	Severity
1	■				45.24	71.03	1	50.01%	1	95.08%
2	■				45.24	71.03	3	81.20%	3	145.69%
			■		45.24	71.03				
3	■				0	17.76	Healthy		1	23.46%
4	■				0	17.76	3	14.72%	1	23.46%
			■		11.31	0				
5	■				0	17.76	3	14.72%	1	23.46%
			■		11.31	0				
6	■				0	5.92	Healthy		1	11.16%

significant damage along the x-direction happens on the 3rd story, while the dominate damage along the y-direction is on the 1st story. In this way, the 1st and the 2nd accelerometers detected different damaged stories. Combining the measurement data from the 1st and the 2nd accelerometers, the AIS was able to identify both damaged stories in the damage pattern. For Pattern 2, because the most significant damage on the 1st and the 3rd story are both along the y-direction, both accelerometers detected the 3rd story as damaged while missed the 1st story. As a result, the AIS only recognized one of the damage locations.

As for the damage-severity-estimation, even though the estimations made by the AIS are generally higher than the actual severities, these estimations are still within the acceptable range in Pattern 3, 4, 5, 6, and also the x-direction in Pattern 1 (severity deviation smaller than 6%). For Pattern 2, the estimations are about the sum of the severities on the 1st and the 3rd stories.

Compared with the results in previous model cases, the results here are more satisfactory. One possible reason is that both the 1st and the 2nd accelerometers are employed and the information about the x-direction and the y-direction are analyzed.

4.2.3.4 Model Case 4

The situation in Model Case 4 is the same with Model Case 3, except that the structural model in this case is asymmetric while the one in Model Case 3 is symmetric. The

asymmetry of the structural model is created by replacing one $400\ kg$ slab on the 4th story with a $550\ kg$ one.

The excitation method in this model case is an external force applied at the roof along the direction of $\pm(\vec{\imath} - \vec{\jmath})$. With this excitation method, the measurement data from the 1st (x-direction at the 1st story) and the 2nd (y-direction at the 1st story) accelerometers is used. Results from the AIS about the six damage patterns in this case are listed in Table 4-7.

The AIS' performance in damage-location-determination here is exactly the same with the result in Model Case 3. This may results from the fact that the analytical structure models in both cases are the same 12-DOF finite element model with the same excitation method. The difference between the two cases is that the structural model in Model Case 3 is symmetric while the one in Model Case 4 is asymmetric. The identical results from both cases suggest that the symmetry of the structural model does not affect the AIS'

Table 4-7: Results from the AIS about the damage patterns in Model Case 4.

Damage Pattern Index	Real Damage Condition						AIS Result			
	Location (Story)				Severity (Stiffness Loss)		X-Direction Sensor		Y-Direction Sensor	
	1	2	3	4	x (%)	y (%)	Location	Severity	Location	Severity
1	■				45.24	71.03	1	45.86%	1	95.50%
2	■				45.24	71.03	3	81.26%	3	145.01%
			■		45.24	71.03				
3	■				0	17.76	Healthy		1	19.84%
4	■				0	17.76	3	11.67%	1	19.84%
			■		11.31	0				
5	■				0	17.76	3	11.67%	1	19.84%
			■		11.31	0				
6	■				0	5.92	Healthy		1	13.81%

performance in the damage-location-determination task.

Although the symmetry does not affect the AIS's performance in the damage-location-determination task, it does have an influence on the results in the damage-severity-estimation. Estimations made by the AIS in this case are different with the estimations in Model Case 3: The AIS generated more accurate damage-severity-estimations about Pattern 1, 3, 4, and 5 in this case. While, the estimation about Pattern 2 is as accurate as and the estimation about Pattern 6 is less accurate than the corresponding results in Model Case 3. Overall, the performance of the trained AIS in Mode Case 4 is similar with its performance in Model Case 3, which is acceptable.

4.2.3.5 Model Case 5

The configuration of Model Case 5 is the same with Model Case 4, except that the structural model in Model Case 5 is 120-DOF while the one in Model Case 4 is 12-DOF. Both the structural models are asymmetric. And the excitation methods in both cases are the same external force applied at the roof along the direction of $\pm(\vec{\imath} - \vec{\jmath})$.

With the external force applied along the direction of $\pm(\vec{\imath} - \vec{\jmath})$, the measurement data from the 1st (x-direction at the 1st story) and the 2nd (y-direction at the 1st story) accelerometers is used. Results from the AIS about the six damage patterns in this case are listed in Table 4-8.

As indicated by Table 4-8, the AIS successfully pointed out the correct damage location for Pattern 1, 3, 4, 5, and 6. In addition, the AIS found damage in one of the damage locations in Pattern 2.

In the damage-severity-estimation part, the AIS is more accurate about the damage along the x-direction. Its estimations along the y-direction are accurate in Pattern 3, 4, 5, and 6 (severity deviation $< 10\%$). But the estimations made by the AIS along the y-direction in Pattern 1 and 2 are much higher than the actual severities. In brief, the overall performance of the trained AIS in this case is satisfactory, with an exception in the damage-severity-estimation along the y-direction, which is not accurate.

It is noteworthy that the structure model in this case is a 120-DOF one and asymmetric, which is the most different one in the benchmark problem with the 4-DOF structure model used for the AIS training. Considering this significant difference, the proposed

Table 4-8: Results from the AIS about the damage patterns in Model Case 5.

Damage Pattern Index	Real Damage Condition						AIS Result			
	Location (Story)				Severity (Stiffness Loss)		X-Direction Sensor		Y-Direction Sensor	
	1	2	3	4	x (%)	y (%)	Location	Severity	Location	Severity
1	■				54.50	74.99	1	58.06%	1	103.93%
2	■				54.14	74.78	3	111.38%	3	163.24%
			■		59.60	76.00				
3	■				0	19.15	Healthy		1	24.55%
4	■				0	19.15	3	15.76%	1	24.55%
			■		15.20	0				
5	■				0	20.37	3	19.37%	1	27.77%
			■		15.20	0				
6	■				0	6.30	Healthy		1	15.24%

AIS' performance in this case is still satisfactory and implies its promising applicability to real world scenarios.

4.2.4 Benchmark Problem Summary

In the preceding part of this section, the proposed AIS was trained using a 4-DOF structure model, which was minutely analyzed in Section 3.3.1.3. After that the trained AIS was applied to a benchmark problem proposed by the IASC-ASCE Structural Health Monitoring Task Group.

There are five modal cases with eight damage patterns per model case in the benchmark problem. The proposed AIS were evaluated using all the five cases of the benchmark problem. The trained AIS exhibited satisfactory damage-location-determination capacity and acceptable damage-estimation-accuracy.

The significance of this investigation is that, the structure models, the SPVs, and the simulation method of the benchmark problem are obviously different with their counterparts in the AIS training. The 4-DOF structure model used for training is a model more simpler than the more accurate and more realistic 12- and 120-DOF structural models in the benchmark problem, which are constructed based on measurements from a physical structure with the finite-element-method.

Results of the AIS in the benchmark problem indicate that the proposed AIS can be potentially trained using a much simplified structure model of the structure under monitoring, and still exhibits satisfactory performance in SHM tasks. This characteristic makes the proposed AIS more applicable to real world SHM scenarios.

5 Conclusions and Future Studies

A parameter-insensitive artificial immune system (AIS) is proposed in this thesis, whose most distinct characteristic is its unique approach to construct FVs, which employ the pattern in modal-parameter-change instead of using modal parameters directly, and its three phase architecture, including damage-existence-detection (Phase 1), damage-location-determination (Phase 2), and damage-severity-estimation (Phase 3).

Through a series of comparisons between the performance of the proposed method and the conventional one in three structure models (2-DOF, 3-DOF and 4-DOF), it is clearly shown that the proposed FVs formed by pattern in modal-parameter-change have superior characteristics, compared with the ones constructed by modal parameters directly: FVs representing different damage locations are better separated in the feature space, while FVs standing for the same damage location are better clustered. More importantly, the proposed FVs are less sensitive to structural-parameter-value (SPV) differences.

In order to fully take advantage of the sensitivity of the proposed FV to damage locations, the AIS is divided into three phases: damage-existence-detection (Phase 1), damage-location-determination (Phase 2), and damage-severity-estimation (Phase 3). Output from the previous phase works as the input to the next phase.

The proposed method is applied to an AIS in a 4-DOF structure model. The AIS is trained using 21 known structural-damage-conditions, including the "healthy" condition. To evaluate the performance of the trained AIS, 440 unknown structural-damage-conditions with randomly selected SPV sets and damage severities are generated using the same 4-DOF structure model. The AIS acquired an overall success rate of 95.23% in damage-existence-detection and damage-location-determination, and accurate results (nearly 90% cases are within a 5% severity deviation) in damage-severity-estimation.

In addition to the 4-DOF structure model test, a benchmark study, which was proposed by the International Association for Structural Control-American Society of Civil Engineers (IASC-ASCE) Structural Health Monitoring Task Group, is employed to further assess the efficacy of the proposed AIS in practical scenarios. The overall performance of the proposed AIS in this benchmark study is satisfactory, which is significant considering that the AIS is trained using a 4-DOF structure model while the models in this benchmark study are 12-DOF and 120-DOF finite-element-models with different SPV sets.

In summary, the proposed AIS exhibits consistent and satisfactory performance in SHM scenarios, especially when there is a discrepancy between the training SPV and the SPV of the structural under monitoring. The tolerance of the proposed AIS to this discrepancy significantly extends the AIS' applicability to real world SHM tasks, and contributes to the exploration of developing the AIS to be a more general method instead of an individual structure dependent system.

Besides the overall satisfactory performance of the proposed AIS, there exist some limitations that need to be further investigated in future studies. One major limitation to this study is the practical issues involved in the modal parameter extraction. In this thesis, modal parameters are extracted from the structural free vibration initiated by an initial displacement. This is acceptable in the proof-of-concept demonstration. However, in real-world scenarios, a more convenient and realistic excitation method for one structure is the ambient excitation, caused by its surrounding environment (such as the wind or the traffic). The difficulties and challenges involved in the modal parameter extraction with the ambient vibration should be investigated in future studies.

The proposed AIS is designed to have a 3-phase procedure, separating the damage-existence-detection, the damage-location-determination, and the damage-severity-estimation tasks. The focus of this thesis is on the 2^{nd} phase (damage-location-determination). Due to the definition used in the proposed method, the feature vector representing the health condition cannot be plotted in the feature space for phase 2. This does not cause any problem, because phase 2 is only performed when the damage has been detected in phase 1. In other words, if the structure is healthy, the AIS will not use phase 2 to determinate the damage location, therefore will not encounter the "undefined" condition. There exists the possibility of modifying the definition to include the healthy condition in the feature space, which requires further study about the mathematic principles behind the proposed feature space.

6 Bibliography

Albergante, L. "Wireless discussion forums: Automatic management via artificial immune systems." *Performance Evaluation of Computer and Telecommunication Systems.* Edinburgh, 2008. 74-81.

Burj Khalifa. http://en.wikipedia.org/wiki/Burj_Khalifa (accessed March 10, 2014).

Casciati, F. "An overview of structural health monitoring expertise within the European Union." Edited by Zhishen Wu and Masato Abe. *Structural Health Monitoring and Intelligent Infrastructure.* Tokyo: Taylor & Francis, 2003. 31-37.

Chen, Bo, and Chuanzhi Zang. "A hybrid immune model for unsupervised structural damage pattern recognition." *Expert Systems with Applications*, 2011: 1650-1658.

Chen, Bo, and Chuanzhi Zang. "Artificial immune pattern recognition for structure damage classification." *Computers and Structures*, 2009: 1394-1407.

Dasgupta, Dipankar, Senhua Yu, and Fernando Nino. "Recent advances in artificial immune systems: models and applications." *Applied Soft Computing*, 2011: 1574-1587.

de Castro, Leandro N., and Fernando J. Von Zuben. "Learning and optimization using the clonal selection principle." *IEEE Transactions on Evolutionary Computation* 6 (June 2002): 239-251.

Doebling, Scott W., Charles R. Farrar, Michael B. Prime, and Daniel W. Shevitz. *Damage identification and health monitoring of structural and mechanical systems from changes in their vibration characteristics: a literature review.* Los Alamos: Los Alamos National Laboratory, 1996.

Ellis, B. R., and A. J. Bougard. "Dynamic testing and stiffness evaluation of a six-storey timber framed building during construction." *Engineering Structures*, 2001: 1232-1242.

Farrar, Charles R., and Keith Worden. "An introduction to structural health monitoring." *Philosophical Transactions: Mathematical, Physical and Engineering Science* 365 (February 2007): 303-315.

Forrest, Stephanie, Alan S. Perelson, Lawrence Allen, and Rajesh Cherukuri. "Self-nonself discrimination in a computer." *IEEE Computer Society Symposium on Research in Security and Privacy.* Los Alamitos, 1994. 202-212.

Gadi, Manoel Fernando Alonso, Xidi Wang, and Alair Pereira do Lago. "Credit card fraud detection with artificial immune system." In *Artificial Immune Systems*, edited by Peter J. Bentley, Doheon Lee and Sungwon Jung, 119-131. Phuket: Springer Berlin Heidelberg, 2008.

Honarvar, Farhang, Farzaneh Salehi, Vahid Safavi, Arman Mokhtari, and Anthony N. Sinclair. "Ultrasonic monitoring of erosion/corrosion thinning rates in industrial piping systems." *Ultrasonics*, 2013: 1251-1258.

Johnson, E. A., H. F. Lam, L. S. Katafygiotis, and J. L. Beck. "Phase I IASC-ASCE structural health monitoring benchmark problem using simulated data." *Journal of Engineering Mechanics* 130 (January 2004): 3-15.

Lerner, Brenda Wilmoth, and K. Lee Lerner. *Immune System.* Vol. 3, in *The Gale Encyclopedia of Science*, by Brenda Wilmoth Lerner and K. Lee Lerner, 2246-2254. Detrioit: Gale, 2008.

Li, Hua, Cui Wang, and Anna Wang. "Medicial image registration based on more features and artificial immune algorithm." *International Joint Conference on Artificial Intelligence.* Hainan Island, 2009. 469-472.

NEEShub - a platform for research, collaboration and education. http://nees.org/dataview/spreadsheet/scmbp (accessed March 16, 2014).

Nguyen, Van Truong, Xuan Hoai Nguyen, and Chi Mai Luong. "A novel combination of negative and positive selection in artificial immune system." *IEEE RIVF International Conference on Computing & Communication Technologies.* IEEE, 2013. 6-11.

Ou, J. P., and H. Li. "The state-of-the-art and practice of structural health monitoring for civil infrastructures in the mainland of China." In *Structural Health Monitoring and Intelligent Infrastructure*, 69-93. London: Taylor & Francis Group, 2006.

Pines, Darryll, and A Emin Aktan. "Status of structural health monitoring of long-span bridges in the United States." *Progress in Structural Engineering and Materials* 4, no. 4 (Octber/December 2002): 372-380.

Puteh, M., A. R. Hamdan, K. Omar, and A. A. Bakar. "Flexible immune network recognition system for mining heterogeneous data." In *Artificial Immune Systems*, edited by Peter J. Bentley, Doheon Lee and Sungwon Jung, 232-241. Phuket: Springer Berlin Heidelberg, 2008.

Sohn, Hoon, et al. *A review of structural health monitoring literature: 1996-2001.* Los Alamos: Los Alamos National Laboratory, 2004.

Srinivasan, M. G., and C. A. Kot. "Effects of damage on the modal parameters of a cylindrical shell." *Processing of the 10th International Modal Analysis Conference.* 1992. 529-535.

Vieira, Ian N., Beatriz L.P. de Lima, and Breno P. Jacob. "Optimization of steel catenary risers for offshore oil production using artificial immune system." In *Artificial Immune Systems*, edited by Peter J. Bentley, Doheon Lee and Sungwon Jung, 254-265. Phuket: Springer Berlin Heidelberg, 2008.

Worden, Keith, Charles R. Farrar, Graeme Manson, and Gyuhae Park. "The fundamental axioms of structural health monitoring." *Proceedings: Mathematical, Physical and Engineering Sciences.* The Royal Society, 2007. 1639-1664.

Xiao, Wenchang. *Structural health monitoring and fault diagnosis based on artificial immune system.* MS Thesis, Mechanical Engineering, Worcester Polytechnic Institute, Worcester: Worcester Polytechnic Institute, 2012.